

Spin-Wave Calculations for Low-Dimensional Magnets

Dissertation
zur Erlangung des Doktorgrades
der Naturwissenschaften

vorgelegt beim Fachbereich Physik
der Johann Wolfgang Goethe - Universität
in Frankfurt am Main

von
Ivan Spremo
aus Ljubljana

Frankfurt 2006
(D F 1)

vom Fachbereich Physik der
Johann Wolfgang Goethe - Universität als Dissertation angenommen.

Dekan:	Prof. Dr. W. Aßmus
Gutachter:	Prof. Dr. P. Kopietz
	Prof. Dr. M.-R. Valenti

Datum der Disputation: 21. Juli 2006

Für meine Eltern Marija und Danilo

und

für Christine

Contents

1	Introduction	1
2	Magnetic insulators	5
2.1	Exchange interaction	5
2.2	Order parameters and disorder in low dimensions	9
2.3	Low-energy excitations	11
3	Quantum Monte Carlo methods for spin systems	13
3.1	Handscomb's scheme	14
3.2	Stochastic Series Expansion	15
3.3	ALPS	16
4	Representing spin operators in terms of canonical bosons	17
4.1	Ordered state: Dyson-Maleev bosons	17
4.2	Spin-waves in non-collinear spin configurations	18
4.2.1	General bosonic Hamiltonian	18
4.2.2	Classical ground state	21
4.3	Holstein-Primakoff bosons	22
4.4	Schwinger bosons	23
5	Spin-wave theory at constant order parameter	25
5.1	Thermodynamics at constant order parameter	26
5.1.1	Thermodynamic potentials and equations of state	26
5.1.2	Conjugate field	28
5.2	Spin waves in a Heisenberg ferromagnet	29
5.2.1	Classical ground state	29
5.2.2	Linear spin-wave theory	31
5.2.3	Dyson-Maleev Vertex	32
5.2.4	Hartree-Fock approximation	33
5.2.5	Two-loop correction	34
5.3	Low-temperature thermodynamics	36
5.3.1	Density of states and Bose-Einstein integrals	36

5.3.2	One-dimensional ferromagnet	37
5.3.3	Two-dimensional ferromagnet	42
5.3.4	Three-dimensional ferromagnet	43
6	Two-dimensional antiferromagnet in a uniform magnetic field	45
6.1	Spin waves in uniform magnetic field	45
6.1.1	Classical ground state	46
6.1.2	Spin-wave dispersion	49
6.2	Observables	54
6.2.1	Uniform and staggered magnetization	55
6.2.2	Uniform susceptibility	60
6.2.3	Specific heat	63
6.2.4	Staggered correlation length	64
6.3	Applications to an antiferromagnet on a distorted honeycomb lattice	66
6.3.1	Experimental motivation	66
6.3.2	Distorted honeycomb lattice	68
6.3.3	Energy dispersion	70
6.3.4	Zero-temperature uniform and staggered magnetization	72
6.3.5	Finite-temperature magnetization curve	76
6.3.6	Finite-temperature susceptibility	78
6.3.7	Specific heat	80
7	Conclusion	83
	Deutsche Zusammenfassung	91
	Veröffentlichungen	97
	Lebenslauf	99
	Danksagung	101

Chapter 1

Introduction

[..] I have sought a more practical definition. And what I came up with is the following definition: Any thing that makes money under the rubric of nanotechnology is nanotechnology.

Suchan Chae, Associate Professor of Economics, Rice University

In industry or in art it is becoming increasingly popular to give products or concepts a catchy name in hope to achieve broader acceptance among customers. A similar trend towards short and memorable labels can also be observed in engineering and science, whereas here the audience are the scientific community on the one side and potential investors on the other side. One of such catch phrases that became broadly known during the past decades and is now part of the everyday language is *nanotechnology* [1], denoting physics on a sub-micron scale. Although he did not use the explicit term, Feynman's visionary talk from 1959 entitled 'There's Plenty of Room at the Bottom' [2] already defined the field of nanotechnology; today its wide scope ranges from carbon nanotubes to smart dust. Another modern area of research which is usually filed under nanotechnology is *spintronics* (short for spin-based electronics).

The moniker spintronics was originally coined after the discovery of giant magnetoresistance (GMR) in Fe-Cr-Fe layers with antiferromagnetic interlayer exchange interaction [3]. Today the term is used in a much broader sense: it includes all electronic concepts or devices that use spin degree of freedom in addition to charge degrees of freedom. The most prominent example of a spintronic device would be a quantum computer where the electron spin would represent a qubit (short for quantum bit) [4, 5]. However, a practical realization of the quantum computer is still an engineering challenge due to a long list of obstacles [6], most notably the inherent stability-decoherence problem.

Among spintronic products spin-valves are the most widespread and successful at present. A spin-valve is based on GMR; it consists typically of layered magnetic thin films with different hystereses, which change electrical resistance depending on

the direction of the applied magnetic field. They are used as magnetic sensors in automotive industry and hard disk read/write heads. The progress in performance of mass-storage devices like hard drives gives a good impression of how fast spintronics is developing in comparison with conventional electronics. The so-called Kryder's law states that the density of information (bits per unit area) that can be stored on a hard disk doubles approximately every 18 months [7]. This is exactly the rate predicted by the famous Moore's law for the number of transistors on an integrated circuit [8]. Thus, Kryder's law is essentially Moore's law for storage and spintronics is essentially developing at the pace of traditional micro electronics.

Although nanotechnology in general and spintronics in particular are still occupying small niches in the market, their potential for the future is huge. Research interest in this field has been growing steadily during the past years. A number of programs have been granted by governmental organizations like the 'National Nanotechnology Initiative' (NNI) in the United States [9] and 'Nanotechnologies and nano-sciences, knowledge-based multifunctional materials and new production processes and devices' (NMP) in the European Union [10].

From the scientific point of view, one of the major drivers behind the keyword spintronics is the physics of low-dimensional quantum spin systems. The field of low-dimensional magnetism was established in the wake of quantum mechanics through two ground-breaking theoretical achievements: first, the introduction of the one-dimensional Ising model in 1925 [11], and second, the exact calculation of the ground state of the one-dimensional Heisenberg model within the Bethe ansatz method in 1931 [12]. In the following four decades the focus was clearly on theoretical research. Numerous exact results were derived, most notably the proof of absence of spontaneous symmetry breaking in low-dimensional models with continuum symmetry at finite temperatures [13, 14]. We review basic aspects of quantum spin systems in Chapter 2, with special emphasis on ferro- and antiferromagnetic Heisenberg models in low dimensions. In Chapter 3 we give a brief introduction in Stochastic Series Expansion [15], a quantum Monte Carlo method for spin systems utilized in the later parts of the present work.

The field of low-dimensional Heisenberg magnets received a boost after the discovery of the high-temperature superconductivity in the 1980s [16]. The copper oxide layers in the high T_c superconductors - the most prominent example is La_2CuO_4 - are a very good experimental realization of a two-dimensional $S = 1/2$ Heisenberg antiferromagnet on a square lattice [17]. The problem has been attacked within several theoretical approaches, e.g. Schwinger boson theory [18] and nonlinear sigma model [17]. In a series of papers, Takahashi succeeded calculating the thermodynamics of the one and two dimensional Heisenberg magnets by incorporating the constraint of vanishing order parameter at finite temperatures into the spin-wave theory [19, 20, 21].

In Chapter 4 we present various mappings of spin degrees of freedom to boson

canonical operators; these are crucial for the understanding of the spin-wave theory. We generalize one of the representations, the Dyson-Maleev transformation [22, 23, 24], to a case with a non-collinear spin configuration. We use this formulation in the spin-wave calculations of the subsequent chapters.

A variant of spin-wave theory for low-dimensional systems is developed in Chapter 5. By calculating thermodynamic observables at constant order parameter we resolve ambiguities regarding the choice of the zero order parameter constraint which plagues Takahashi's approach. In addition to this, we are able to go beyond linear spin-wave theory and systematically calculate two-loop correction to the free energy. We use our method to determine the low-temperature physics of Heisenberg ferromagnets in one, two and three spatial dimensions.

During the last two decades solid state chemists and crystal growers have synthesized low-dimensional magnets with tailored properties, e.g the layered cuprate high-temperature superconductors (for a review, see [25]) or transition metal compounds (for a review, see [26]). Due to the interplay of dimensionality, strong interactions and quantum fluctuations these materials exhibit a multitude of interesting phenomena. Particularly new phases of matter like resonating valence bond state [27], spin-Peierls transition [28] and magnetic plateaus [29] gave the research field a strong impetus.

In the case of a two-dimensional Heisenberg antiferromagnet the influence of frustration, arising e.g. from competing nearest-neighbor bonds or lattice topology, on the existence of the long range order has been extensively investigated (see [30] and references therein). Chapter 6 is devoted to similar issues in a special case of a non-frustrated antiferromagnet on a bipartite lattice in two dimensions; among other observables we 'measure' the long range order by calculating the staggered correlation length at low temperatures and fields. Furthermore, we expand the $T = 0$ spin-wave method for Heisenberg antiferromagnets in the vicinity of an external magnetic field proposed by Zhitomirsky and Nikuni [31] to the finite temperature case. After setting the formal framework, we determine the uniform and staggered magnetization in presence of a uniform magnetic field, the uniform susceptibility and the specific heat. Additionally, we perform quantum Monte Carlo simulations and subsequently show that numerical findings are qualitatively comparable to spin-wave results. Finally, we validate our theoretical results through comparison with the measurements performed on a novel quasi two-dimensional metal-organic antiferromagnet on a distorted honeycomb lattice [32].

We give a résumé of the thesis and a critical analysis of what still has to be done in the closing Chapter 7.

Chapter 2

Magnetic insulators

In this chapter we give a short introduction to the collective magnetic phenomena of magnetic insulators. In Sec. 2.1 we show how the dominant magnetic interaction - the exchange interaction - arises from the static Coulomb interaction. Sec. 2.2 recapitulates the concepts of order parameter and of spontaneous symmetry breaking. A classic theorem on order in low dimensions by Hohenberg, Mermin and Wagner is also discussed. In Sec. 2.3 we discuss the nature of low-lying excitations in magnetic systems and outline a basic idea of the spin-wave theory.

The scope of this chapter is aimed at readers which are not very familiar with the fundamentals of localized quantum magnetism. The style is concise and the references for further reading are given.

2.1 Exchange interaction

In the present work we deal with magnetic insulators, i. e. with solids where permanent magnetic dipoles are localized on a lattice. Despite this simplification the theory of the origin of magnetic interaction is still quite complex. Therefore we first introduce the basic concepts of ferro- and antiferromagnetism for the case of a two-electron system. Subsequently, we indicate how the obtained results can be generalized to a more realistic many-body system. Similar approaches can be found in a classic solid-state textbook by Ashcroft and Mermin [33] and in a book by Auerbach [34].

The experimentally observed magnetic transition temperatures are of order

$$T_c \approx 10^2 - 10^3 \text{ K} \quad (2.1)$$

in transition metal and rare earth compounds [35]. We therefore expect the magnetic interactions in this systems to have the same order of magnitude.

Starting from classical physics one might expect that the ferromagnetism arises from the dipole-dipole interaction. The dipolar interaction energy of two magnetic

moments \mathbf{m}_1 and \mathbf{m}_2 separated by a distance \mathbf{r} is given by

$$V_{\text{d-d}} = \frac{1}{|\mathbf{r}|^3} \mathbf{m}_1 \cdot \mathbf{m}_2 - \frac{3}{|\mathbf{r}|^5} (\mathbf{m}_1 \cdot \mathbf{r})(\mathbf{m}_2 \cdot \mathbf{r}). \quad (2.2)$$

Atomic dipole moments have a magnitude $|\mathbf{m}_1| \approx |\mathbf{m}_2| \approx g\mu_B$ where g is gyromagnetic ratio and μ_B is Bohr magneton. In a magnet they are typically about 1\AA apart, therefore the strength of the dipole-dipole interaction (2.2) is approximately

$$V_{\text{d-d}} \approx 10^0 \text{ K}, \quad (2.3)$$

which is far too weak to explain Eq. (2.1).

Another naïve guess for the source of magnetism would be spin-orbit coupling. The magnitude of the spin-orbit interaction is determined by the charge of the atomic nucleus as [36]

$$V_{\text{s-o}} \propto \alpha^2 Z^4, \quad (2.4)$$

with the atomic number Z and the fine-structure constant

$$\alpha = \frac{e^2}{\hbar c} \approx \frac{1}{137}, \quad (2.5)$$

where e denotes the elementary charge of an electron and c is the speed of light in vacuum. Although according to Eq. (2.4) the strength of the spin-orbit coupling increases rapidly with atomic number, it is still not the dominant magnetic interaction. Nevertheless, both dipole-dipole and spin-orbit interaction can give rise to anisotropies.

Exchange interaction originates mainly from the following fundamental properties of electrons:

- the spin of a electron,
- Pauli exclusion principle,
- the kinetic energy of a electron, and
- the Coulomb interaction between electrons.

Depending on the nature of the noninteracting wave functions the coupling between electronic spins can be ferro- or antiferromagnetic. In the following we illustrate this on a simplest non-trivial example, two localized electrons interacting via Coulomb potential.

First we approximate the strength of the two-body Coulomb repulsion

$$U(\mathbf{r}_1, \mathbf{r}_2) = \frac{e^2}{|\mathbf{r}_1 - \mathbf{r}_2|} \approx 10^5 \text{ K}, \quad (2.6)$$

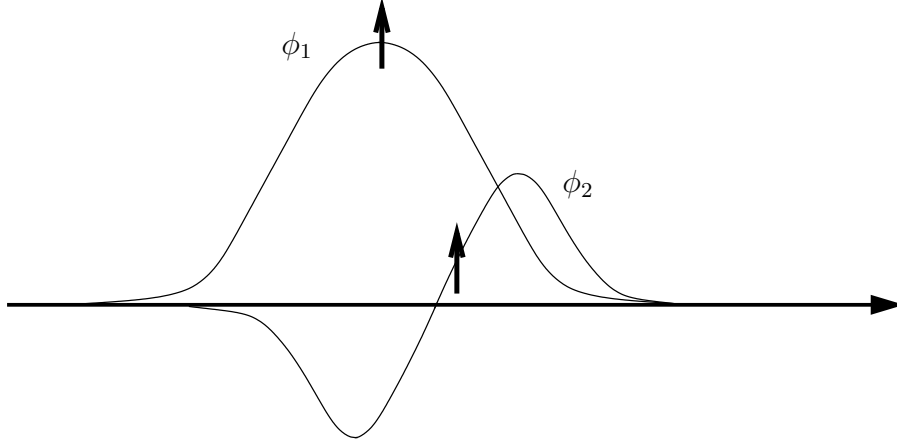


Figure 2.1: One-dimensional representation of the orbitals ϕ_1 and ϕ_2 for two ferromagnetically coupled electrons.

where we have assumed the average distance between the electrons to be 1\AA . The Coulomb interaction is thus five orders of magnitude larger than the corresponding dipolar interaction and is an appropriate candidate for the source of the magnetic interaction.

Now let us consider two orthogonal electronic orbitals ϕ_1 and ϕ_2 which occupy the same region of space. In Fig. 2.1 the one-dimensional case of two such wave-functions is shown. We write the electron fields in terms of canonical fermion operators:

$$\psi_{\sigma}^{\dagger}(\mathbf{r}) = \sum_{i=1}^2 \phi_i^* c_{i\sigma}^{\dagger} \quad , \quad \sigma = \uparrow, \downarrow . \quad (2.7)$$

In this basis the two-body Coulomb interaction is given by

$$V = \sum_{i \neq j} U_{ij} n_i n_j + \sum_{i=1}^2 U_{ii} \rho_{i\uparrow} \rho_{i\downarrow} + \sum_{i \neq j} \sum_{\sigma \sigma'} J_F c_{i\sigma}^{\dagger} c_{j\sigma'}^{\dagger} c_{i\sigma'} c_{j\sigma} , \quad (2.8)$$

with

$$\rho_{i\sigma} \equiv c_{i\sigma}^{\dagger} c_{i\sigma} , \quad (2.9)$$

and

$$n_i \equiv \sum_{\sigma = \uparrow, \downarrow} \rho_{i\sigma} . \quad (2.10)$$

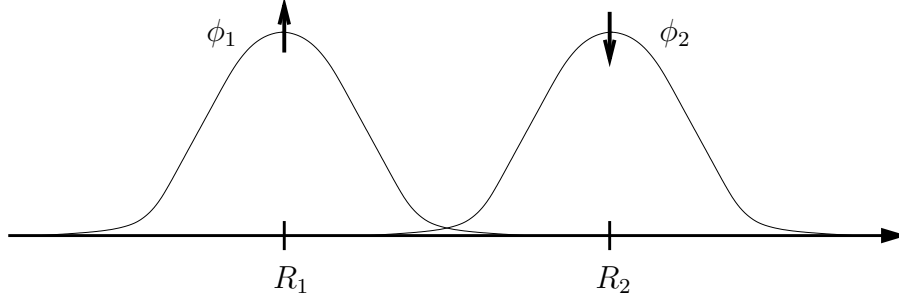


Figure 2.2: One-dimensional representation of the orbitals ϕ_1 and ϕ_2 for two anti-ferromagnetically coupled electrons. The equilibrium positions of the corresponding protons are denoted by R_1 and R_2 .

The interaction parameters in Eq. (2.8) are given by direct integrals

$$U_{ij} = \frac{1}{2} \int d^3r_1 d^3r_2 V_c(\mathbf{r}_1, \mathbf{r}_2) |\phi_i(\mathbf{r}_1)|^2 |\phi_j(\mathbf{r}_2)|^2, \quad (2.11)$$

and by exchange integrals

$$J_F = \frac{1}{2} \int d^3r_1 d^3r_2 \phi_i(\mathbf{r}_1) \phi_j(\mathbf{r}_2) V_c(\mathbf{r}_1, \mathbf{r}_2) \phi_j^*(\mathbf{r}_1) \phi_i^*(\mathbf{r}_2) > 0. \quad (2.12)$$

The ferromagnetic exchange integral J_F depends on the spatial overlap between the single particle orbitals ϕ_1, ϕ_2 . In spin space spanned by the states

$$\{|\sigma_1, \sigma_2\rangle\} \quad , \quad \sigma_i = \uparrow, \downarrow, \quad (2.13)$$

the exchange term acts as a Heisenberg interaction

$$\mathcal{H} = \sum_{\sigma\sigma'} J_F c_{i\sigma}^\dagger c_{j\sigma'}^\dagger c_{i\sigma'} c_{j\sigma} = -2J_F \left(\mathbf{S}_i \cdot \mathbf{S}_j + \frac{1}{4} n_i n_j \right), \quad (2.14)$$

with the $S = 1/2$ spin operators \mathbf{S}_i . In other words: electrons with overlapping orbitals give rise to a ferromagnetic exchange interaction. A parallel alignment of spins reduces the effect of Coulomb repulsion.

Now let us treat two electrons with spatially well separated non-orthogonal orbits. The simplest example of such a system is the H_2 molecule which was first discussed by Heitler and London [37]. In Fig. 2.2 we show the atomic wave functions ϕ_1 and ϕ_2 centered on atoms with respective positions R_1 and R_2 .

Using the Pauli principle it can be shown in the framework of the Heitler-London approximation that the singlet state is energetically more favorable than the triplet

state. Hence the spins align antiparallel in the ground state. The energy splitting between the triplet and the singlet

$$J_A \equiv E_t - E_s > 0, \quad (2.15)$$

is the antiferromagnetic coupling of the Heisenberg Hamiltonian

$$\mathcal{H} = J_A \mathbf{S}_1 \cdot \mathbf{S}_2. \quad (2.16)$$

The antiparallel alignment of the spins reduces their kinetic energy.

In the case of N spins \mathbf{S}_i on a discrete lattice the two-spin Heisenberg Hamiltonians (2.14, 2.16) can be very often directly generalized to

$$\mathcal{H} = \sum_{ij}^N J_{ij} \mathbf{S}_i \cdot \mathbf{S}_j, \quad (2.17)$$

with appropriate (anti)ferromagnetic couplings J_{ij} . We close our treatment of the origin of the exchange coupling here and do not discuss under which circumstances Eq. (2.17) is justified. A thorough discussion of this complex topic is given in Ref. [38].

Finally, it should be mentioned that there are further mechanisms beside exchange interaction that give rise to collective magnetic phenomena. Most prominent examples are itinerant magnetism [39] and super-exchange interaction [40]. We do not discuss these interaction mechanisms as they are not taken into account in the present work.

2.2 Order parameters and disorder in low dimensions

The notions of order parameter and of symmetry breaking play a fundamental role in the characterization of different phases. In this chapter we recapitulate basic concepts used in the theory of phase transitions and give physical examples of order parameters in ferro- and antiferromagnets. Finally, we address the issue of low dimensionality and its consequences on the symmetry breaking.

An order parameter can be defined as a quantity which vanishes in a disordered phase and is finite in the ordered phase [41]. In a slightly more formal approach, an order parameter is defined as the thermodynamic variable conjugate to the external thermodynamic field. The order parameter couples linearly to the corresponding conjugate field. The linear response of the order parameter to the external field involves the susceptibility. In other words, the susceptibility measures the fluctuations of the order parameter.

In the case of a ferromagnetic phase transition the corresponding order parameter

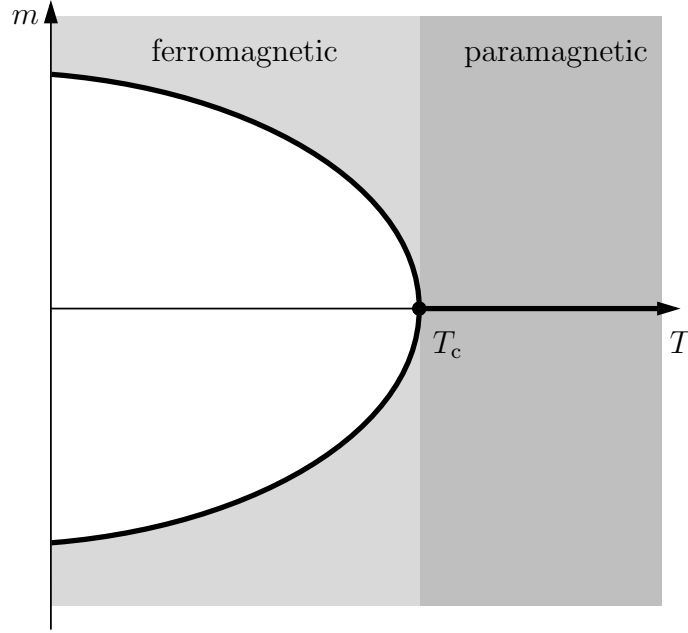


Figure 2.3: A phase diagram for a ferromagnet. The surface of the equation of state is projected onto the $m - T$ plane. The solid line denotes magnetization as a function of temperature at zero external magnetic field.

is the magnetization per site, here denoted by m , and the conjugate field is the uniform magnetic field H . For an antiferromagnet the order parameter is the staggered magnetization per site, here denoted by n , and the conjugate field is the staggered magnetic field H_s . We will come back to these concepts in Sec. 5.1 when we discuss the thermodynamics of Heisenberg magnets at constant order parameter.

In Fig. 2.3 a typical phase diagram of a ferromagnet is sketched. Below the critical temperature T_c the order parameter m is finite even in the absence of the ordering field. Hence, in the ferromagnetic phase the system has a spontaneously broken symmetry. This implies true long-range order. When the temperature is approaching T_c from below, the magnetization continuously decreases and is zero at and above the critical point T_c . This is generic behavior of a system which undergoes a second-order phase transition. An antiferromagnet shows a quantitatively similar phase diagram with the staggered magnetization n as an order parameter.

In low dimensions thermal excitations disorder the spins at infinitesimally small temperatures and the phase transition from the ordered into the disordered state occurs at $T_c = 0$. Mermin and Wagner proved exactly that there is no spontaneous symmetry-breaking at finite temperatures in isotropic one and two dimensional quantum Heisenberg models with finite-range interactions [13]. Their proof utilizes the Bogoliubov inequality [42], which in turn follows from the Cauchy-Schwarz inequality.

The reasoning of Mermin and Wagner can be generalized to a larger class of models with continuous symmetries; for recent results, see Ref. [43] and references therein. Historically, Hohenberg was the first to use the Bogoliubov inequality in order to show the absence of superfluidity at finite temperatures in one and two dimensions [14]. Hence, the corresponding theorem is often called Hohenberg-Mermin-Wagner theorem. We will make use of this exact statement later in the present work.

In a three dimensional Heisenberg magnet spontaneous symmetry breaking occurs at a finite critical temperature $T_c > 0$, which is of the order of the exchange interaction.

With the zero temperature version of the Bogoliubov inequality it can be shown exactly that the ground state of a low-dimensional Heisenberg model is disordered if there is a finite gap in the excitation spectrum [34]. A prominent one-dimensional example for a such behaviour are antiferromagnetic integer spin chains which show the so-called Haldane-gap in their spectrum [44].

We stop our discussion of order and disorder in Heisenberg magnets at this point and give references for further reading. A concise introduction into the field of phase transitions can be found in the Chap. 4 of the textbook by Negele and Orland [45]. The book by Sachdev [28] provides a modern view on quantum phase transitions with special emphasis on magnetic systems.

2.3 Low-energy excitations

In this section we present the main physical idea behind spin-wave theory, a highly successful approach to the low-temperature sector of ordered spin systems.

We start with the *Goldstone theorem*, an exact statement on the existence of gapless excitations. Goldstone theorem states that a broken continuous symmetry in the ground state of a Hamiltonian with short-range interactions implies the existence of low-energy excitations called *Goldstone modes* [46]. If the order parameter correlation function diverges at some wave vector $\bar{\mathbf{q}}$, then the energy of the Goldstone mode vanishes as $\mathbf{q} \rightarrow \bar{\mathbf{q}}$. Examples for Goldstone modes in condensed matter are e.g. acoustic phonons in solids that break translational symmetry and spin waves in Heisenberg ferromagnets with a finite-range exchange interaction [47].

Spin-wave theory for the low-lying excitations in ferromagnets was proposed independently by Bloch [48] and Holstein and Primakoff [49]. Here one starts with the equations of motion for the spin \mathbf{S}_i at the site i of a Heisenberg ferromagnet in the presence of an uniform magnetic field. It is a convention to choose the z axis of the system to be along the direction of the external field. Then the equation of motion for the z -component of the spin S_i^z is second order in small parameters S_i^x , S_i^y and can be consequently neglected

$$S_i^z \approx S. \quad (2.18)$$

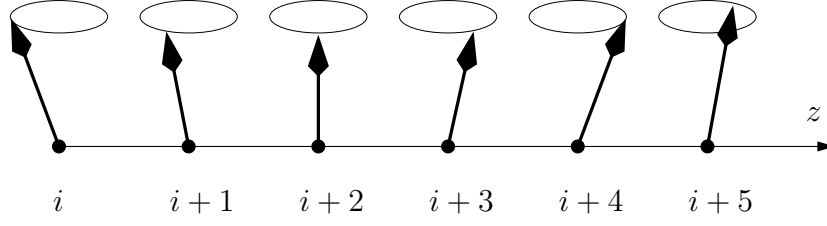


Figure 2.4: Lattice spins $\mathbf{S}_i, \dots, \mathbf{S}_{i+5}$ in the spin-wave state.

By transforming the equations for the remaining two spin components into the momentum space one can show that in the excited state the spins precess with the same frequency but different phases about the direction of the external field. In other words, a wave of spins is excited, as shown in Fig. 2.4. At low temperatures the amplitude of the *spin wave* is small. Hence, the excitations in the vicinity of the ground state can be approximated through non-interacting spin waves: this approach is called *linear* spin-wave theory. With this theory Bloch was able to derive the $T^{3/2}$ law for the spontaneous magnetization in three dimensional ferromagnets. In Sec. 5.3 we will obtain this classic result within our modified spin-wave theory at constant order parameter.

In the 1950s the spin-wave approach was extended to the Néel state of an antiferromagnet by Anderson [50] and Kubo [51]. In a seminal work [22, 23] Dyson was able to show that for the three-dimensional Heisenberg ferromagnet at low temperatures the asymptotic expansions of the thermodynamic variables can be calculated. Harris and co-workers determined in a systematic manner the dynamical properties like spin-spin correlations and spin-wave damping of Heisenberg antiferromagnets by utilizing a generalized version of Dyson's method [52].

Experimentally, three standard methods have been established for the observation of spin waves. Inelastic neutron scattering is used for determination of the magnon dispersion, Brillouin scattering is capable of resolving the energy of magnons on the meV scale and ferromagnetic resonance displays the effect of anisotropies on the dispersion of spin waves.

Chapter 3

Quantum Monte Carlo methods for spin systems

Quantum Monte Carlo is a common name for a class of nonperturbative numerical methods for quantum many-body systems at finite temperatures. The goal is calculation of the thermal expectation value of an operator \mathcal{A}

$$\langle \mathcal{A} \rangle = \frac{1}{Z} \text{Tr} (\mathcal{A} e^{-\beta \mathcal{H}}) , \quad (3.1)$$

with the Hamiltonian \mathcal{H} , the inverse temperature (we set Boltzmann constant equal to 1)

$$\beta \equiv \frac{1}{T} , \quad (3.2)$$

and the partition function

$$Z = \text{Tr} e^{-\beta \mathcal{H}} . \quad (3.3)$$

Quantum Monte Carlo relies on the the Monte Carlo method [53] for the evaluation of the integrals appearing in the expressions for the expectation values. Monte Carlo is a stochastic method based on an idea to sample the integrals statistically. Statistical uncertainty can be reduced with longer simulation time, because independent of the dimension of the integral the sampling error decreases as $1/\sqrt{N}$ where N is the number of points at which the integrand is sampled.

Different quantum Monte Carlo schemes have been developed in order to treat bosonic and fermionic many-body models; for examples and for an extensive list of references, see Ref. [45]. For spin systems a method proposed by Handscomb [54, 55] has been very successful. However, Handscomb's scheme is limited to $S = 1/2$ systems, hence a generalized version called Stochastic Series Expansion was put forward by Sandvik [15].

In Sec. 3.1 we briefly review the method of Handscomb and discuss its limitations. A short overview of the Stochastic Series Expansion is given in Sec. 3.2. In the last

section of this chapter we present ALPS, an open source project providing simulation codes for strongly correlated quantum mechanical systems.

3.1 Handscomb's scheme

In this section give a review of the basic ideas of Handscomb's simulation scheme.

The Hamiltonian may generally be expressed in terms of noncommuting terms

$$\mathcal{H} = \sum_{i=1}^M \mathcal{H}_i, \quad (3.4)$$

where M is large but finite and

$$[\mathcal{H}_i, \mathcal{H}_j] \neq 0 \quad , \quad \text{for } i \neq j. \quad (3.5)$$

Handscomb proposed to expand $e^{-\beta\mathcal{H}}$ in a Taylor series and express the powers of \mathcal{H} as sums of products of the operators \mathcal{H}_i [54, 55]. The resulting partition function is then given by

$$Z = \sum_{n=0}^{\infty} \sum_{\{C_n\}} \frac{(-\beta)^n}{n!} \text{Tr} \left(\prod_{l=1}^n \mathcal{H}_{i_l} \right), \quad (3.6)$$

where C_n denotes any sequence (i_1, i_2, \dots, i_n) of n indices in the range $1 \leq i \leq M$. Next, a sample space consisting of the set of all such sequences C_n for all $n \geq 0$ is defined. The thermal average (3.1) of the operator \mathcal{A} can now be written as

$$\langle \mathcal{A} \rangle = \sum_{n=0}^{\infty} \sum_{\{C_n\}} A(C_n) W(C_n), \quad (3.7)$$

with the weight factor

$$W(C_n) = \frac{1}{Z} \frac{(-\beta)^n}{n!} \text{Tr} \left(\prod_{l=1}^n \mathcal{H}_{i_l} \right), \quad (3.8)$$

and

$$A(C_n) = \frac{\mathcal{A} \text{Tr} (\prod_{l=1}^n \mathcal{H}_{i_l})}{\text{Tr} (\prod_{l=1}^n \mathcal{H}_{i_l})}. \quad (3.9)$$

For the $S = 1/2$ Heisenberg model the traces in Eqs. (3.8,3.9) can be calculated analytically. Then a random walk in the C_n -space can be constructed in various ways [55, 56] and the average value of $A(C_n)$ can be estimated over the sequences occurring in a realization of the defined walk.

For spins larger than $S = 1/2$ the evaluation of the traces is not possible and the original formulation of the Handscomb's scheme outlined above cannot be used.

3.2 Stochastic Series Expansion

Based on the Handscomb's approach, Sandvik proposed a simulation scheme which is applicable to spin systems with arbitrary spins [15].

Here the Hamiltonian is decomposed into a sum of bond Hamiltonians:

$$\mathcal{H} = \sum_{b=1}^B \mathcal{H}_b, \quad (3.10)$$

where

$$b = \langle i(b), j(b) \rangle, \quad (3.11)$$

denotes one of the B bonds connecting lattice sites $i(b)$ and $j(b)$.

In order to avoid difficulties in calculating the traces which plague Handscomb's approach, Sandvik suggested to choose a representation with basis vectors $\{|\alpha\rangle\}$ such that \mathcal{H}_b operating on a basis vector gives either zero or a basis vector

$$\mathcal{H}_b|\alpha\rangle \sim |\alpha'\rangle, \quad |\alpha\rangle, |\alpha'\rangle \in \{|\alpha\rangle\}. \quad (3.12)$$

In this basis the density matrix $e^{-\beta\mathcal{H}}$ is expanded in a Taylor series and the trace in partition function (3.3) is written as a sum over diagonal matrix elements

$$Z = \sum_{n=0}^{\infty} \sum_{\{S_n\}} \sum_{\alpha} \frac{(-\beta)^n}{n!} \langle \alpha | \prod_{p=1}^n \mathcal{H}_{b_p} | \alpha \rangle, \quad (3.13)$$

where S_n denotes any concatenation $\prod_{p=1}^n \mathcal{H}_{b_p}$ of n bond Hamiltonians, also called operator string. The thermal expectation value of an operator \mathcal{A} is now given by

$$\langle \mathcal{A} \rangle = \frac{1}{Z} \sum_{n=0}^{\infty} \sum_{\{S_n\}} \sum_{\alpha} \frac{(-\beta)^n}{n!} \langle \alpha | \mathcal{A} \prod_{p=1}^n \mathcal{H}_{b_p} | \alpha \rangle. \quad (3.14)$$

This average is estimated through importance sampling in a combined space of basis vectors $|\alpha\rangle$ and index sequences S_n .

The original implementation of the Stochastic Series Expansion has been further developed, e.g. by introducing the operator-loop update [57].

3.3 ALPS

ALPS (Algorithms and Libraries for Physics Simulations) is an international open-source software project focused on development of programs and libraries for the simulation of strongly correlated quantum lattice models [58]. The aim of the project is to provide non-experts in the field of numerical simulation with most important algorithms like classical and quantum Monte Carlo and density matrix renormalization group.

The user of ALPS is provided with a standardized file where the parameters of the system and of the method can be chosen. Lattices and models are defined in separate files using a XML syntax.

In the present work we have performed quantum Monte Carlo calculations using the Stochastic Series Expansion routine `sse` from the ALPS package [59]. The simulations were performed on a nearest-neighbor Heisenberg antiferromagnet on two-dimensional 24×24 square and hexagonal lattices. We present the results for magnetization curves, uniform susceptibility and specific heat in Chap. 6.

Chapter 4

Representing spin operators in terms of canonical bosons

Having summarized the main ideas of the spin-wave theory in the last section of the Chap. 2, we substantiate them with a more formal approach in this chapter. In Sec. 4.1 we recapitulate the Dyson-Maleev representation which is extended to the case of non-collinear spin configurations in Sec. 4.2. In Sec. 4.3 we give a few remarks on another way of performing the spin-wave expansion, the Holstein-Primakoff formalism. We close this chapter with a short presentation of a Schwinger-Boson approach, which is suitable for both ordered and symmetric phase.

Spin-wave theory is a subject of many excellent textbooks on magnetism [60, 34], so we do not dwell into detail in this chapter.

4.1 Ordered state: Dyson-Maleev bosons

In the broken-symmetry phase of the quantum Heisenberg model one of the components of the spin operators has a finite expectation value. It is therefore natural to seek for a spin representation which describes the quantum fluctuations around the classical expectation value of the spin.

Dyson [22] and Maleev [24] independently proposed a mapping of the spin operators onto bosons. The resulting bosonic degrees of freedom can be identified as *magnons* or *spin waves* [60]. As we will show explicitly in the subsequent section, the spin Hamiltonian can be transformed to a general bosonic Hamiltonian

$$\mathcal{H}^{\text{DM}} = E_{\text{cl}} + \sum_{\nu=1}^6 \mathcal{H}_{\nu}^{\text{DM}}, \quad (4.1)$$

where \mathcal{H}_{ν} is a term containing ν canonical boson operators. In the case of a ferromag-

net the classical ground state energy E_{cl} is equal to the exact ground state energy. For an antiferromagnet it is just a lowest order spin-wave approximation to the exact value. The terms up to \mathcal{H}_2 are part of the noninteracting Hamiltonian, which can be mapped to a system of harmonic oscillators through an adequate canonical transformation. Higher order terms introduce interactions between bosons. These terms can be treated perturbatively, which is formally justified by the fact that Eq. (4.1) is an expansion in powers of $S^{-1/2}$

$$\mathcal{H}_\nu^{\text{DM}} \sim S^{2-\nu/2}. \quad (4.2)$$

Following Dyson [22], the magnon-magnon interactions are often called *dynamic* interactions in the literature.

However, another type of interaction results from the mapping of the spin component operators to a boson operator b . The Fock space of the bosons is infinite-dimensional, while the physical spin subspace is spanned by the states

$$\{|n\rangle\}_S = \{|0\rangle, |1\rangle, |2\rangle, \dots, |2S\rangle\}, \quad (4.3)$$

with

$$b^\dagger b |n\rangle = n |n\rangle. \quad (4.4)$$

The unphysical states with $n > 2S$ can be eliminated by appropriate projection operators. Dyson was first to point out that the introduction of the projection operators corresponds to an additional interaction between magnons which he called *kinematic* interaction [22]. Dyson also rigorously proved that kinematic interactions can be neglected in a three-dimensional quantum Heisenberg ferromagnet [22]. The problem of kinematic interactions is very complex and has not been completely tackled for lower dimensions or other types of ordering mechanisms. One usually ignores the effect of kinematical interactions, although efforts have been made to take it into account by imposing constraints on the magnon occupation number [61]. We will follow the common procedure and neglect the kinematic interaction throughout this work.

4.2 Spin-waves in non-collinear spin configurations

We extend the idea of the spin-wave expansion to the general case of the Heisenberg magnet in the presence of an external magnetic field and briefly discuss the corresponding classical ground state.

4.2.1 General bosonic Hamiltonian

In this section we treat a general Heisenberg magnet in the presence of an arbitrary magnetic field. As a result we obtain the full Dyson-Maleev bosonic Hamiltonian in coordinate space.

Consider the Heisenberg Hamiltonian

$$\mathcal{H} = \frac{1}{2} \sum_{i,j} J_{ij} \mathbf{S}_i \cdot \mathbf{S}_j - g\mu_B \sum_i \mathbf{B}_i \cdot \mathbf{S}_i, \quad (4.5)$$

where the sums are over all N sites \mathbf{r}_i of a D -dimensional lattice, and the \mathbf{S}_i are spin- S operators. For the time being, we do not impose any constraints on the exchange couplings $J_{ij} = J(\mathbf{r}_i, \mathbf{r}_j)$. The inhomogeneous magnetic field \mathbf{B}_i couples to the spins via the second term in the Hamiltonian (4.5), which is the Zeeman energy with the gyromagnetic factor g and the Bohr magneton μ_B .

In the following we formulate the problem in a coordinate-free vector notation which was introduced by Schütz et al. [62] in the context of persistent spin currents in mesoscopic Heisenberg rings and was further developed in Ref. [63].

Assume that the external magnetic field induces a permanent magnetic dipole moment at site i

$$\mathbf{m}_i = g\mu_B \langle \mathbf{S}_i \rangle, \quad (4.6)$$

where $\langle \cdot \rangle$ denotes the thermal average. It is then convenient to decompose the spin operators into the components of a rotating local coordinate system

$$\mathbf{S}_i = S_i^\parallel \hat{\mathbf{m}}_i + \mathbf{S}_i^\perp, \quad (4.7)$$

with the unit vector

$$\hat{\mathbf{m}}_i = \frac{\mathbf{m}_i}{|\mathbf{m}_i|} \quad (4.8)$$

setting the direction of the longitudinal fluctuations. Next, we supplement $\hat{\mathbf{m}}_i$ by two additional unit vectors $\hat{\mathbf{e}}_i^1$ and $\hat{\mathbf{e}}_i^2$ such that $\{\hat{\mathbf{e}}_i^1, \hat{\mathbf{e}}_i^2, \hat{\mathbf{m}}_i\}$ forms a right-handed orthonormal triad. There is a local gauge freedom in the choice of the transversal basis; the vectors $\hat{\mathbf{e}}_i^1$ and $\hat{\mathbf{e}}_i^2$ can be arbitrarily rotated around $\hat{\mathbf{m}}_i$. By defining the corresponding spherical basis vectors

$$\mathbf{e}_i^p = \hat{\mathbf{e}}_i^1 + ip\hat{\mathbf{e}}_i^2, \quad p = \pm, \quad (4.9)$$

we can expand the transverse component of the spin operator \mathbf{S}_i in this basis:

$$\mathbf{S}_i^\perp = \frac{1}{2} \sum_{p=\pm} S_i^{-p} \mathbf{e}_i^p. \quad (4.10)$$

Substituting the decompositions (4.7) and (4.10) into Eq. (4.5) yields:

$$\mathcal{H} = \mathcal{H}^\parallel + \mathcal{H}^\perp + \mathcal{H}', \quad (4.11)$$

where

$$\mathcal{H}^{\parallel} = \frac{1}{2} \sum_{i,j} J_{ij} \hat{\mathbf{m}}_i \cdot \hat{\mathbf{m}}_j S_i^{\parallel} S_j^{\parallel} - \sum_i \mathbf{H}_i \cdot \hat{\mathbf{m}}_i S_i^{\parallel}, \quad (4.12)$$

$$\mathcal{H}^{\perp} = \frac{1}{2} \sum_{i,j} J_{ij} \mathbf{S}_i^{\perp} \cdot \mathbf{S}_j^{\perp} \quad (4.13)$$

$$= \frac{1}{8} \sum_{i,j} \sum_{p,p'} J_{ij} (\mathbf{e}_i^p \cdot \mathbf{e}_j^{p'}) S_i^{-p} S_j^{-p'}, \quad (4.14)$$

$$\mathcal{H}' = - \sum_i \mathbf{S}_i^{\perp} \cdot (\mathbf{H}_i - \sum_j J_{ij} S_j^{\parallel} \hat{\mathbf{m}}_j), \quad (4.15)$$

with

$$\mathbf{H}_i = g\mu_B \mathbf{B}_i. \quad (4.16)$$

The part \mathcal{H}' of the Hamiltonian describes the coupling between transverse and longitudinal spin fluctuations generated by the external magnetic field.

Now we expand the spin operators in terms of canonical boson operators via a Dyson-Maleev transformation in the local frame:

$$S_i^{\parallel} = S - n_i, \quad (4.17a)$$

$$S_i^{-} = \sqrt{2S} \left[1 - \frac{n_i}{(2S)} \right] b_i, \quad (4.17b)$$

$$S_i^{+} = \sqrt{2S} b_i^{\dagger}, \quad (4.17c)$$

where

$$n_i = b_i^{\dagger} b_i \quad (4.18)$$

is the boson occupation number operator. Note that the Dyson-Maleev transformation for the Heisenberg antiferromagnet is not unique. For collinear spin configurations an alternative version with $S_j^{-} = \sqrt{2S} b_j$ and $S_i^{+} = \sqrt{2S} b_j^{\dagger} [1 - n_j/(2S)]$ on the other sublattice is more convenient, because the three-body term in the Hamiltonian is removed [64]. However, physical results do not depend on this choice.

Now the spin Hamiltonian (4.5) can be expanded in powers of the inverse spin, see Eq. (4.1). The classical ground state energy is given by

$$E_{\text{cl}} = \frac{S^2}{2} \sum_{ij} J_{ij} \hat{\mathbf{m}}_i \cdot \hat{\mathbf{m}}_j - S \sum_i \mathbf{H}_i \cdot \hat{\mathbf{m}}_i, \quad (4.19)$$

and the following terms contribute to the bosonic Hamiltonian (4.1):

$$\mathcal{H}'_1 = -\frac{\sqrt{2S}}{2} \sum_i \left(b_i^\dagger \mathbf{e}_i^+ + b_i \mathbf{e}_i^- \right) \cdot \left(\mathbf{H}_i - S \sum_j J_{ij} \hat{\mathbf{m}}_j \right), \quad (4.20)$$

$$\mathcal{H}_2^\parallel = -\frac{S}{2} \sum_{ij} J_{ij} \hat{\mathbf{m}}_i \cdot \hat{\mathbf{m}}_j (n_i + n_j) + \sum_i \mathbf{H}_i \cdot \hat{\mathbf{m}}_i n_i, \quad (4.21)$$

$$\begin{aligned} \mathcal{H}_2^\perp = \frac{S}{4} \sum_{ij} J_{ij} [& (\mathbf{e}_i^+ \cdot \mathbf{e}_j^-) b_i^\dagger b_j + (\mathbf{e}_i^- \cdot \mathbf{e}_j^+) b_j^\dagger b_i \\ & + (\mathbf{e}_i^+ \cdot \mathbf{e}_j^+) b_i^\dagger b_j^\dagger + (\mathbf{e}_i^- \cdot \mathbf{e}_j^-) b_j b_i], \end{aligned} \quad (4.22)$$

$$\begin{aligned} \mathcal{H}'_3 = & -\frac{1}{2\sqrt{2S}} \sum_i n_i b_i \mathbf{e}_i^+ \cdot \left(\mathbf{H}_i - S \sum_j J_{ij} \hat{\mathbf{m}}_j \right) \\ & -\frac{\sqrt{2S}}{2} \sum_j J_{ij} \left(b_i^\dagger \mathbf{e}_i^+ + b_i \mathbf{e}_i^- \right) \cdot \hat{\mathbf{m}}_j n_j, \end{aligned} \quad (4.23)$$

$$\mathcal{H}_4^\parallel = \frac{1}{2} \sum_{ij} J_{ij} \hat{\mathbf{m}}_i \cdot \hat{\mathbf{m}}_j n_i n_j, \quad (4.24)$$

$$\begin{aligned} \mathcal{H}_4^\perp = & -\frac{1}{8} \sum_{ij} J_{ij} [(\mathbf{e}_i^+ \cdot \mathbf{e}_j^-) b_j^\dagger n_i b_i + (\mathbf{e}_i^- \cdot \mathbf{e}_j^+) b_i^\dagger n_j b_j \\ & + (\mathbf{e}_i^+ \cdot \mathbf{e}_j^+) (n_j b_j b_i + n_i b_i b_j)], \end{aligned} \quad (4.25)$$

$$\mathcal{H}'_5 = -\frac{1}{2\sqrt{2S}} \sum_{ij} J_{ij} (\mathbf{e}_i^- \cdot \hat{\mathbf{m}}_j) n_j n_i b_i, \quad (4.26)$$

$$\mathcal{H}_6^\perp = \frac{1}{16S} \sum_{ij} J_{ij} (\mathbf{e}_i^- \cdot \mathbf{e}_j^-) n_i b_i n_j b_j. \quad (4.27)$$

Note that the bosonic Hamiltonian \mathcal{H} is not hermitian. However, one can use the standard many-body-methods as long as the assumption that the Hamiltonian is hermitian does not enter the calculations. So far, no approximations besides neglecting kinematic interactions were made. In Chap. 5 we use the results of this section in the simple case of collinear spin configurations. In Chap. 6 we apply the formalism to the antiferromagnet in the presence of a uniform external magnetic field.

4.2.2 Classical ground state

In this section we consider the classical ground state of the general Heisenberg magnet (4.5) in the presence of an external magnetic field.

In the classical limit $S \rightarrow \infty$ and $J_{i,j} S^2 \rightarrow \text{const}$, the transverse part of the spins vanishes and the quantum spin operators can be replaced with classical vectors in the

direction of $\hat{\mathbf{m}}_i$:

$$\mathbf{S}_i \rightarrow S\hat{\mathbf{m}}_i \quad (4.28)$$

In order to find a configuration $\{\hat{\mathbf{m}}_i\}$ that characterizes the classical ground state we have to minimize the classical ground state energy E_{cl} given in Eq. (4.19). Together with the normalization constraint $\hat{\mathbf{m}}_i^2 = 1$ this leads to the condition

$$\hat{\mathbf{m}}_i \times \left(\mathbf{H}_i - S \sum_j J_{ij} \hat{\mathbf{m}}_j \right) = 0. \quad (4.29)$$

For given \mathbf{H}_i and J_{ij} , this is a system of non-linear equations for the spin directions $\hat{\mathbf{m}}_i$ in the classical ground state. As expected, Eq. (4.29) states that the classical spins align parallel to the sum of external and exchange field.

Let us now have a look at the expression (4.20) for the one-boson part \mathcal{H}'_1 of the Dyson-Maleev Hamiltonian (4.1). From the condition for the minimum of the classical ground state energy, Eq. (4.29), it follows that \mathcal{H}'_1 is proportional to the sum of the scalar products of the type

$$\mathbf{e}_i^\pm \cdot \hat{\mathbf{m}}_i = 0. \quad (4.30)$$

Basis vectors \mathbf{e}_i^\pm and $\hat{\mathbf{m}}_i$ are orthogonal by construction. Therefore, the contribution to \mathcal{H} linear in bosons vanishes

$$\mathcal{H}'_1 = 0. \quad (4.31)$$

Note that the part \mathcal{H}'_1 vanishes only when we consider fluctuations around the classical ground state. If one takes into account the “true” instead of the classical canting angle, \mathcal{H}'_1 is finite [31, 65].

4.3 Holstein-Primakoff bosons

A different transformation was introduced by Holstein and Primakoff [49]

$$S_i^\parallel = S - n_i, \quad (4.32a)$$

$$S_i^- = \sqrt{2S - n_i} b_i, \quad (4.32b)$$

$$S_i^+ = b_i^\dagger \sqrt{2S - n_i}, \quad (4.32c)$$

where n_i is given in Eq. (4.18). The square roots can be expanded in powers of $1/S$

$$\sqrt{2S - n_i} = \sqrt{2S} \left[1 - \frac{n_i}{4S} - \frac{n_i^2}{32S^2} - \mathcal{O}\left(\frac{1}{S^3}\right) \right], \quad (4.33)$$

which is expansion in spin fluctuations around the direction of the classical spin.

In this formalism the spin Hamiltonian is mapped to a boson Hamiltonian con-

taining an infinite number of terms

$$\mathcal{H}^{\text{HP}} = E_{\text{cl}} + \sum_{\nu=1}^{\infty} \mathcal{H}_{\nu}^{\text{HP}}, \quad (4.34)$$

where \mathcal{H}_{ν} are sorted by powers of inverse spin similar to Eq. (4.2). In explicit calculations the Holstein-Primakoff Hamiltonian (4.34) has to be truncated appropriately. The truncation of the Hamiltonian couples the physical with the unphysical subspaces. In other words, it gives rise to the kinematic interaction.

Note that the lowest-order terms of the Dyson-Maleev and the Holstein-Primakoff Hamiltonian are related through simple equalities

$$\mathcal{H}_1^{\text{HP}} = \mathcal{H}_1^{\text{DM}}, \quad (4.35)$$

$$\mathcal{H}_2^{\text{HP}} = \mathcal{H}_2^{\text{DM}}, \quad (4.36)$$

$$\mathcal{H}_3^{\text{HP}} = \frac{1}{2} \left[\mathcal{H}_3^{\text{DM}} + (\mathcal{H}_3^{\text{DM}})^{\dagger} \right], \quad (4.37)$$

$$\mathcal{H}_4^{\text{HP}} = \frac{1}{2} \left[\mathcal{H}_4^{\text{DM}} + (\mathcal{H}_4^{\text{DM}})^{\dagger} \right]. \quad (4.38)$$

At the level of linear spin-wave theory the two approaches are therefore equivalent. We will use the Dyson-Maleev formalism throughout this work.

4.4 Schwinger bosons

The vacuum state of the Dyson-Maleev or Holstein-Primakoff bosons is a broken-symmetry state. These approaches are therefore suitable for the description of the fluctuations around the magnetically ordered state. In the Schwinger boson representation which was first used for the evaluation of the Clebsch-Gordan coefficients [66] the spin rotational invariance of the Hamiltonian is manifest. The long-range order is equivalent to the condensation of the Schwinger bosons. Thus, the Schwinger boson approach can address both the ordered and the symmetric state.

In the Schwinger boson representation a spin operator is written in terms of two boson operators b_+ , b_-

$$S_i^{\parallel} = \frac{1}{2} \left(b_{i+}^{\dagger} b_{i+} - b_{i-}^{\dagger} b_{i-} \right), \quad (4.39a)$$

$$S_i^{-} = b_{i-}^{\dagger} b_{i+}, \quad (4.39b)$$

$$S_i^{+} = b_{i+}^{\dagger} b_{i-}, \quad (4.39c)$$

with the local constraints on their Fock space

$$\sum_{\sigma=\pm} b_{i\sigma}^\dagger b_{i\sigma} = 2S, \quad (4.40)$$

which project out the unphysical states and thus eliminate the kinematic interactions.

Using the representation (4.39), the spin Hamiltonian is mapped onto an interacting boson Hamiltonian, which can be approximated within mean-field theory. This approach was introduced by Arovas and Auerbach in the context of low-dimensional Heisenberg magnets [18]. We do not go further into the details of this method; a very good introduction is given in the book by Auerbach [34].

Let us close our short foray into the Schwinger boson representation with a comparison with the Holstein-Primakoff boson representation. Using the constraint (4.40) we can eliminate the b_+ boson and obtain the relation:

$$\begin{array}{ll} \text{Schwinger boson} & \text{Holstein - Primakoff boson} \\ b_- & \leftrightarrow b \\ b_+ & \leftrightarrow \sqrt{2S - b^\dagger b}. \end{array} \quad (4.41)$$

This correspondence shows explicitly that Schwinger bosons provide a symmetric representation in the spin space, while Holstein-Primakoff (and Dyson-Maleev) bosons single out the S^\parallel direction.

Chapter 5

Spin-wave theory at constant order parameter

In low-dimensional magnets without long-range magnetic order the conventional spin-wave approach described in Chap. 4 is not applicable, because it relies on the existence of long-range magnetic order. Nevertheless, even in the absence of long-range magnetic order the low-energy excitations of many magnetic materials can be described as renormalized spin-waves as long as their wavelength is much shorter than the correlation length [67].

For example, in two-dimensional quantum Heisenberg ferromagnets [68] and antiferromagnets [17] at low but finite temperatures, where the order parameter correlation length ξ is exponentially large, spin-waves with wave vectors $|\mathbf{k}| \gg \xi^{-1}$ are well-defined elementary excitations [64]. Other examples for systems where the low-energy physics is dominated by elementary excitations of the spin-wave type are Haldane gap antiferromagnets and one-dimensional Heisenberg ferromagnets with arbitrary spin.

To study the low-temperature properties of these systems, several methods have been proposed. The Schwinger-boson mean-field theory introduced by Arovas and Auerbach [18] manifestly takes the spin-rotational invariance of the disordered phase into account. However, going beyond the mean-field approximation within the Schwinger boson approach has turned out to be quite difficult [69]. At the mean field level the modified spin-wave theory proposed by Takahashi [19] is an alternative to the Schwinger-boson approach. Up to numerical prefactors, the modified spin-wave theory yields results which are identical with the predictions of Schwinger boson mean field theory [18]. However, also within the modified spin-wave theory it is difficult to go beyond the mean-field analysis and for complex magnetic systems the approach is plagued by ambiguities, as we shall discuss in Sec. 5.1.1.

We propose in this chapter a method based on a conventional spin-wave expansion where the thermodynamic calculations are performed at constant order parameter. In Sec. 5.1 we set up the formalism. In Sec. 5.2 we recapitulate the spin-wave theory for

a Heisenberg ferromagnet and perturbatively treat the interactions between magnons up to second order. The low-temperature thermodynamic behavior for $D = 1, 2, 3$ ferromagnets is presented in Sec. 5.3.

5.1 Thermodynamics at constant order parameter

In this section we discuss the calculation of thermodynamic variables at constant order parameter. We derive general equations of state and discuss the role of the external field.

5.1.1 Thermodynamic potentials and equations of state

Although the method developed here is valid for a variety of systems with order parameter \mathcal{M} and corresponding conjugate field H , we shall in the following focus on the Heisenberg magnet with the zero-field Hamiltonian

$$\mathcal{H} = \frac{1}{2} \sum_{i,j} J_{ij} \mathbf{S}_i \cdot \mathbf{S}_j . \quad (5.1)$$

where the sum runs over all sites \mathbf{r}_i of a D -dimensional lattice with N sites and $J_{ij} = J(\mathbf{r}_i, \mathbf{r}_j)$ are the exchange integrals. We assume periodic boundary conditions for simplicity. In order to keep this section as general as possible we do not impose any further restrictions on the exchange couplings and the topology of the lattice. Note that we use calligraphic letters for \mathcal{M} and \mathcal{H} in order to stress the fact that they are operators.

Let us first recall some elementary thermodynamics, see for example Ref. [45]. If we fix the field H and the temperature T , thermodynamic observables can be obtained from the Helmholtz free energy

$$F(H) = -T \ln \text{Tr} \left[e^{-(\mathcal{H} - H\mathcal{M})/T} \right] , \quad (5.2)$$

where the dependence on T is suppressed for brevity and the Boltzmann constant is set to unity. The order parameter is thus given by

$$M(H) = \langle \mathcal{M} \rangle = - \frac{\partial F(H)}{\partial H} , \quad (5.3)$$

where $\langle \cdot \rangle$ denotes the thermal expectation value.

Alternatively, we may choose to fix the order parameter M and adjust the conjugated field H appropriately. The corresponding thermodynamic potential is the Gibbs free energy $G(M)$, which is related to the Helmholtz free energy via a Legen-

dre transformation

$$\begin{aligned} G(M) &= MH(M) + F(H(M)) \\ &= -T \ln \text{Tr} \left[e^{-[\mathcal{H} - H(\mathcal{M} - M)]/T} \right], \end{aligned} \quad (5.4)$$

where the function $H(M)$ should be obtained from Eq. (5.3). From $G(M)$ we obtain the equation of state in the form

$$H = H(M) \quad (5.5)$$

via the reciprocity relation

$$H(M) = \frac{\partial G(M)}{\partial M}. \quad (5.6)$$

The equilibrium order parameter for vanishing field is thus a local extremum of $G(M)$. If the system has a finite spontaneous order parameter

$$M_0 = \lim_{H \rightarrow 0^+} M(H), \quad (5.7)$$

then the generic behavior of $G(M)$ is [70]

$$G(M) = \begin{cases} G(M_0) + \frac{(M - M_0)^2}{2\chi} + \mathcal{O}[(M - M_0)^3] & \text{for } |M| \geq M_0, \\ G(M_0) & \text{for } |M| < M_0. \end{cases} \quad (5.8)$$

Here

$$\chi^{-1} = \left. \frac{\partial H(M)}{\partial M} \right|_{M_0} = \left. \frac{\partial^2 G(M)}{\partial M^2} \right|_{M_0} \quad (5.9)$$

is the inverse longitudinal susceptibility. These expressions are also valid in the absence of spontaneous symmetry breaking, where $M_0 = 0$. Note that in general $G(M) = G(-M)$, because the spectrum of \mathcal{M} is symmetric with respect to the origin.

The zero-temperature version of the method outlined above has been used previously by Georges and Yedidia to study spontaneous symmetry breaking in the ground state of the Hubbard model [71]. Note that in the limit $T \rightarrow 0$ Eq. (5.4) can be written as

$$G(M) = \langle 0 | \mathcal{G}(M) | 0 \rangle, \quad (5.10)$$

where $|0\rangle$ is the ground state of the “free-energy operator”

$$\mathcal{G}(M) = \mathcal{H} - H(M)[\mathcal{M} - M]. \quad (5.11)$$

As shown in Ref. [71], the expansion at constant order parameter is advantageous for

the calculation of corrections to the mean field approximation. This idea has been successfully applied to a one-dimensional Hubbard model with next-nearest neighbor hopping by Zedler and Kopietz [72].

The parameter $H(M)$ in Eq. (5.4) can be viewed as a Lagrange multiplier which enforces the condition of constant magnetization. The idea of imposing a constraint on the magnetization of low-dimensional magnets was first introduced by Takahashi in the context of the so-called modified spin-wave theory for the Heisenberg ferromagnet [19, 20]. Recently, Takahashi's modified spin-wave theory has also been applied to more complex problems, such as frustrated magnets [73], disordered magnets [74], or magnetic molecular clusters [75]. However, the modified spin-wave theory has several shortcomings:

1. it is very difficult to systematically calculate corrections due to interactions between spin-waves,
2. the absence of long-range magnetic order is not obtained as a result, i.e. the magnetization is set to zero by hand. This leads to some arbitrariness in the choice of the constraint if the method is applied to systems with more complicated magnetic order, such as ferrimagnets [76].

In the rest of this chapter we will show that this problems can be resolved within conventional spin-wave expansion by performing the calculations at constant order parameter. References to the results of Takahashi's modified spin-wave theory will be given when appropriate.

5.1.2 Conjugate field

In this section we discuss a Heisenberg magnet in the presence of a weak symmetry breaking field. In the following we make use of the general results from Sec. 4.2.1.

Consider the Heisenberg Hamiltonian

$$\mathcal{H} = \frac{1}{2} \sum_{i,j} J_{ij} \mathbf{S}_i \cdot \mathbf{S}_j - \sum_i \mathbf{H}_i \cdot \mathbf{S}_i, \quad (5.12)$$

where a weak conjugate field \mathbf{H}_i is imposed that uniquely defines the order parameter.

In the classical ground state the spins of the Heisenberg model assume a collinear configuration, i. e. the longitudinal components $\hat{\mathbf{m}}_i$ fulfill the simple relation

$$\hat{\mathbf{m}}_i \times \hat{\mathbf{m}}_j = 0 \quad , \quad \text{for all } i, j. \quad (5.13)$$

Therefore, the general condition for the ground state configuration (4.29) simplifies to

$$\mathbf{H}_i \times \hat{\mathbf{m}}_j = 0 \quad , \quad \text{for all } i, j. \quad (5.14)$$

From Eq. (5.14) follows directly for all i, j

$$\mathbf{H}_i \cdot \mathbf{S}_j^\perp = 0, \quad (5.15)$$

$$\hat{\mathbf{m}}_i \cdot \mathbf{S}_j^\perp = 0, \quad (5.16)$$

where the transverse spin component is given by Eq. (4.10). Hence, the term \mathcal{H}' denoting the coupling between transverse and longitudinal spin fluctuations vanishes, as it follows from Eq. (4.15). Now we can decompose the Hamiltonian (5.12) into

$$\mathcal{H} = \mathcal{H}^\parallel + \mathcal{H}^\perp, \quad (5.17)$$

where the longitudinal and transverse part are given by Eqs. (4.12) and (4.14), respectively. Eqs. (4.21, 4.24) and (4.22, 4.25, 4.27) are the corresponding terms of the Dyson-Maleev Hamiltonian. We do not further evaluate the spin-wave Hamiltonian in this section.

5.2 Spin waves in a Heisenberg ferromagnet

For a ferromagnet the corresponding magnetic order parameter is the uniform magnetization and the conjugate field is the uniform magnetic field. The ferromagnetic Hamiltonian is rotational invariant. We are therefore completely free in our choice of the direction of the symmetry-breaking field. Traditionally, the uniform field defines the z direction

$$\mathbf{H}_i = H \hat{\mathbf{e}}_z. \quad (5.18)$$

To keep things simple we set the exchange integrals to constants and let them couple only nearest next-neighbors on a D -dimensional hypercubic lattice

$$J_{i,j} = \begin{cases} J < 0 & , \text{ for } i, j \text{ next neighbors,} \\ 0 & , \text{ else.} \end{cases} \quad (5.19)$$

5.2.1 Classical ground state

The classical ground state configuration is simply

$$\hat{\mathbf{m}}_i = \hat{\mathbf{e}}_z, \quad (5.20)$$

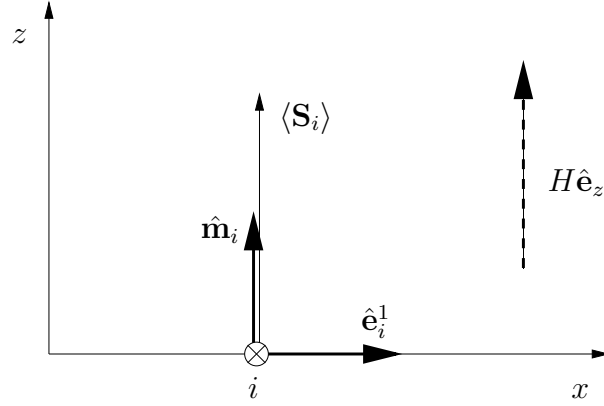


Figure 5.1: Spin configuration on an arbitrary lattice site i in the classical ground state of the Heisenberg ferromagnet. The dashed arrow represents a uniform magnetic field $H\hat{e}_z$ in the z direction. The small solid arrows represent the vectors of the local basis that matches the direction defined by the local magnetization $\langle \mathbf{S}_i \rangle$. Not shown is the basis vector $\hat{e}_i^2 = \hat{e}_y$ which points into the plane of the paper.

i.e. all spin vectors align parallel to the uniform magnetic field, as shown in Fig. 5.1. We complete the local basis set with the unit vectors:

$$\hat{e}_i^1 = \hat{e}_x, \quad (5.21a)$$

$$\hat{e}_i^2 = \hat{e}_y, \quad (5.21b)$$

which is a formal expression of the fact that in the ferromagnetic spin configuration the local and the laboratory bases coincide. This is a trivial example of the general ideas presented in Sec. 4.2.

The relevant scalar products in the basis (5.20, 5.21) are for all i, j

$$\hat{\mathbf{m}}_i \cdot \hat{\mathbf{m}}_j = 1, \quad (5.22)$$

$$\hat{\mathbf{m}}_i \cdot \mathbf{H}_j = H \quad (5.23)$$

$$\mathbf{e}_i^p \cdot \mathbf{e}_j^{p'} = 2\delta_{p,-p'}. \quad (5.24)$$

The classical ground state energy (4.19) thus yields

$$E_{\text{cl}} = -|\tilde{J}_0|NS^2 \left(\frac{1}{2} + h \right), \quad (5.25)$$

with the dimensionless uniform field

$$h \equiv \frac{H}{|\tilde{J}_0|S}. \quad (5.26)$$

and

$$\tilde{J}_0 \equiv 2DJ . \quad (5.27)$$

In Sec. 5.2.2 we focus on the non-interacting case, whereas in Secs. 5.2.4 and 5.2.5 the dynamic interactions between Dyson-Maleev bosons are treated perturbatively.

5.2.2 Linear spin-wave theory

The one-body Hamiltonian given by Eqs. (4.21, 4.22) simplifies substantially in the basis (5.20, 5.21)

$$\mathcal{H}_2 = \frac{|J|S}{2} \sum_{ij} (b_i^\dagger - b_j^\dagger)(b_i - b_j) + H \sum_i n_i . \quad (5.28)$$

In order to diagonalize \mathcal{H}_2 we perform the Fourier transformation of the boson operators [60]

$$b_i = \frac{1}{\sqrt{N}} \sum_{\mathbf{k}} e^{i\mathbf{k} \cdot \mathbf{r}_i} b_{\mathbf{k}} , \quad (5.29)$$

where the sum runs over all N wave-vectors of the first Brillouin zone. The Hamiltonian \mathcal{H}_2 is diagonal in reciprocal space

$$\mathcal{H}_2 = |\tilde{J}_0|S \sum_{\mathbf{k}} (\epsilon_{\mathbf{k}} + h) b_{\mathbf{k}}^\dagger b_{\mathbf{k}} , \quad (5.30)$$

with the dimensionless energy dispersion

$$\epsilon_{\mathbf{k}} = 1 - \gamma_{\mathbf{k}} . \quad (5.31)$$

The information on the geometry of the underlying D -dimensional hypercubic lattice is summarized in the structure factor

$$\gamma_{\mathbf{k}} = \frac{1}{D} \sum_{\mu=1}^D \cos(\mathbf{k} \cdot \mathbf{a}_\mu) , \quad (5.32)$$

where \mathbf{a}_μ are the primitive lattice vectors. The low-temperature properties are determined by the behavior at long wavelengths, hence we expand the structure factor for small wave vectors \mathbf{k}

$$\gamma_{\mathbf{k}} = 1 - \frac{(ka)^2}{2D} + \mathcal{O}((ka)^4) , \quad (5.33)$$

where we assume for the lattice spacings

$$a = |\mathbf{a}_\mu| \quad (5.34)$$

and herewith

$$k = |\mathbf{k}|. \quad (5.35)$$

The thermodynamics of the diagonal Hamiltonian (5.30) is very simple; it is equivalent to the standard textbook problem of free bosons on a lattice [77]. The corresponding Helmholtz free energy is

$$F^{(0)}(h) = E_{\text{cl}} + T \sum_{\mathbf{k}} \ln \left[1 - e^{-|\tilde{J}_0|S(\epsilon_{\mathbf{k}}+h)/T} \right]. \quad (5.36)$$

We use the superscript (0) to remind that this is a zeroth order result in terms of perturbation theory. From Eq. (5.3) we then obtain the usual spin-wave result for the magnetization

$$M(h) = NS - \sum_{\mathbf{k}} n_{\mathbf{k}}, \quad (5.37)$$

with the occupation number for free bosons:

$$n_{\mathbf{k}} = \left[e^{|\tilde{J}_0|S(\epsilon_{\mathbf{k}}+h)/T} - 1 \right]^{-1}. \quad (5.38)$$

5.2.3 Dyson-Maleev Vertex

Within the Dyson-Maleev formalism the dynamical spin-wave interactions are contained in the two-body interaction term

$$\mathcal{H}_4 = -\frac{|J|}{2} \sum_{ij} b_i^\dagger b_j^\dagger \left[b_i b_j - \frac{1}{2}(b_i^2 + b_j^2) \right]. \quad (5.39)$$

This expression follows from Eqs. (4.24, 4.25) in the special basis (5.20, 5.21). The three body term (4.27) does not contribute.

Performing the Fourier transformation (5.29) on canonical boson operators, we obtain

$$\mathcal{H}_4 = \frac{|\tilde{J}_0|}{2N} \sum_{\mathbf{k}'_1, \mathbf{k}'_2, \mathbf{k}_1, \mathbf{k}_2} \delta_{\mathbf{k}'_1 + \mathbf{k}'_2, \mathbf{k}_1 + \mathbf{k}_2} V(\mathbf{k}'_1, \mathbf{k}'_2; \mathbf{k}_1, \mathbf{k}_2) b_{\mathbf{k}'_1}^\dagger b_{\mathbf{k}'_2}^\dagger b_{\mathbf{k}_2} b_{\mathbf{k}_1}, \quad (5.40)$$

where $\delta_{\mathbf{k}, \mathbf{k}'}$ is the Kronecker delta. The Dyson-Maleev vertex can be written as:

$$V(\mathbf{k}'_1, \mathbf{k}'_2; \mathbf{k}_1, \mathbf{k}_2) = -\frac{1}{4} [\gamma_{\mathbf{k}_1 - \mathbf{k}'_1} + \gamma_{\mathbf{k}_1 - \mathbf{k}'_2} + \gamma_{\mathbf{k}_2 - \mathbf{k}'_1} + \gamma_{\mathbf{k}_2 - \mathbf{k}'_2} - 2\gamma_{\mathbf{k}'_1} - 2\gamma_{\mathbf{k}'_2}], \quad (5.41)$$

with $\gamma_{\mathbf{k}}$ defined in Eq. (5.32). Note that the formulation (5.41) of V is symmetric under the exchange of momenta of two incoming or two outgoing momenta

$$V(\mathbf{k}'_1, \mathbf{k}'_2; \mathbf{k}_1, \mathbf{k}_2) = V(\mathbf{k}'_1, \mathbf{k}'_2; \mathbf{k}_2, \mathbf{k}_1) = V(\mathbf{k}'_2, \mathbf{k}'_1; \mathbf{k}_1, \mathbf{k}_2) = V(\mathbf{k}'_2, \mathbf{k}'_1; \mathbf{k}_2, \mathbf{k}_1). \quad (5.42)$$

This symmetry plays an important role in the determination of the combinatorial factors entering perturbative calculations.

The long-wavelength limit of the Dyson-Maleev vertex (5.41) is to leading order in k given by

$$V(\mathbf{k}'_1, \mathbf{k}'_2; \mathbf{k}_1, \mathbf{k}_2) = -\frac{(\mathbf{k}_1 \cdot \mathbf{k}_2)a^2}{2D} + \mathcal{O}((ka)^4). \quad (5.43)$$

Here we have made use of the fact that if all momenta are small, the vertex is independent of the momentum transfer $\mathbf{k}_1 - \mathbf{k}'_1 = \mathbf{k}'_2 - \mathbf{k}_2$.

5.2.4 Hartree-Fock approximation

We estimate the effect of \mathcal{H}_4 within the self-consistent Hartree-Fock approximation in this section.

We write our spin-wave Hamiltonian as

$$\mathcal{H} = (\mathcal{H}_2 + \delta\mathcal{H}^{(1)}) + (\mathcal{H}_4 - \delta\mathcal{H}^{(1)}), \quad (5.44)$$

and choose the one-body Hamiltonian $\delta\mathcal{H}^{(1)}$ such that the thermal expectation value of the residual interaction $\mathcal{H}_4 - \delta\mathcal{H}^{(1)}$ in the ensemble defined by the Hartree-Fock Hamiltonian $\mathcal{H}_2 + \delta\mathcal{H}^{(1)}$ vanishes

$$\langle \mathcal{H}_4 - \delta\mathcal{H}^{(1)} \rangle_{\mathcal{H}_2 + \delta\mathcal{H}^{(1)}} = 0. \quad (5.45)$$

We obtain

$$\delta\mathcal{H}^{(1)} = \sum_{\mathbf{k}} \Sigma^{(1)}(\mathbf{k}) b_{\mathbf{k}}^\dagger b_{\mathbf{k}} - \frac{|\tilde{J}_0|}{N} \sum_{\mathbf{k}, \mathbf{k}'} V(\mathbf{k}, \mathbf{k}'; \mathbf{k}, \mathbf{k}') n_{\mathbf{k}}^{(1)} n_{\mathbf{k}'}^{(1)}, \quad (5.46)$$

with the Hartree-Fock self-energy

$$\Sigma^{(1)}(\mathbf{k}) = 4 \frac{|\tilde{J}_0|D}{2NS} \sum_{\mathbf{k}'} V(\mathbf{k}, \mathbf{k}'; \mathbf{k}, \mathbf{k}') n_{\mathbf{k}'}^{(1)}. \quad (5.47)$$

The combinatorial factor 4 of the Feynman diagram for the Hartree-Fock self-energy shown in Fig. 5.2 results from the symmetry of the vertex V , see Eq. (5.42). The thermal occupation number of the Hartree-Fock magnon states with momentum \mathbf{k} is denoted by

$$n_{\mathbf{k}}^{(1)} = \left[e^{|\tilde{J}_0|S(\epsilon_{\mathbf{k}}^{(1)} + \hbar)/T} - 1 \right]^{-1}, \quad (5.48)$$

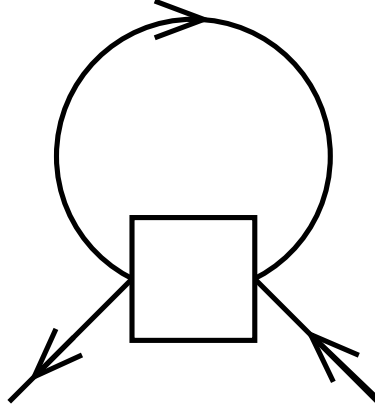


Figure 5.2: Feynman diagram describing the Hartree-Fock self-energy of the ferromagnetic Heisenberg model, see Eq. (5.47). The solid arrows denote the Hartree-Fock magnon propagators and the square is the Dyson-Maleev vertex.

with the renormalized magnon dispersion

$$\epsilon_{\mathbf{k}}^{(1)} = Z\epsilon_{\mathbf{k}}. \quad (5.49)$$

The dimensionless Hartree-Fock renormalization factor Z satisfies the self-consistency condition:

$$Z = 1 - \frac{1}{NS} \sum_{\mathbf{k}} (1 - \gamma_{\mathbf{k}}) n_{\mathbf{k}}^{(1)}. \quad (5.50)$$

Within self-consistent Hartree-Fock approximation we obtain for the Helmholtz free energy after some standard manipulations

$$F^{(1)}(h) = E_{\text{cl}} + T \sum_{\mathbf{k}} \ln \left[1 - e^{-|\tilde{J}_0|S(\epsilon_{\mathbf{k}}^{(1)} + h)/T} \right] + \frac{|\tilde{J}_0|NS^2}{2} (1 - Z)^2. \quad (5.51)$$

Note that the quantity ZS corresponds to the second variational parameter S' introduced by Takahashi [19], so that at this level of approximation our theory is exactly equivalent to Takahashi's modified spin wave theory [19, 20].

5.2.5 Two-loop correction

In this section we calculate the lowest order fluctuation correction to the Helmholtz free energy $F(h)$.

The relevant second-order Feynman diagram is shown in Fig. 5.3. Evaluating the

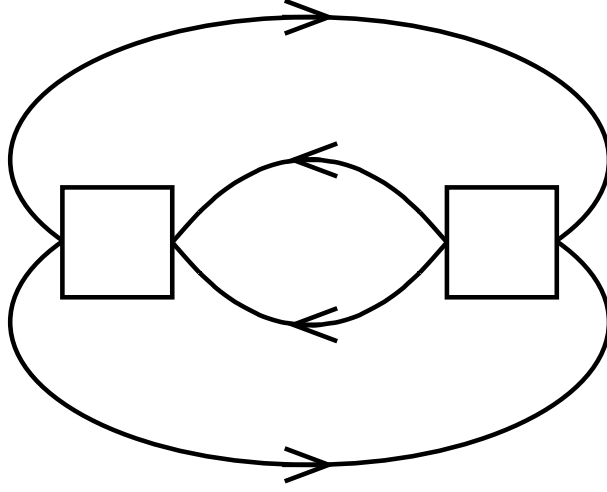


Figure 5.3: Feynman diagram describing the leading fluctuation correction to the free energy of the ferromagnetic Heisenberg model, see Eq. (5.53).

diagram, we obtain the leading fluctuation correction to $F(h)$

$$\begin{aligned} \delta F^{(2)}(h) = & 2 \left(\frac{|\tilde{J}_0|}{2N} \right)^2 \sum_{\mathbf{k}, \mathbf{k}', \mathbf{q}} \frac{W(\mathbf{k}, \mathbf{k}', \mathbf{q})}{E_{\mathbf{k}}^{(1)} + E_{\mathbf{k}'}^{(1)} - E_{\mathbf{k}+\mathbf{q}}^{(1)} - E_{\mathbf{k}'-\mathbf{q}}^{(1)}} \\ & \times \left[\left(1 + n_{\mathbf{k}}^{(1)}\right) \left(1 + n_{\mathbf{k}'}^{(1)}\right) n_{\mathbf{k}+\mathbf{q}}^{(1)} n_{\mathbf{k}'-\mathbf{q}}^{(1)} - n_{\mathbf{k}}^{(1)} n_{\mathbf{k}'}^{(1)} \left(1 + n_{\mathbf{k}+\mathbf{q}}^{(1)}\right) \left(1 + n_{\mathbf{k}'-\mathbf{q}}^{(1)}\right) \right], \end{aligned} \quad (5.52)$$

where

$$W(\mathbf{k}, \mathbf{k}', \mathbf{q}) = V(\mathbf{k}, \mathbf{k}'; \mathbf{k} + \mathbf{q}, \mathbf{k}' - \mathbf{q}) V(\mathbf{k} + \mathbf{q}, \mathbf{k}' - \mathbf{q}; \mathbf{k}, \mathbf{k}') , \quad (5.53)$$

and

$$E_{\mathbf{k}}^{(1)} \equiv |\tilde{J}_0| S \epsilon_{\mathbf{k}}^{(1)} . \quad (5.54)$$

At low temperatures one may replace the Dyson-Maleev vertices in Eq. (5.53) by their long-wavelength limit (5.43) and perform the integrations in Eq. (5.53) analytically [64].

Up to this order the free Helmholtz free energy is thus given by

$$F^{(2)}(h) = F^{(1)}(h) + \delta F^{(2)}(h) . \quad (5.55)$$

We will use Eqs. (5.51) and (5.55) in Sec. 5.3 for the calculation of the low-temperature behavior.

5.3 Low-temperature thermodynamics

In this section we explicitly calculate the low-temperature properties of a Heisenberg ferromagnet on a D -dimensional hypercubic lattice within spin-wave theory at constant order parameter.

The section is organized as follows. In Sec. 5.3.1 we present a general technique for the evaluation of the integrals arising in expressions for the magnetization and the thermodynamic potentials. In the subsequent Secs. 5.3.2-5.3.4 we discuss the cases of $D = 1, 2, 3$ spatial dimensions.

5.3.1 Density of states and Bose-Einstein integrals

First, let us introduce the formal framework we will use throughout this section for the evaluation of the momentum sums.

It is convenient to define the D -dimensional density of states

$$\rho_D(\epsilon) \equiv \frac{1}{N} \sum_{\mathbf{k}} \delta(\epsilon - 2D\epsilon_{\mathbf{k}}), \quad (5.56)$$

where $\delta(\epsilon)$ is the Dirac delta function and the sum is over the D -dimensional reciprocal lattice. We restrict the analysis of this section to the energy spectrum of noninteracting magnons $\epsilon_{\mathbf{k}}$. Extension to the higher-order perturbational results is straightforward. Formally, the momentum sums appearing in the thermodynamic observables can now be reduced to integrals of the type

$$\frac{1}{N} \sum_{\mathbf{k}} n_{\mathbf{k}} \rightarrow \int_0^\infty d\epsilon \frac{\rho_D(\epsilon)}{e^{\epsilon t^{-1} + v} - 1}, \quad (5.57)$$

$$\frac{1}{N} \sum_{\mathbf{k}} \ln \left[1 - e^{-|\tilde{J}_0|S(\epsilon_{\mathbf{k}} + h)/T} \right] \rightarrow \int_0^\infty d\epsilon \rho_D(\epsilon) \ln \left(1 - e^{-\epsilon t^{-1} - v} \right), \quad (5.58)$$

where

$$t \equiv \frac{T}{|J|S}, \quad (5.59)$$

$$v \equiv \frac{H}{T}. \quad (5.60)$$

As we are interested in the low-temperature behavior we can expand ρ_D for small wave vectors. Then, we need for the evaluation of the above one-dimensional integrals the

Bose-Einstein integral function [78]

$$\mathfrak{F}_\sigma(v) = \frac{1}{\Gamma(\sigma)} \int_0^\infty dx \frac{x^{\sigma-1}}{e^{x+v} - 1}, \quad (5.61)$$

with the gamma function $\Gamma(\sigma)$ [79]. Analytical properties of the Bose-Einstein integral function have been thoroughly discussed in the literature [78, 80]. For small positive $v \ll 1$ we have

$$\mathfrak{F}_\sigma(v) = \frac{(-v)^{\sigma-1}}{(\sigma-1)!} \left(\sum_{r=1}^{\sigma-1} \frac{1}{r} - \ln v \right) + \sum_{n \neq \sigma-1} \frac{(-v)^n}{n!} \zeta(\sigma-n), \quad (5.62)$$

if σ is a positive integer, and

$$\mathfrak{F}_\sigma(v) = \Gamma(1-\sigma)v^{\sigma-1} + \sum_{n=0}^{\infty} \frac{(-v)^n}{n!} \zeta(\sigma-n), \quad (5.63)$$

if σ is not a positive integer [80]. Here $\zeta(\sigma)$ is the ordinary Riemann zeta function [79]. Useful relations for the evaluation of the integrals appearing in the expressions for the Helmholtz free energy are

$$\int_0^\infty dx v^{\sigma-1} \ln(1 - e^{-x-v}) = -\Gamma(\sigma) \mathfrak{F}_{\sigma+1}(v), \quad (5.64)$$

$$\int_0^\infty dx v^{\sigma-1} e^{x+v} (e^{x+v} - 1)^{-2} = \Gamma(\sigma) \mathfrak{F}_{\sigma-1}(v). \quad (5.65)$$

We perform all explicit calculations in the thermodynamic limit, i.e. we transform the sums over the Brillouin zone to integrals according to

$$\frac{1}{N} \sum_{\mathbf{k}} \xrightarrow{N \rightarrow \infty} V_u \int_{\text{BZ}} \frac{d^D k}{(2\pi)^D}, \quad (5.66)$$

where V_u is the volume of the unit cell in real space and the integral is over the first Brillouin zone. In the following sections we present the results for ferromagnets on hypercubic lattices in $D = 1, 2, 3$ dimensions.

5.3.2 One-dimensional ferromagnet

Let us first consider the case of one dimension, where we know from the Mermin-Wagner-Hohenberg theorem that the Heisenberg ferromagnet does not have any long-range order at any finite temperature T .

Within linear spin-wave theory the density of states for the one-dimensional chain

is in the thermodynamic limit given by

$$\rho_1(\epsilon) = \frac{1}{2\pi} \int_0^{2\pi} dk \delta[\epsilon - 2 + 2 \cos(ka)] . \quad (5.67)$$

We evaluate the above integral over the first Brillouin zone

$$\rho_1(\epsilon) = \begin{cases} \frac{1}{2\pi} [\epsilon (1 - \frac{\epsilon}{4})]^{-1/2} & : 0 \leq \epsilon \leq 4, \\ 0 & : \epsilon > 4, \end{cases} \quad (5.68)$$

using the identity

$$\delta[f(k)] = \sum_i \frac{1}{|f'(k_i)|} \delta(k - k_i), \quad (5.69)$$

with

$$f(k_i) = 0 \quad \text{and} \quad f'(k_i) \neq 0. \quad (5.70)$$

In the long-wavelength limit we expand $\rho_1(\epsilon)$ in powers of the small parameter ϵ

$$\rho_1(\epsilon) = \frac{1}{2\pi} \epsilon^{-1/2} \left[1 + \frac{1}{8} \epsilon + \frac{3}{128} \epsilon^2 + \mathcal{O}(\epsilon^3) \right]. \quad (5.71)$$

Using the Bose-Einstein integral function discussed in the previous section we obtain for the magnetization per site

$$m \equiv \frac{M}{N} \quad (5.72)$$

to leading order in v and t

$$\frac{m(H)}{S} = 1 - \frac{\zeta(\frac{1}{2})}{2S\sqrt{\pi}} \sqrt{t} - \frac{1}{2S} \sqrt{\frac{t}{v}} + \mathcal{O}(t, t^{3/2}v^{-1/2}). \quad (5.73)$$

Keeping in mind that $v = H/T$, it is clear that this expression predicts a divergent magnetization for $H \rightarrow 0$, so at first glance it seems impossible to extract a meaningful result for the susceptibility

$$\chi = \lim_{h \rightarrow 0} \partial M / \partial H. \quad (5.74)$$

Fortunately, this is not quite true: we can obtain a perfectly finite result for the susceptibility if we use Eq. (5.9) to calculate the *inverse* susceptibility. Solving Eq. (5.73) for H as a function of M we obtain

$$H(M) = \frac{T^2}{4JS \left[S - m - \frac{\zeta(\frac{1}{2})}{2\sqrt{\pi}} \sqrt{t} \right]^2}. \quad (5.75)$$

According to Eq. (5.9) this implies for the inverse susceptibility

$$\chi^{-1} = \frac{T^2}{2NJS \left[S - m - \frac{\zeta(\frac{1}{2})}{2\sqrt{\pi}}\sqrt{t} \right]^3}. \quad (5.76)$$

Anticipating that in one dimension $m = 0$, we obtain for the susceptibility per site at low temperatures

$$\frac{\chi}{N} = \frac{2JS^4}{T^2} \left[1 - \frac{3}{S} \frac{\zeta(\frac{1}{2})}{2\sqrt{\pi}}\sqrt{t} + \mathcal{O}(t) \right]. \quad (5.77)$$

Apart from a different normalization, this expression agrees with the prediction of the modified spin-wave theory advanced by Takahashi [19], who argued that Eq. (5.77) is indeed the correct asymptotic low-temperature behavior of the susceptibility for arbitrary S .

Note that for $S = 1/2$ the nearest neighbor Heisenberg chain is exactly solvable via the Bethe-Ansatz [81, 82], so that in this case one can obtain an independent check of Eq. (5.77). Indeed, from a numerical analysis of Bethe-Ansatz integral equations Takahashi found perfect agreement with Eq. (5.77) for $S = 1/2$ [19], which is remarkable because a priori linear spin-wave theory is only expected to be accurate in the ordered state and for large S . We shall further comment on this surprising agreement at the end of this section.

The Gibbs potential per site is within linear spin-wave theory

$$\frac{G_0(M)}{NT} = -\frac{JS^2}{T} - \frac{\zeta(\frac{3}{2})}{2\sqrt{\pi}}\sqrt{t} + \frac{1}{NT} \left[H(0)|M| + \frac{M^2}{2\chi} + \mathcal{O}(|M|^3) \right], \quad (5.78)$$

where χ is given in Eq. (5.77) and

$$H(0) = \frac{T^2}{4JS^3} + \mathcal{O}(T^{5/2}), \quad (5.79)$$

see Eq. (5.75). In writing down Eq. (5.78) we have used the fact that our spin-wave calculation yields $G_0(M)$ only for $M \geq 0$ and that the exact $G(M)$ is an even function of M . Note that $G_0(M)$ assumes a minimum at $M = 0$, indicating the absence of long-range order. However, as shown in Fig. 5.4, linear spin-wave theory predicts an unphysical cusp in the Gibbs potential at $M = 0$.

The finite slope $H(0) = \partial G_0 / \partial M|_{M=0+}$ can be identified with the variational parameter $-\mu$ introduced by Takahashi [19], which in his calculation plays the role of a chemical potential for the Dyson-Maleev bosons, enforcing the condition of zero magnetization. On the other hand, it is physically clear that for $T > 0$ any finite value of the external field will always be accompanied with a finite magnetization, so that an exact calculation of $G(M)$ should yield $\lim_{M \rightarrow 0} H(M) = 0$. Therefore we expect

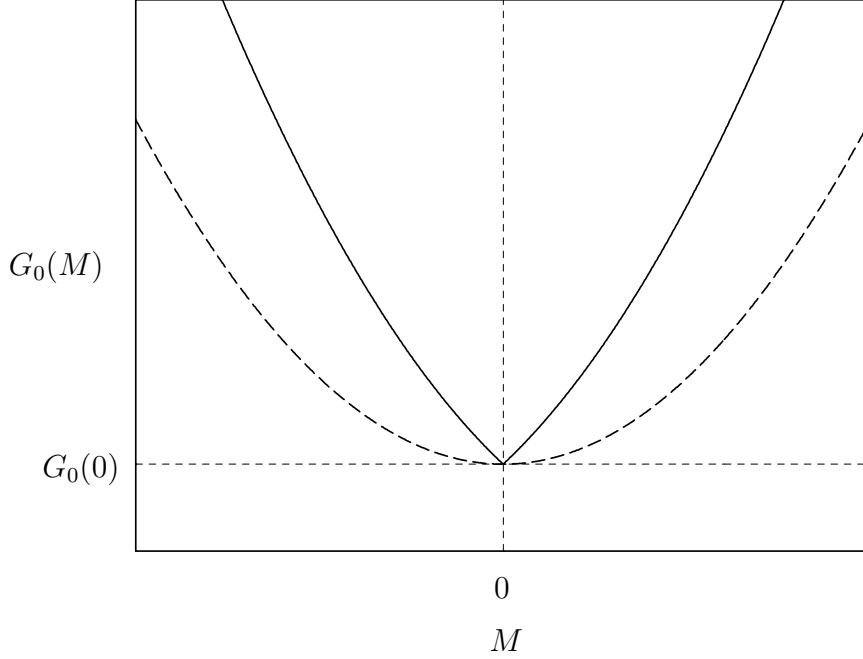


Figure 5.4: Gibbs-potential $G_0(M)$ of the one-dimensional Heisenberg ferromagnet within linear spin-wave theory, see Eq. (5.78). The cusp at $m = 0$ is an unphysical artefact of the spin-wave expansion. The dashed line is the subtracted Gibbs potential $\tilde{G}_0(M) = G_0(M) - H(0)|M|$.

that the exact Gibbs potential in one dimension has the form given in Eq. (5.8).

The cusp of the spin-wave result for the Gibbs potential seems to be related to the fact that in our simple spin-wave calculation we have ignored the kinematic interaction between spin waves. Fortunately, this cusp is irrelevant for the calculation of the zero-field thermodynamics, which can be also obtained from the subtracted Gibbs potential

$$\tilde{G}_0(M) = G_0(M) - H(0)|M|, \quad (5.80)$$

see Fig. 5.4. Note that $\tilde{G}_0(M)$ has the generic behavior given in Eq. (5.8), with the susceptibility approximated by Eq. (5.77).

Because fluctuation effects are usually stronger in lower dimensions, we now explicitly calculate the two-loop correction to the mean-field susceptibility (5.77).

In one dimension the Hartree-Fock renormalization factor Z is close to unity at low temperatures [19],

$$1 - Z = \mathcal{O}(T^2), \quad (5.81)$$

so that for the calculation of the first two terms in low-temperature expansion of thermodynamic observables it is sufficient to set $Z = 1$. Therefore, at the Hartree-Fock level the dynamical interaction between spin waves does not contribute to the

low-temperature asymptotics in $D = 1$.

The leading behavior of the first fluctuation correction to the Helmholtz free energy is

$$\frac{\delta F^{(2)}(H)}{TN} = \frac{1}{16} \frac{t^{3/2}}{(2S)^2 v^{1/2}} + \mathcal{O}(t^{3/2}, t^{1/2}v) . \quad (5.82)$$

The resulting equation of state is

$$\frac{m^{(2)}(H)}{S} = 1 - \frac{\zeta(\frac{1}{2})}{2S\sqrt{\pi}}\sqrt{t} - \frac{1}{2S}\sqrt{\frac{t}{v}} + \frac{1}{16} \left[\frac{1}{2S}\sqrt{\frac{t}{v}} \right]^3 + O(t, t^{3/2}v^{-1/2}) . \quad (5.83)$$

Comparing this result with the corresponding expression obtained within linear spin-wave theory given in Eq. (5.73), we see that the two-loop correction gives rise to an additional term proportional to the third power of $(2S)^{-1}(t/v)^{1/2}$. However, linear spin-wave theory predicts that this parameter is actually close to unity, as is easily seen by setting $m = 0$ in Eq. (5.73). Hence, *the leading fluctuation correction to the Hartree-Fock theory is not controlled by a small parameter*. Note that the extra power of S^{-1} that appears in the two-body part of the effective boson Hamiltonian is cancelled by the singular H -dependence of the two-loop correction.

If we nevertheless truncate the expansion at the two-loop order we obtain from Eq. (5.83) for the leading low-temperature behavior of the susceptibility

$$\frac{\chi^{(2)}}{N} \sim C_\chi \frac{JS^4}{T^2} , \quad (5.84)$$

with $C_\chi \approx 1.96$, which is slightly smaller than the mean-field prediction $C_\chi = 2$, and significantly smaller than the result $C_\chi = 3$ obtained within Schwinger-Boson mean-field theory [18]. We suspect that corrections involving more loops will involve higher powers of the parameter $(2S)^{-1}(t/v)^{1/2}$ in Eq. (5.84), which give rise to additional finite renormalizations of C_χ . Hence, a numerically accurate expression for low-temperature behavior of the susceptibility of a one-dimensional Heisenberg ferromagnet cannot be obtained from a truncation of the $1/S$ spin-wave expansion at some finite order.

Note that quantum Monte-Carlo simulations for the $S = 1/2$ nearest neighbor Heisenberg chain [83] give $C_\chi = 1.58 \pm 0.03$, supporting the scenario described above. In the light of these results it is puzzling that from the numerical analysis of the Bethe-Ansatz integral equations for $S = 1/2$ Takahashi obtained $C_\chi = 2$ [19, 81, 82]. Possibly this is related to difficulties in extracting the true asymptotic low temperature behavior of the susceptibility from the Bethe ansatz integral equations [19, 84, 85].

5.3.3 Two-dimensional ferromagnet

In two dimensions the Mermin-Wagner theorem states that no spontaneous symmetry-breaking occurs in the Heisenberg ferromagnet at any finite temperature T . The analysis is therefore similar to the $D = 1$ case.

In linear spin-wave theory the density of states for the square lattice with the lattice constant a is

$$\rho_2(\epsilon) = \frac{1}{4\pi^2} \int_0^{2\pi} dk_1 \int_0^{2\pi} dk_2 \delta[\epsilon - 4 + 2\cos(k_1 a) + 2\cos(k_2 a)] . \quad (5.85)$$

As in the one-dimensional case we make use of the delta function relation (5.69) to evaluate the momentum space integrals

$$\rho_2(\epsilon) = \begin{cases} \frac{8}{\pi^2(8-\epsilon)} K\left(\frac{\epsilon}{8-\epsilon^2}\right) & : 0 \leq \epsilon \leq 4, \\ \frac{8}{\pi^2\epsilon} K\left(\frac{\epsilon}{8-\epsilon^2}\right) & : 4 \leq \epsilon \leq 8, \\ 0 & : \epsilon > 8, \end{cases} \quad (5.86)$$

where $K(\epsilon)$ is the complete elliptic integral of the first kind [79]. Because we are interested in low-temperature properties, we expand $\rho_2(\epsilon)$ in the small parameter ϵ

$$\rho_2(\epsilon) = \frac{1}{4\pi} \left[1 + \frac{1}{8}\epsilon + \frac{3}{128}\epsilon^2 + \mathcal{O}(\epsilon^3) \right] . \quad (5.87)$$

Following a procedure similar to that of the previous section leads us to the expression for the normalized magnetization

$$m(H) = 1 - \frac{t}{4\pi S} \left[-\ln v + \frac{v}{2} + \frac{\zeta(2)}{8}t + \mathcal{O}(t^2, v^2) \right] . \quad (5.88)$$

Like in the one-dimensional case, $m(H)$ again diverges for $H \rightarrow 0$. Solving Eq. (5.88) for H as a function of m we obtain

$$H(m) = T e^{-4\pi S(1-m)/t} [1 + \mathcal{O}(t)] , \quad (5.89)$$

i. e. in two dimensions the conjugate field is exponentially small at low temperatures. Taking into account that $m = 0$ in $D = 2$, we obtain for the susceptibility

$$\chi = \frac{e^{4\pi S/t}}{4\pi JS} [1 + \mathcal{O}(t)] . \quad (5.90)$$

which grows exponentially fast for $T \rightarrow 0$. Eqs. (5.88, 5.89, 5.90) agree with the

corresponding results of Takahashi's modified spin-wave theory [19].

In two dimensions the Gibbs free energy takes the form

$$\frac{G_0(M)}{NT} = -\frac{\zeta(2)}{4\pi} + e^{-4\pi S/t} \left(\frac{1}{4\pi} |m| + \frac{m^2}{2} \right) + \mathcal{O}(t, m^3) . \quad (5.91)$$

The qualitative behavior of the Gibbs free energy is similar to that in $D = 1$: within linear spin-wave theory $G_0(M)$ has again a minimum at $m = 0$ with an unphysical cusp. However, it is known that a two-loop calculation is necessary to obtain the correct low-temperature asymptotics of the susceptibility [68]. The two-loop correction leaves the exponential factor unchanged but modifies the power of T in the prefactor of Eq. (5.90)

$$\chi^{(2)} \sim T^2 e^{4\pi JS^2/T} . \quad (5.92)$$

This result is not modified in a higher-order perturbation theory [17, 68].

5.3.4 Three-dimensional ferromagnet

We close this chapter with the linear spin-wave theory for the three-dimensional ferromagnet.

In the thermodynamic limit we obtain for the normalized magnetization to leading order in t and v

$$m(H) = S - \frac{\zeta(\frac{3}{2})}{(2\sqrt{\pi})^3} t^{3/2} + \frac{1}{4\pi} t^{3/2} v^{1/2} + \mathcal{O}(t^{5/2}, t^{3/2} v) . \quad (5.93)$$

Setting $H = 0$ we recover the well-known Bloch $T^{3/2}$ -law for the leading correction to the spontaneous magnetization per site $m(0)$ in the ordered state of the Heisenberg ferromagnet.

Taking the derivative of Eq. (5.93) with respect to H , we see that the longitudinal susceptibility $\chi(H) = \partial M / \partial H$ diverges for $H \rightarrow 0$ as $H^{-1/2}$. This divergence of the uniform longitudinal susceptibility of a three-dimensional Heisenberg magnet in the ordered state is not widely appreciated. Renormalization group calculations for the classical Heisenberg ferromagnet [86, 87] and diagrammatic calculations for the corresponding quantum model [88] indicate that this divergence is not an artefact of the linear spin-wave approximation. Due to this divergence the Gibbs-potential of the Heisenberg ferromagnet in $D = 3$ does not have the generic form given in Eq. (5.8).

We rewrite Eq. (5.93) as

$$\left(\frac{H}{T} \right)^{1/2} = \frac{4\pi(m - m(0))}{t^{3/2}} , \quad (5.94)$$

so we cannot solve for H as a function of m unless $m > m_0$. In the light of the general

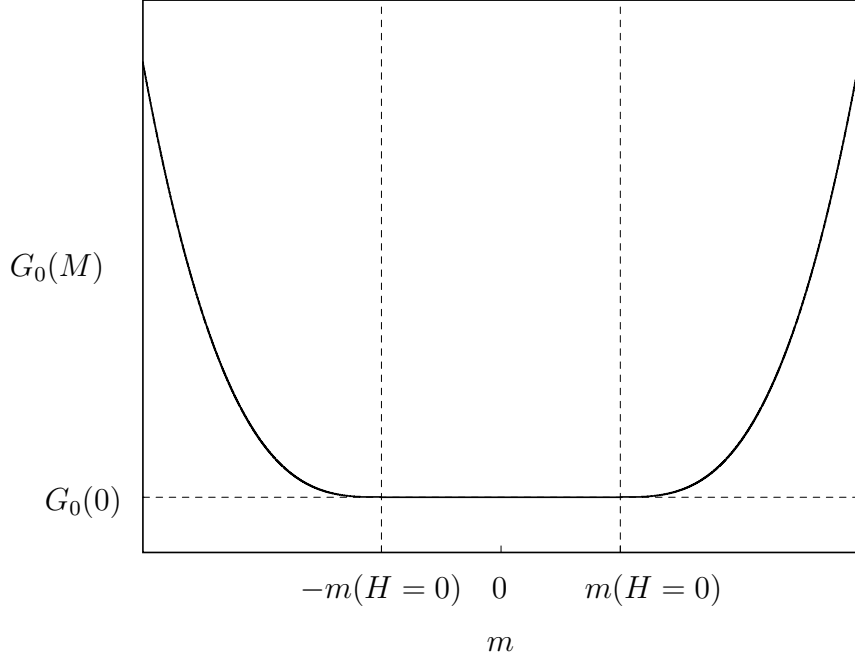


Figure 5.5: Gibbs-potential $G_0(m)$ of the three-dimensional Heisenberg ferromagnet within linear spin-wave theory. Due to the divergent longitudinal susceptibility in $D = 3$, the Gibbs potential grows like $(m - m(0))^3$ for $|m|$ slightly above $|m(0)|$, see Eq. (5.95).

discussion above this is not surprising, because for $|m| < |m(0)|$ the Gibbs potential should be constant [70]. The final result for the Gibbs potential in the thermodynamic limit within the non-interacting spin-wave approximation is for $m \geq m(0)$

$$\frac{G_0(M)}{NT} = -\frac{3JS^2}{T} - \frac{\zeta(\frac{5}{2})}{(2\sqrt{\pi})^3} t^{3/2} + \frac{16\pi^2}{3t^3} (m - m(0))^3 + \mathcal{O}[(m - m(0))^4]. \quad (5.95)$$

The behavior of $G_0(M)$ is shown in Fig. 5.5.

The leading m -dependence of Eq. (5.95) is proportional to $(m - m(0))^3$, because the inverse susceptibility vanishes. Note that for $D > 4$ the uniform longitudinal susceptibility of the Heisenberg ferromagnet is finite [86, 87], so that in this case the Gibbs potential has the generic form (5.8).

Chapter 6

Two-dimensional antiferromagnet in a uniform magnetic field

Quantum antiferromagnets in an external magnetic field exhibit a multitude of non-conventional quantum-mechanical phenomena and have been intensely studied in the past years [31, 89]. Especially the high-field regime near to the saturation point is interesting from the theoretical point of view [89]. In addition to this, advances in experimental techniques make precise measurements in the field regimes comparable to the strength of the exchange coupling possible.

The work presented in this chapter was strongly motivated by our co-operation with the chemists and the experimental physicists here at University of Frankfurt who synthesized novel two-dimensional metal-organic antiferromagnets and characterized them [32].

This chapter is organized as follows. In Sec. 6.1 we apply the formalism of the spin-wave expansion for non-collinear spin configurations to an antiferromagnet on a bipartite lattice in the presence of a uniform magnetic field. In Sec. 6.2 thermodynamic observables are calculated within linear spin-wave theory. In Sec. 6.3 we present results for a distorted honeycomb lattice and compare with quantum Monte Carlo findings and experimental measurements.

6.1 Spin waves in uniform magnetic field

We present a thorough analysis of the classical ground state for the antiferromagnet subject to a uniform magnetic field. By diagonalizing the quadratic part of the Dyson-Maleev Hamiltonian we derive an expression for the spin-wave spectrum.

6.1.1 Classical ground state

Let us consider a Heisenberg model with antiferromagnetic exchange couplings $J_{ij} > 0$ in an external magnetic field

$$\mathcal{H} = \frac{1}{2} \sum_{\langle i,j \rangle} J_{ij} \mathbf{S}_i \cdot \mathbf{S}_j - g\mu_B \sum_i \mathbf{B}_i \cdot \mathbf{S}_i, \quad (6.1)$$

where the sum runs over all next-neighbor pairs of a D -dimensional bipartite lattice.

A lattice is called *bipartite* if it can be divided into two equivalent sublattices such that the nearest neighbors of all sites belonging to one sublattice are located on the other sublattice. The two sublattices will be labeled A and B throughout the text. Examples of common bipartite lattices in one and two dimensions are shown in Fig. 6.1.

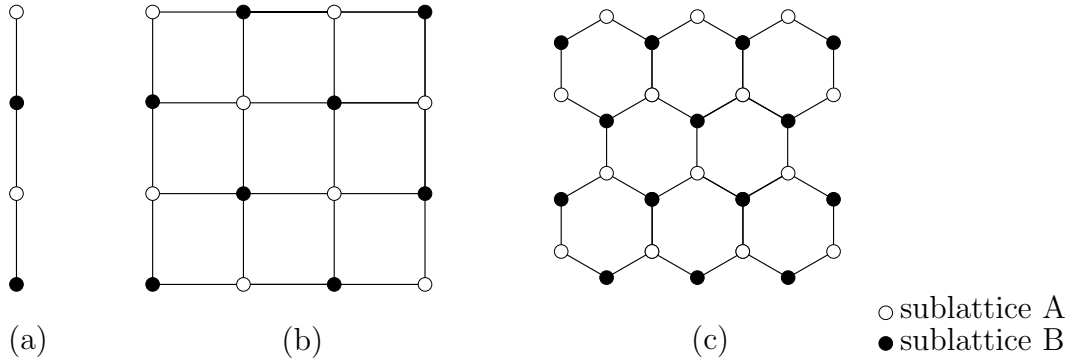


Figure 6.1: Examples of bipartite lattices are: (a) linear chain in $D = 1$ and (b) square and (c) honeycomb lattice in $D = 2$.

We choose the x axis of an orthonormal laboratory frame $\{\hat{\mathbf{e}}_x, \hat{\mathbf{e}}_y, \hat{\mathbf{e}}_z\}$ in the direction of the uniform external magnetic field:

$$\mathbf{B}(\mathbf{r}) = B\hat{\mathbf{e}}_x. \quad (6.2)$$

For technical reasons that will become clear in Sec. 6.2 a formal staggered field in the z direction is also introduced

$$\mathbf{B}_s(\mathbf{r}_i) = \zeta_i B_s \hat{\mathbf{e}}_z, \quad (6.3)$$

with

$$\zeta_i = \begin{cases} 1 & : \mathbf{r}_i \in A, \\ -1 & : \mathbf{r}_i \in B. \end{cases} \quad (6.4)$$

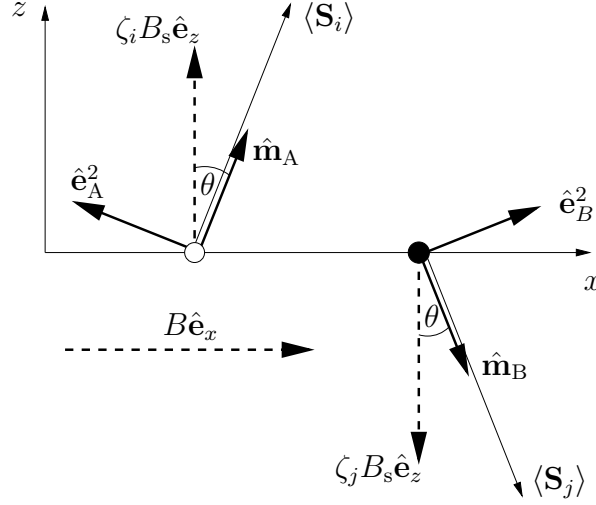


Figure 6.2: Spin configuration in the classical ground state of a bipartite antiferromagnet. The dashed arrows represent a uniform magnetic field $B\hat{\mathbf{e}}_x$ in the x direction and a staggered magnetic field $B_s\hat{\mathbf{e}}_z$ in the z direction. The small solid arrows represent the vectors of a “co-moving” basis that matches the direction defined by the local magnetization $\langle \mathbf{S}_i \rangle$ or $\langle \mathbf{S}_j \rangle$. Not shown are the basis vectors $\hat{\mathbf{e}}_A^1 = \hat{\mathbf{e}}_B^1 = \hat{\mathbf{e}}_y$ which point into the plane of the paper.

The total magnetic field is thus

$$\mathbf{H}_i \equiv g\mu_B \mathbf{B}_i = g\mu_B [B\hat{\mathbf{e}}_x + \zeta_i B_s \hat{\mathbf{e}}_z] . \quad (6.5)$$

Then the classical ground state configuration is

$$\hat{\mathbf{m}}_i = \zeta_i \cos \theta \hat{\mathbf{e}}_z + \sin \theta \hat{\mathbf{e}}_x , \quad (6.6)$$

i.e. the spins are canted in the direction of the uniform magnetic field by a canting angle θ , as shown in Fig. 6.2. For convenience we introduce the notation

$$n_0 = \cos \theta , \quad (6.7)$$

$$m_0 = \sin \theta . \quad (6.8)$$

Then the directions of the classical spins on the two sublattices in the ground state configuration are given by:

$$\hat{\mathbf{m}}_A = m_0 \hat{\mathbf{e}}_x + n_0 \hat{\mathbf{e}}_z , \quad (6.9a)$$

$$\hat{\mathbf{m}}_B = m_0 \hat{\mathbf{e}}_x - n_0 \hat{\mathbf{e}}_z . \quad (6.9b)$$

We complete the local orthonormal basis set on each sublattice with

$$\hat{\mathbf{e}}_A^1 = \hat{\mathbf{e}}_B^1 = \hat{\mathbf{e}}_y , \quad (6.10)$$

and

$$\hat{\mathbf{e}}_A^2 = -n_0 \hat{\mathbf{e}}_x + m_0 \hat{\mathbf{e}}_z , \quad (6.11a)$$

$$\hat{\mathbf{e}}_B^2 = n_0 \hat{\mathbf{e}}_x + m_0 \hat{\mathbf{e}}_z . \quad (6.11b)$$

The corresponding spherical basis vectors $\mathbf{e}_A^p, \mathbf{e}_B^p$, with $p = \pm$, can easily be obtained from Eq. (4.9). Note that by rotating the unit vectors $\hat{\mathbf{e}}_A^1, \hat{\mathbf{e}}_A^2$ around the axis $\hat{\mathbf{m}}_A$ an infinite number of equivalent orthonormal basis sets can be defined. The same is true for the sublattice B. Here, we have chosen a convenient set of vectors.

Physically, m_0 corresponds to the classical limit of the normalized uniform magnetization

$$m = \frac{1}{NS} \sum_i \langle \hat{\mathbf{e}}_x \cdot \mathbf{S}_i \rangle , \quad (6.12)$$

while n_0 corresponds to the $S \rightarrow \infty$ limit of the normalized staggered magnetization

$$n = \frac{1}{NS} \sum_i \zeta_i \langle \hat{\mathbf{e}}_z \cdot \mathbf{S}_i \rangle . \quad (6.13)$$

By symmetry, the uniform magnetization points into the x direction, while the staggered magnetization points into the z direction. The natural dimensionless measure for the strength of the fields is

$$h = \chi_0 g \mu_B B , \quad (6.14)$$

$$h_s = \chi_0 g \mu_B B_s , \quad (6.15)$$

with the classical uniform susceptibility:

$$\chi_0 = (2\tilde{J}_0 S)^{-1} . \quad (6.16)$$

Here

$$\tilde{J}_0 = \frac{1}{N} \sum_{\langle ij \rangle} J_{ij} \quad (6.17)$$

is the $\mathbf{k} = 0$ component of the Fourier transform of the exchange coupling

$$\tilde{J}_{\mathbf{k}} = \frac{1}{N} \sum_{\langle ij \rangle} e^{-i\mathbf{k} \cdot (\mathbf{r}_i - \mathbf{r}_j)} J_{ij} . \quad (6.18)$$

For the special choice of the field \mathbf{H}_i given in Eq. (6.2) the relevant scalar products

in the basis (6.9, 6.10, 6.11) are

$$\hat{\mathbf{m}}_A \cdot \hat{\mathbf{m}}_B = m_0^2 - n_0^2, \quad (6.19)$$

$$\hat{\mathbf{m}}_A \cdot \mathbf{H}_A = \hat{\mathbf{m}}_B \cdot \mathbf{H}_B = 2\tilde{J}_0 S(hm_0 + h_s n_0), \quad (6.20)$$

$$\hat{\mathbf{m}}_A \cdot \mathbf{e}_B^p = -\hat{\mathbf{m}}_B \cdot \mathbf{e}_A^p = 2ipn_0m_0, \quad (6.21)$$

$$\mathbf{e}_A^p \cdot \mathbf{e}_B^{p'} = 2[\delta_{p,p'}n_0^2 + \delta_{p,-p'}m_0^2]. \quad (6.22)$$

Now the classical ground state energy (4.19) reads:

$$E_{\text{cl}} = -\tilde{J}_0 N S^2 \left(\frac{n_0^2 - m_0^2}{2} + 2hm_0 + 2h_s n_0 \right). \quad (6.23)$$

The general condition (4.29) for the ground state reduces to the simple relation

$$h = m_0[1 + h_s/n_0], \quad (6.24)$$

which together with the normalization condition

$$n_0^2 + m_0^2 = 1 \quad (6.25)$$

determines the classical Néel order parameter n_0 and the classical uniform magnetization m_0 as functions of the fields h and h_s .

6.1.2 Spin-wave dispersion

In this section we derive the spin-wave spectrum of the Heisenberg antiferromagnet subject to a uniform external magnetic field. In order to treat quantum fluctuations around the classical ground state we take into account terms of the spin-wave Hamiltonian which are linear and quadratic in bosons and neglect terms of higher orders in $S^{-1/2}$. We work in the local basis defined in Eqs. (6.9, 6.10, 6.11) of the last section.

As we are considering only fluctuations around the classical ground state, the one-boson term \mathcal{H}'_1 defined in Eq. (4.20) vanishes, see Eq. (4.31) and the accompanying discussion.

To obtain the spin-wave dispersion, we have to diagonalize the quadratic part of the Hamiltonian:

$$\mathcal{H}_2 = \mathcal{H}_2^{\parallel} + \mathcal{H}_2^{\perp}, \quad (6.26)$$

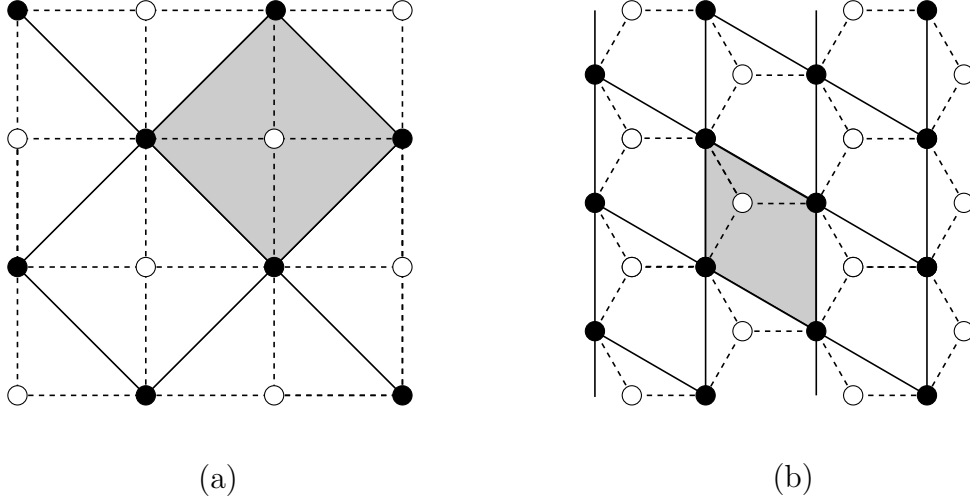


Figure 6.3: Reciprocal sublattices (solid lines) for an underlying (a) square and (b) honeycomb lattice (dashed lines). Shaded areas are the respective reduced Brillouin zones.

which in our special co-moving basis is given by

$$\begin{aligned} \mathcal{H}_2 = & \frac{S}{2} \sum_{i,j} J_{ij} \left[(n_0^2 - m_0^2) (n_i + n_j) + n_0^2 (b_i^\dagger b_j + b_j^\dagger b_i) + m_0^2 (b_i^\dagger b_j^\dagger + b_j b_i) \right] \\ & + 2\tilde{J}_0 S (hm_0 + h_s n_0) \sum_i n_i . \end{aligned} \quad (6.27)$$

It is convenient to express \mathcal{H}_2 in momentum space first. We perform a Fourier transformation of the boson operators separately on each sublattice,

$$b_i = \sqrt{\frac{2}{N}} \sum_{\mathbf{k}} e^{i\mathbf{k} \cdot \mathbf{r}_i} a_{\mathbf{k}} , \quad \text{for } \mathbf{r}_i \in A , \quad (6.28a)$$

$$b_i = \sqrt{\frac{2}{N}} \sum_{\mathbf{k}} e^{i\mathbf{k} \cdot \mathbf{r}_i} b_{\mathbf{k}} , \quad \text{for } \mathbf{r}_i \in B , \quad (6.28b)$$

where the wave-vector sums are over the reduced Brillouin zone of the bipartite lattice. The *reduced* Brillouin zone is defined as the first Brillouin zone of one of the sublattices. In the context of magnetism a reduced Brillouin zone is sometimes also referred to as a *magnetic* Brillouin zone. Examples for the square and the honeycomb lattice are shown in Fig. 6.3.

If we apply Eqs. (6.28) to the quadratic Dyson-Maleev Hamiltonian \mathcal{H}_2 we obtain:

$$\mathcal{H}_2 = \tilde{J}_0 S \sum_{\mathbf{k}} [A(a_{\mathbf{k}}^\dagger a_{\mathbf{k}} + b_{\mathbf{k}}^\dagger b_{\mathbf{k}}) + B_{\mathbf{k}} b_{-\mathbf{k}} a_{\mathbf{k}} + B_{\mathbf{k}}^* a_{\mathbf{k}}^\dagger b_{-\mathbf{k}}^\dagger + C_{\mathbf{k}} b_{\mathbf{k}}^\dagger a_{\mathbf{k}} + C_{\mathbf{k}}^* a_{\mathbf{k}}^\dagger b_{\mathbf{k}}] , \quad (6.29)$$

with

$$A = 1 + 2h_s/n_0 , \quad (6.30a)$$

$$B_{\mathbf{k}} = n_0^2 \gamma_{\mathbf{k}} , \quad (6.30b)$$

$$C_{\mathbf{k}} = m_0^2 \gamma_{\mathbf{k}} . \quad (6.30c)$$

For a more compact notation we introduce the structure factor

$$\gamma_{\mathbf{k}} = \frac{\tilde{J}_{\mathbf{k}}}{\tilde{J}_0} . \quad (6.31)$$

In general, $\gamma_{\mathbf{k}}$ and with it also the coefficients $B_{\mathbf{k}}, C_{\mathbf{k}}$ are complex numbers with a phase angle $\phi_{\mathbf{k}}$

$$\gamma_{\mathbf{k}} = |\gamma_{\mathbf{k}}| e^{i\phi_{\mathbf{k}}} \Rightarrow B_{\mathbf{k}} = |B_{\mathbf{k}}| e^{i\phi_{\mathbf{k}}} , \quad C_{\mathbf{k}} = |C_{\mathbf{k}}| e^{i\phi_{\mathbf{k}}} , \quad (6.32)$$

which makes handling of \mathcal{H}_2 somewhat tedious. However, from Eq. (6.18) it follows immediately that

$$\tilde{J}_{-\mathbf{k}} = \tilde{J}_{\mathbf{k}}^* \Leftrightarrow \phi_{-\mathbf{k}} = -\phi_{\mathbf{k}} , \quad (6.33)$$

therefore the phase factors can be removed from Eq. (6.29) via the gauge transformation

$$\tilde{a}_{\mathbf{k}} = e^{i\phi_{\mathbf{k}}} a_{\mathbf{k}} . \quad (6.34)$$

In the next step, we introduce the symmetric (+) and antisymmetric (−) combinations of the boson operators

$$c_{\mathbf{k}\sigma} = \frac{1}{\sqrt{2}} [\tilde{a}_{\mathbf{k}} + \sigma b_{\mathbf{k}}] , \quad \sigma = \pm 1 , \quad (6.35)$$

which also obey canonical boson commutation relations

$$[c_{\mathbf{k}\sigma}, c_{\mathbf{k}'\sigma'}^\dagger] = \delta_{\mathbf{k},\mathbf{k}'} \delta_{\sigma,\sigma'} . \quad (6.36)$$

Now the Hamiltonian (6.29) assumes the block-diagonal form

$$\begin{aligned} \mathcal{H}_2 = & \frac{\tilde{J}_0 S}{2} \sum_{\mathbf{k}\sigma} [(A + \sigma |C_{\mathbf{k}}|) (c_{\mathbf{k}\sigma}^\dagger c_{\mathbf{k}\sigma} + c_{-\mathbf{k}\sigma}^\dagger c_{-\mathbf{k}\sigma}) \\ & + \sigma |B_{\mathbf{k}}| (c_{\mathbf{k}\sigma}^\dagger c_{-\mathbf{k}\sigma}^\dagger + c_{\mathbf{k}\sigma} c_{-\mathbf{k}\sigma})] . \end{aligned} \quad (6.37)$$

Finally, the diagonalization is completed by means of the standard Bogoliubov trans-

formation,

$$\begin{pmatrix} c_{\mathbf{k}\sigma} \\ c_{-\mathbf{k}\sigma}^\dagger \end{pmatrix} = \begin{pmatrix} u_{\mathbf{k}\sigma} & -\sigma v_{\mathbf{k}\sigma} \\ -\sigma v_{\mathbf{k}\sigma} & u_{\mathbf{k}\sigma} \end{pmatrix} \begin{pmatrix} d_{\mathbf{k}\sigma} \\ d_{-\mathbf{k}\sigma}^\dagger \end{pmatrix}, \quad (6.38)$$

where

$$u_{\mathbf{k}\sigma} = \sqrt{\frac{A + \sigma|C_{\mathbf{k}}| + \epsilon_{\mathbf{k}\sigma}}{2\epsilon_{\mathbf{k}\sigma}}}, \quad (6.39a)$$

$$v_{\mathbf{k}\sigma} = \sqrt{\frac{A + \sigma|C_{\mathbf{k}}| - \epsilon_{\mathbf{k}\sigma}}{2\epsilon_{\mathbf{k}\sigma}}}, \quad (6.39b)$$

with the dimensionless energy dispersion

$$\epsilon_{\mathbf{k}\sigma} = \sqrt{(A + \sigma|C_{\mathbf{k}}|)^2 - |B_{\mathbf{k}}|^2}. \quad (6.40)$$

The transformation (6.38) is canonical, i.e. the bosonic nature of the operators is conserved

$$[d_{\mathbf{k}\sigma}, d_{\mathbf{k}'\sigma'}^\dagger] = \delta_{\mathbf{k},\mathbf{k}'}\delta_{\sigma,\sigma'}. \quad (6.41)$$

The quadratic spin-wave Hamiltonian \mathcal{H}_2 is diagonal in terms of the new bosonic degrees of freedom

$$\mathcal{H}_2 = \delta E_2 + \tilde{J}_0 S \sum_{\mathbf{k}\sigma} \epsilon_{\mathbf{k}\sigma} d_{\mathbf{k}\sigma}^\dagger d_{\mathbf{k}\sigma}, \quad (6.42)$$

with the lowest-order quantum correction to the classical ground state energy

$$\delta E_2 = \frac{\tilde{J}_0 S}{2} \sum_{\mathbf{k}\sigma} [\epsilon_{\mathbf{k}\sigma} - (A + \sigma|C_{\mathbf{k}}|)]. \quad (6.43)$$

By inserting Eqs. (6.30) into Eq. (6.40) we obtain the explicit form of the spin-wave dispersion

$$\epsilon_{\mathbf{k}\sigma} = \left[\left(1 + \frac{2h_s}{n_0} + \sigma|\gamma_{\mathbf{k}}| \right) \left(1 + \frac{2h_s}{n_0} - \sigma(n_0^2 - m_0^2)|\gamma_{\mathbf{k}}| \right) \right]^{1/2}. \quad (6.44)$$

Note that the presence of the external magnetic field splits the dispersion into two branches, denoted by $\sigma = \pm$. Using the fact that $|C_{\mathbf{k}}| = |C_{-\mathbf{k}}|$ and substituting A by expression (6.30a) yields for Eq. (6.43)

$$\delta E_2 = -\tilde{J}_0 N S \left[\left(1 + \frac{2h_s}{n_0} \right) - \frac{1}{2N} \sum_{\mathbf{k}\sigma} \epsilon_{\mathbf{k}\sigma} \right]. \quad (6.45)$$

The low-temperature properties of the magnet are determined by the long-wavelength

behavior of the energy dispersion, which follows from a expansion for small \mathbf{k} ,

$$|\gamma_{\mathbf{k}}| \approx 1 - \frac{1}{2} \sum_{\alpha\beta} k_{\alpha} A_{\alpha\beta} k_{\beta}, \quad (6.46)$$

where \mathbf{A} is a symmetric matrix and k_{α} are the components of \mathbf{k} . An orthogonal basis can always be chosen such that \mathbf{A} is diagonal, with eigenvalues A_{α} . In this basis

$$|\gamma_{\mathbf{k}}| \approx 1 - \frac{1}{2} \sum_{\alpha} A_{\alpha} k_{\alpha}^2. \quad (6.47)$$

The matrix \mathbf{A} is positive, since

$$|\gamma_{\mathbf{k}}| \leq \sum_{\nu} \left| \frac{J_{\nu}}{\bar{J}_0} \right| = 1, \quad (6.48)$$

where the last equality assumes that all couplings have the same sign. We can thus define effective length scales ℓ_{α} by setting

$$A_{\alpha} = \ell_{\alpha}^2. \quad (6.49)$$

For a D -dimensional hypercubic lattice with lattice spacing a we have $\ell_{\alpha}^2 = a^2/D$. We will give the results for the experimentally relevant case of the distorted honeycomb lattice in Sec. 6.3.3.

For $h_s = 0$ only the mode $\epsilon_{\mathbf{k}-}$ is gapless for $\mathbf{k} \rightarrow 0$, while the mode $\epsilon_{\mathbf{k}+}$ has the gap $2m_0$. To give a more explicit form for the long-wavelength spin-wave dispersions, we further assume $h_s \ll n_0$. Then

$$\epsilon_{\mathbf{k}-} \approx n_0 \left[\frac{4h_s}{n_0} + \sum_{\alpha} (\ell_{\alpha} k_{\alpha})^2 \right]^{1/2}, \quad (6.50)$$

$$\begin{aligned} \epsilon_{\mathbf{k}+} \approx & \left[4m_0^2 + \frac{4h_s}{n_0} (1 + m_0^2) \right. \\ & \left. + (n_0^2 - 2m_0^2) \sum_{\alpha} (\ell_{\alpha} k_{\alpha})^2 \right]^{1/2}. \end{aligned} \quad (6.51)$$

For $n_0 \rightarrow 0$ the expansion (6.50) is not appropriate any longer and for $h_s = 0$ the dispersion $\epsilon_{\mathbf{k}-}$ becomes purely quadratic at $n_0 = 0$. Before this happens, there is a critical field $0 < h^* < 1$ at which the curvature of the dispersion $\epsilon_{\mathbf{k}-}$ changes sign. The positive curvature for $h > h^*$ results in an instability of magnons towards a spontaneous decay into two magnon states [89]. Furthermore, if an anisotropic exchange is considered, the anisotropy gap Δ is strongly renormalized by magnon interactions [90, 91]. As the influence of these instabilities on the thermodynamic

properties is unclear at the moment, they will not be further considered in this work.

Let us conclude this section with some remarks regarding the case of vanishing external uniform magnetic field. From $h = 0$ it follows immediately that $m = m_0 = 0$, and the normalization condition (6.25) becomes $n_0 = 1$. Then the coefficients in the diagonalized spin-wave Hamiltonian are given by

$$A = 1 + 2h_s, \quad (6.52a)$$

$$B_{\mathbf{k}} = \gamma_{\mathbf{k}}, \quad (6.52b)$$

$$C_{\mathbf{k}} = 0. \quad (6.52c)$$

As one would expect, we obtain a doubly degenerate mode with energy dispersion

$$\epsilon_{\mathbf{k}\sigma} = \epsilon_{\mathbf{k}} = \sqrt{(1 + 2h_s)^2 - |\gamma_{\mathbf{k}}|^2}. \quad (6.53)$$

The contribution to the ground state energy now reads

$$\delta E_2 = -\tilde{J}_0 N S \left[(1 + 2h_s) - \frac{1}{N} \sum_{\mathbf{k}} \epsilon_{\mathbf{k}} \right]. \quad (6.54)$$

The expression in the square brackets is usually called Oguchi correction [92] in the literature.

We have to bear in mind that throughout this section we have neglected interactions between magnons and that fluctuations around the classical ground state were considered. However, if we take into account the spin-wave interactions and the renormalized canting angle θ , we would get only small corrections to the noninteracting case [31].

6.2 Observables

We are primarily interested in experimentally relevant thermodynamic observables like the magnetization, the uniform susceptibility and the specific heat for low-dimensional systems, which in our case are two-dimensional Heisenberg antiferromagnets.

As we have learned from the Hohenberg-Mermin-Wagner theorem in Sec. 2.2, at finite temperatures $T > 0$ no spontaneous symmetry breaking occurs. The absence of long-range antiferromagnetic order leads to infrared divergences in conventional spin-wave theory. However, we can formally enforce a vanishing antiferromagnetic order parameter

$$n = 0, \quad (6.55)$$

by an appropriate choice of the staggered field h_s that regularizes the divergent inte-

grals. This issue was discussed for the ferromagnetic case in great detail in Chap. 5.

Note that h_s is not a physical external magnetic field like h , but an internal effective field that is generated by strong fluctuations. In fact h_s is equivalent to the Lagrange multiplier introduced in Takahashi's modified spin wave theory [21]. It is well known that the internal field is related to a finite correlation length ξ , as we will further discuss in Sec. 6.2.4.

6.2.1 Uniform and staggered magnetization

In this section we calculate the leading spin-wave corrections to the normalized uniform- and staggered magnetization as defined in Eqs. (6.12) and (6.13). We discuss general finite-temperature results and their $T \rightarrow 0$ limits.

For fixed temperature T , the magnetization can be obtained from the field dependence of the Helmholtz free energy which for our quadratic spin-wave Hamiltonian \mathcal{H}_2 reads

$$F(h, h_s) = E_2 - T \sum_{\mathbf{k}} \sum_{\sigma=\pm} \ln(n_{\mathbf{k}\sigma} + 1), \quad (6.56)$$

with the Bose function

$$n_{\mathbf{k}\sigma} = [e^{\tilde{J}_0 S \epsilon_{\mathbf{k}\sigma}/T} - 1]^{-1}. \quad (6.57)$$

Up to this order in the spin-wave expansion the ground state energy is a sum of the classical value (6.23) and the leading correction (6.43)

$$E_2 = E_{\text{cl}} + \delta E_2. \quad (6.58)$$

We know from elementary thermodynamics that the (staggered) magnetization can be obtained as the partial derivative of the free energy with respect to the (staggered) magnetic field

$$m = -\frac{1}{2\tilde{J}_0 N S^2} \frac{\partial F(h, h_s)}{\partial h}, \quad (6.59)$$

$$n = -\frac{1}{2\tilde{J}_0 N S^2} \frac{\partial F(h, h_s)}{\partial h_s}. \quad (6.60)$$

A closer look at the Eqs. (6.56-6.58) shows that the free energy essentially depends on the classical ground-state energy E_{cl} and - through the spin-wave correction to the ground-state energy δE_2 and the Bose factor $n_{\mathbf{k}\sigma}$ - on the spin-wave dispersion $\epsilon_{\mathbf{k}\sigma}$. In the following, we therefore focus on the derivatives

$$\frac{\partial E_{\text{cl}}}{\partial h}, \quad \frac{\partial \epsilon_{\mathbf{k}\sigma}}{\partial h} \quad \text{and} \quad \frac{\partial E_{\text{cl}}}{\partial h_s}, \quad \frac{\partial \epsilon_{\mathbf{k}\sigma}}{\partial h_s}. \quad (6.61)$$

First, we differentiate Eq. (6.23) with respect to h and take into account that

$$n_0 \frac{\partial n_0}{\partial h} = -m_0 \frac{\partial m_0}{\partial h}, \quad (6.62)$$

which follows directly from the normalization condition $n_0^2 + m_0^2 = 1$. Using the condition for the classical canted ground state (6.24) we show that the part of the derivative proportional to $\partial m_0 / \partial h$ vanishes and we obtain

$$-\frac{1}{2\tilde{J}_0 NS^2} \frac{\partial E_{\text{cl}}}{\partial h} = m_0. \quad (6.63)$$

The derivative of the classical ground-state energy with respect to the uniform field gives the uniform magnetization, as expected.

In order to evaluate the derivative of the dispersion (6.44) slightly more work is needed. With the explicit relations:

$$\frac{\partial m_0}{\partial h} = \frac{n_0^3}{n_0^3 + h_s}, \quad (6.64)$$

$$\frac{\partial(2h_s/n_0)}{\partial h} = \frac{2h_s m_0}{n_0^3 + h_s}, \quad (6.65)$$

we obtain

$$\begin{aligned} \frac{\partial \epsilon_{\mathbf{k}\sigma}}{\partial h} = & \frac{2}{\epsilon_{\mathbf{k}\sigma}} \frac{m_0}{n_0^3 + h_s} \left[h_s \left(1 + \frac{2h_s}{n_0} + \sigma |\gamma_{\mathbf{k}}| m_0^2 \right) \right. \\ & \left. + \sigma |\gamma_{\mathbf{k}}| n_0^3 \left(1 + \frac{2h_s}{n_0} + \sigma |\gamma_{\mathbf{k}}| \right) \right]. \end{aligned} \quad (6.66)$$

With this expression it is straightforward to calculate the derivatives of δE_2 and $n_{\mathbf{k}\sigma}$.

Now we can write down an expression for the uniform magnetization

$$\begin{aligned} m = & \frac{m_0}{n_0^3 + h_s} \left\{ n_0^3 + h_s + \frac{2h_s}{n_0} - \frac{1}{NS} \sum_{\mathbf{k}\sigma} \frac{n_{\mathbf{k}\sigma} + \frac{1}{2}}{\epsilon_{\mathbf{k}\sigma}} \left[h_s \left(1 + \frac{2h_s}{n_0} + \sigma |\gamma_{\mathbf{k}}| m_0^2 \right) \right. \right. \\ & \left. \left. + \sigma |\gamma_{\mathbf{k}}| n_0^3 \left(1 + \frac{2h_s}{n_0} + \sigma |\gamma_{\mathbf{k}}| \right) \right] \right\}. \end{aligned} \quad (6.67)$$

This relation is still pretty cumbersome. However, after we derive the corresponding expression for the staggered magnetization we will see that by combining them we obtain more concise and elegant formulas.

The rationale for the derivatives with respect to h_s is similar to the case of the uniform field. We therefore give only a brief presentation of the calculation. The derivative of the classical ground-state energy with respect to the staggered field

yields

$$-\frac{1}{2\tilde{J}_0 N S^2} \frac{\partial E_{\text{cl}}}{\partial h_s} = n_0, \quad (6.68)$$

which is not surprising. With

$$\frac{\partial m_0}{\partial h_s} = -\frac{m_0 n_0^2}{n_0^3 + h_s}, \quad (6.69)$$

$$\frac{\partial(2h_s/n_0)}{\partial h_s} = \frac{2}{n_0} \left(1 - \frac{h_s m_0^2}{n_0^3 + h_s}\right), \quad (6.70)$$

it follows for the derivative of the spin-wave dispersion

$$\begin{aligned} \frac{\partial \epsilon_{\mathbf{k}\sigma}}{\partial h_s} = \frac{2}{\epsilon_{\mathbf{k}\sigma}} \frac{1}{n_0^3 + h_s} & \left[n_0 (n_0 + h_s) \left(1 + \frac{2h_s}{n_0} + \sigma |\gamma_{\mathbf{k}}| m_0^2\right) \right. \\ & \left. + \sigma |\gamma_{\mathbf{k}}| m_0^2 n_0^2 \left(1 + \frac{2h_s}{n_0} + \sigma |\gamma_{\mathbf{k}}|\right) \right]. \end{aligned} \quad (6.71)$$

We obtain for the staggered magnetization

$$\begin{aligned} n = n_0 & \left\{ 1 + \frac{1}{2S} + \frac{1}{2S} \frac{m_0^2 n_0}{n_0^3 + h_s} + \frac{1}{NS} \sum_{\mathbf{k}\sigma} \frac{n_{\mathbf{k}\sigma} + \frac{1}{2}}{\epsilon_{\mathbf{k}\sigma}} \left[\left(1 + \frac{2h_s}{n_0} + \sigma |\gamma_{\mathbf{k}}| m_0^2\right) \right. \right. \\ & \left. \left. - \frac{m_0^2 n_0}{n_0^3 + h_s} \left(\left(1 + \frac{2h_s}{n_0} + \sigma |\gamma_{\mathbf{k}}| m_0^2\right) - \sigma |\gamma_{\mathbf{k}}| \left(1 + \frac{2h_s}{n_0} + \sigma |\gamma_{\mathbf{k}}|\right) \right) \right] \right\} \end{aligned} \quad (6.72)$$

We simplify our expressions for the uniform and staggered magnetization to

$$m = m_0 \left\{ 1 - \frac{1}{s(n_0^3 + h_s)} [n_0^3 R(h, h_s) + h_s I(h, h_s)] \right\}, \quad (6.73)$$

$$n = n_0 \left\{ 1 + \frac{1}{s(n_0^3 + h_s)} [m_0^2 n_0 R(h, h_s) - (n_0 + h_s) I(h, h_s)] \right\}, \quad (6.74)$$

with

$$R(h, h_s) = \frac{1}{N} \sum_{\mathbf{k}\sigma} \frac{n_{\mathbf{k}\sigma} + \frac{1}{2}}{\epsilon_{\mathbf{k}\sigma}} \sigma |\gamma_{\mathbf{k}}| \left(1 + \frac{2h_s}{n_0} + \sigma |\gamma_{\mathbf{k}}|\right), \quad (6.75)$$

and

$$I(h, h_s) = -\frac{1}{2} + \frac{1}{N} \sum_{\mathbf{k}\sigma} \frac{n_{\mathbf{k}\sigma} + \frac{1}{2}}{\epsilon_{\mathbf{k}\sigma}} \left(1 + \frac{2h_s}{n_0} + \sigma m_0^2 |\gamma_{\mathbf{k}}|\right). \quad (6.76)$$

In the final step of the calculation we build linear combinations of m and n in order to express the uniform magnetization in terms of $R(h, h_s)$ and n and the staggered

magnetization in terms of $I(h, h_s)$ and m

$$n_0(n_0 + h_s)m - h_s m_0 n = m_0 n_0^2 \left[1 - \frac{1}{S} R(h, h_s) \right], \quad (6.77)$$

$$m_0 m + n_0 n = 1 - \frac{1}{S} I(h, h_s), \quad (6.78)$$

From the above relations we directly obtain the compact form

$$m = \frac{m_0^2}{h} \left[1 + \frac{n h_s}{n_0^2} - \frac{R(h, h_s)}{S} \right], \quad (6.79)$$

$$n = \frac{1}{n_0} \left[1 - m_0 m - \frac{I(h, h_s)}{S} \right]. \quad (6.80)$$

The parameters n_0 and m_0 on the right-hand sides of Eqs. (6.75,6.76,6.79,6.80) are determined as functions of the fields h and h_s by Eqs. (6.24) and (6.25).

Note that for $S \rightarrow \infty$ the solutions of Eqs. (6.79) and (6.80) correctly approach the classical magnetizations $n = n_0$ and $m = m_0$: in this limit Eq. (6.79) reduces to Eq. (6.24), while Eq. (6.80) simply becomes another way of writing the normalization condition $n_0^2 + m_0^2 = 1$.

We evaluate Eqs. (6.75,6.76,6.79,6.80) in the thermodynamic limit, i.e. we transform Brillouin zone sums to integrals according to

$$\frac{2}{N} \sum_{\mathbf{k}} \xrightarrow{N \rightarrow \infty} V_u \int_{\text{BZ}} \frac{d^2 k}{(2\pi)^2}, \quad (6.81)$$

where V_u is the volume of the magnetic unit cell in real space and the integral is over the reduced Brillouin zone as defined in the previous section.

At any finite temperature the integral $I(h, 0)$ is infrared divergent in two dimensions, signaling the absence of long-range antiferromagnetic order. We set $n = 0$ in Eqs. (6.79) and (6.80), according to the discussion at the beginning of this section. Then these equations can be interpreted as a condition for the staggered field h_s that is necessary to enforce a vanishing staggered magnetization.

Numerically, we calculate the uniform magnetization $m(h, T)$ at finite temperature T by adjusting h_s for fixed external field h such that the condition $n = 0$ is fulfilled in Eqs. (6.79) and (6.80). Using this $h_s(h)$ in Eq. (6.79) then directly yields $m(h, T)$.

We must keep in mind that the staggered field h_s does not respect the rotational symmetry of the original Hamiltonian, which for $h = 0$ corresponds to a global $O(3)$ symmetry and for $h > 0$ is reduced to a global $O(2)$ symmetry around the axis of the uniform field. With the parameterization that explicitly breaks this symmetry, we should therefore only calculate rotationally invariant quantities [64, 93].

Below, we will find a disagreement between a rotationally invariant evaluation of the zero-field uniform susceptibility and the slope of $\partial m/\partial h$ for $h \rightarrow 0$. We attribute this discrepancy to the fact that $\partial m/\partial h|_{h \rightarrow 0}$ does not respect the $O(3)$ symmetry in this limit. Generally, we expect our approach for the finite temperature magnetization to be reasonable only for $h > h_s(h, T)$. In Sec. 6.2.4 we will see that h_s is exponentially small at low temperatures, such that $h > h_s(h, T)$ is fulfilled even for very small external fields. The condition $h > h_s(h, T)$ then roughly gives a limit of validity of our approach in terms of the temperature as $T \lesssim 0.5\tilde{J}_0 S$. The fact that the limits $T \rightarrow 0$ and $h \rightarrow 0$ do not commute in a modified spin-wave expansion was first noticed by Takahashi [21].

At $T = 0$, there are no divergent contributions to the integrals in Eqs. (6.79) and (6.80) in two-spatial dimensions, indicating true long range order. We can thus set

$$h_s = 0, \quad (6.82)$$

and consequently

$$m_0 = h \quad \Rightarrow \quad n_0 = \sqrt{1 - h_0^2}. \quad (6.83)$$

Then the integrals (6.75) and (6.76) are given by

$$R(h) = \frac{1}{2N} \sum_{\mathbf{k}\sigma} \sigma |\gamma_{\mathbf{k}}| \sqrt{\frac{1 + \sigma |\gamma_{\mathbf{k}}|}{1 - \sigma |\gamma_{\mathbf{k}}|(1 - 2h^2)}}, \quad (6.84)$$

$$I(h) = -\frac{1}{2} + \frac{1}{2N} \sum_{\mathbf{k}\sigma} \frac{1 + \sigma |\gamma_{\mathbf{k}}| h^2}{\epsilon_{\mathbf{k}\sigma}}, \quad (6.85)$$

with the spin-wave spectrum:

$$\epsilon_{\mathbf{k}\sigma} = \sqrt{[1 + \sigma |\gamma_{\mathbf{k}}|][1 + \sigma |\gamma_{\mathbf{k}}|(1 - 2h^2)]}. \quad (6.86)$$

We have taken into account that the Bose factor Eq. (6.57) vanishes for $T \rightarrow 0$. The Eqs. 6.79 and 6.80 for uniform and staggered magnetization, respectively, simplify to

$$m(h) = h \left[1 - \frac{R(h)}{S} \right], \quad (6.87)$$

$$n(h) = \frac{1}{\sqrt{1 - h^2}} \left[1 - hm - \frac{I(h)}{S} \right], \quad (6.88)$$

An expression similar to Eq. (6.87) has been obtained previously by Zhitomirsky and Nikuni for the Heisenberg antiferromagnet on a square lattice [31]. Only $m(h)$ was given explicitly and a renormalization of the canting angle θ was found by considering spin-wave interactions. Very recently, the renormalized canting angle was also used

to analyze the behavior of $n(h)$ at $T = 0$ for a more complicated geometry [94].

6.2.2 Uniform susceptibility

In this section we calculate the uniform susceptibility in the framework of the spin-wave theory.

The rotationally invariant uniform zero-field susceptibility per spin is defined as

$$\chi = \frac{1}{TN} \sum_{i,j} \langle \mathbf{S}_i \cdot \mathbf{S}_j \rangle, \quad (6.89)$$

with the spin-spin correlation functions $\langle \mathbf{S}_i \cdot \mathbf{S}_j \rangle$. For a vanishing uniform external magnetic field $h = 0$ the expression for the staggered magnetization (6.80) reduces to

$$n = 1 + \frac{1}{2S} - \frac{2}{NS} \sum_{\mathbf{k}} \frac{n_{\mathbf{k}} + \frac{1}{2}}{\epsilon_{\mathbf{k}}} (1 + 2h_s). \quad (6.90)$$

As explained previously we use a self-consistently determined staggered field h_s to enforce a vanishing order parameter $n = 0$.

Due to the translational invariance of the underlying sublattice the susceptibility (6.89) has a very simple form in momentum space

$$\chi = \frac{1}{T} \langle \mathbf{S}_{\mathbf{q},+} \cdot \mathbf{S}_{-\mathbf{q},+} \rangle_{\mathbf{q}=0}, \quad (6.91)$$

where we have defined the linear combinations

$$\mathbf{S}_{\mathbf{q},\sigma} = \frac{1}{\sqrt{2}} (\mathbf{S}_{\mathbf{q}}^A + \sigma \mathbf{S}_{\mathbf{q}}^B) \quad , \quad \sigma = \pm, \quad (6.92)$$

of the Fourier-transformed spin operators on each sublattice

$$\mathbf{S}_{\mathbf{q}}^{A/B} = \sqrt{\frac{2}{N}} \sum_{\mathbf{r}_i \in A/B} e^{-i\mathbf{q} \cdot \mathbf{r}_i} \mathbf{S}_i. \quad (6.93)$$

It is convenient to decompose Eq. (6.91) into a transverse and a longitudinal part

$$\chi = \chi^{+-} + \chi^{zz}, \quad (6.94)$$

with

$$\chi^{+-} = \frac{1}{2T} \langle S_{\mathbf{q},+}^+ S_{-\mathbf{q},+}^- + S_{\mathbf{q},+}^- S_{-\mathbf{q},+}^+ \rangle_{\mathbf{q}=0} , \quad (6.95)$$

$$\chi^{zz} = \frac{1}{T} \langle S_{\mathbf{q},+}^z S_{-\mathbf{q},+}^z \rangle_{\mathbf{q}=0} . \quad (6.96)$$

We map the spin operators (6.93) onto canonical boson operators via a Dyson-Maleev transformation in momentum space. On a sublattice A we obtain

$$S_{\mathbf{q}}^{A,z} = \sqrt{\frac{N}{2}} S \delta_{\mathbf{q},0} - \sqrt{\frac{2}{N}} \sum_{\mathbf{q}_1, \mathbf{q}_2} \delta_{\mathbf{q}+\mathbf{q}_1, \mathbf{q}_2} a_{\mathbf{q}_1}^\dagger a_{\mathbf{q}_2} , \quad (6.97a)$$

$$S_{\mathbf{q}}^{A,-} = \sqrt{2S} a_{\mathbf{q}} - \frac{1}{\sqrt{2S}} \mathcal{A}_{\mathbf{q}} , \quad (6.97b)$$

$$S_{\mathbf{q}}^{A,+} = \sqrt{2S} a_{-\mathbf{q}}^\dagger , \quad (6.97c)$$

whereas the result on a sublattice B is:

$$S_{\mathbf{q}}^{B,z} = -\sqrt{\frac{N}{2}} S \delta_{\mathbf{q},0} + \sqrt{\frac{2}{N}} \sum_{\mathbf{q}_1, \mathbf{q}_2} \delta_{\mathbf{q}+\mathbf{q}_1, \mathbf{q}_2} b_{\mathbf{q}_2}^\dagger b_{\mathbf{q}_1} , \quad (6.98a)$$

$$S_{\mathbf{q}}^{B,-} = \sqrt{2S} b_{\mathbf{q}}^\dagger - \frac{1}{\sqrt{2S}} \mathcal{B}_{\mathbf{q}}^\dagger , \quad (6.98b)$$

$$S_{\mathbf{q}}^{B,+} = \sqrt{2S} b_{-\mathbf{q}} , \quad (6.98c)$$

with the operators

$$\mathcal{A}_{\mathbf{q}} \equiv \frac{2}{N} \sum_{\mathbf{q}_1, \mathbf{q}_2, \mathbf{q}_3} \delta_{\mathbf{q}+\mathbf{q}_1, \mathbf{q}_2+\mathbf{q}_3} a_{\mathbf{q}_1}^\dagger a_{\mathbf{q}_2} a_{\mathbf{q}_3} \quad (6.99a)$$

$$\mathcal{B}_{\mathbf{q}} \equiv \frac{2}{N} \sum_{\mathbf{q}_1, \mathbf{q}_2, \mathbf{q}_3} \delta_{\mathbf{q}+\mathbf{q}_1, \mathbf{q}_2+\mathbf{q}_3} b_{\mathbf{q}_1}^\dagger b_{\mathbf{q}_2} b_{\mathbf{q}_3} . \quad (6.99b)$$

By substituting Eqs. (6.97,6.98) into Eq. (6.92) we obtain the components of the total spin in the reciprocal space

$$S_{\mathbf{q},+}^z = -\sqrt{\frac{2}{N}} \sum_{\mathbf{q}_1, \mathbf{q}_2} \delta_{\mathbf{q}+\mathbf{q}_1, \mathbf{q}_2} (a_{\mathbf{q}_1}^\dagger a_{\mathbf{q}_2} - b_{\mathbf{q}_2}^\dagger b_{\mathbf{q}_1}) , \quad (6.100a)$$

$$S_{\mathbf{q},+}^- = \sqrt{2S} (a_{\mathbf{q}} + b_{\mathbf{q}}^\dagger) - \frac{1}{\sqrt{2S}} (\mathcal{A}_{\mathbf{q}} + \mathcal{B}_{\mathbf{q}}^\dagger) , \quad (6.100b)$$

$$S_{\mathbf{q},+}^+ = \sqrt{2S} (a_{-\mathbf{q}}^\dagger + b_{-\mathbf{q}}) . \quad (6.100c)$$

Now we can express Eqs. (6.95) and (6.96) in terms of canonical boson operators

$$\begin{aligned}\chi^{+-}(\mathbf{q}) &= \frac{S}{2T} \left\langle (a_{\mathbf{q}} + b_{\mathbf{q}}^{\dagger})(a_{\mathbf{q}}^{\dagger} + b_{\mathbf{q}}) + (a_{-\mathbf{q}}^{\dagger} + b_{-\mathbf{q}})(a_{-\mathbf{q}} + b_{-\mathbf{q}}^{\dagger}) \right\rangle \\ &- \frac{1}{4T} \left\langle (\mathcal{A}_{\mathbf{q}} + \mathcal{B}_{\mathbf{q}}^{\dagger})(a_{\mathbf{q}}^{\dagger} + b_{\mathbf{q}}) + (a_{-\mathbf{q}}^{\dagger} + b_{-\mathbf{q}})(\mathcal{A}_{-\mathbf{q}} + \mathcal{B}_{-\mathbf{q}}^{\dagger}) \right\rangle, \quad (6.101)\end{aligned}$$

$$\begin{aligned}\chi^{zz}(\mathbf{q}) &= \frac{2}{TN} \sum_{\mathbf{q}_1, \mathbf{q}_2, \mathbf{q}_3, \mathbf{q}_4} \delta_{\mathbf{q}+\mathbf{q}_1, \mathbf{q}_2} \delta_{\mathbf{q}_3, \mathbf{q}+\mathbf{q}_4} \\ &\times \left\langle (a_{\mathbf{q}_1}^{\dagger} a_{\mathbf{q}_2} - b_{\mathbf{q}_2}^{\dagger} b_{\mathbf{q}_1})(a_{\mathbf{q}_3}^{\dagger} a_{\mathbf{q}_4} - b_{\mathbf{q}_4}^{\dagger} b_{\mathbf{q}_3}) \right\rangle. \quad (6.102)\end{aligned}$$

Alternatively, we would obtain these results also by formulating the spin-spin correlation functions χ^{+-} , χ^{zz} in terms of canonical boson operators in real space first and then performing the Fourier transformation into the reciprocal space.

We evaluate above expectation values using the bosonic version of the Wick theorem [95]

$$\begin{aligned}\chi^{+-}(\mathbf{q}) &= \frac{S}{2T} \left[(2P_{\mathbf{q}} + 1) + (2P_{-\mathbf{q}} + 1) - (Q_{\mathbf{q}} + Q_{\mathbf{q}}^{\star}) - (Q_{-\mathbf{q}} + Q_{-\mathbf{q}}^{\star}) \right] \\ &\times \left[1 - \frac{2}{NS} \sum_{\mathbf{k}} P_{\mathbf{k}} \right], \quad (6.103)\end{aligned}$$

$$\chi^{zz}(\mathbf{q}) = \frac{2}{TN} \sum_{\mathbf{k}} (P_{\mathbf{k}} + P_{\mathbf{k}+\mathbf{q}} + 2P_{\mathbf{k}}P_{\mathbf{k}+\mathbf{q}} - Q_{\mathbf{k}}Q_{\mathbf{k}+\mathbf{q}}^{\star} - Q_{\mathbf{k}+\mathbf{q}}Q_{\mathbf{k}}^{\star}), \quad (6.104)$$

with the only nonzero contractions

$$\left\langle a_{\mathbf{k}}^{\dagger} a_{\mathbf{q}} \right\rangle = \left\langle b_{\mathbf{k}}^{\dagger} b_{\mathbf{q}} \right\rangle = \delta_{\mathbf{k}, \mathbf{q}} \left[(|u_{\mathbf{k}}|^2 + |v_{\mathbf{k}}|^2) n_{\mathbf{k}} + |v_{\mathbf{k}}|^2 \right] \equiv \delta_{\mathbf{k}, \mathbf{q}} P_{\mathbf{k}}, \quad (6.105)$$

$$\left\langle a_{\mathbf{k}}^{\dagger} b_{\mathbf{q}}^{\dagger} \right\rangle = \left\langle a_{\mathbf{k}} b_{\mathbf{q}} \right\rangle^{\star} = \delta_{\mathbf{k}, \mathbf{q}} |u_{\mathbf{k}}| |v_{\mathbf{k}}| (2n_{\mathbf{k}} + 1) \equiv \delta_{\mathbf{k}, \mathbf{q}} Q_{\mathbf{k}}. \quad (6.106)$$

In general the coefficients of the Bogoliubov transformation $u_{\mathbf{k}}$ and $v_{\mathbf{k}}$ are complex numbers. In our case they are real and are given by Eqs. (6.39a, 6.39b) for vanishing uniform magnetic field $h = 0$. The corresponding expressions for the contractions read

$$P_{\mathbf{k}} = \frac{n_{\mathbf{k}} + \frac{1}{2}}{\epsilon_{\mathbf{k}}} (1 + 2h_s), \quad (6.107)$$

$$Q_{\mathbf{k}} = \frac{n_{\mathbf{k}} + \frac{1}{2}}{\epsilon_{\mathbf{k}}} |\gamma_{\mathbf{k}}|. \quad (6.108)$$

Substituting Eq. (6.107) into the last part of Eq. (6.103) yields immediately the zero

staggered magnetization condition (6.90)

$$1 - \frac{2}{NS} \sum_{\mathbf{k}} P_{\mathbf{k}} = n = 0. \quad (6.109)$$

Hence in the spin-wave approximation the transversal spin-spin correlation function vanishes for all momenta \mathbf{q}

$$\chi^{+-}(\mathbf{q}) = 0, \quad (6.110)$$

and only the longitudinal part contributes to the uniform susceptibility

$$\chi = \chi^{zz}(\mathbf{q} = 0) = \frac{2}{TN} \sum_{\mathbf{k}} n_{\mathbf{k}}(n_{\mathbf{k}} + 1). \quad (6.111)$$

Apart from a different normalization, this is the result of Ref. [21]. We evaluate Eq. (6.111) numerically in the thermodynamic limit.

6.2.3 Specific heat

In this section we determine the low-temperature behavior of the specific heat.

Specific heat per site at a constant uniform field is given by:

$$C_h(T) = \frac{1}{N} \left. \frac{\partial U}{\partial T} \right|_h, \quad (6.112)$$

where U is the internal energy of the system. We rewrite above expression using the chain rule

$$C_h(T) = \frac{1}{N} \left. \frac{\partial U}{\partial S} \right|_h \left. \frac{\partial S}{\partial T} \right|_h, \quad (6.113)$$

with entropy S . Utilizing standard relations between thermodynamic potentials

$$T = \left. \frac{\partial U}{\partial S} \right|_h \quad (6.114)$$

$$-S = \left. \frac{\partial F}{\partial T} \right|_h, \quad (6.115)$$

we obtain for the specific heat

$$C_h(T) = -\frac{T}{N} \left. \frac{\partial^2 F}{\partial T^2} \right|_h, \quad (6.116)$$

where the Helmholtz free energy of the noninteracting spin-wave Hamiltonian is given by Eq. (6.56). Temperature dependence of the free energy is essentially given by a $e^{1/T}$ behavior of the Bose function (6.57). Performing partial derivatives of the free

energy with respect to the temperature yields for the specific heat:

$$C_h(T) = \left(\frac{\tilde{J}_0 S}{T} \right)^2 \frac{1}{N} \sum_{\mathbf{k}} \sum_{\sigma=\pm} (n_{\mathbf{k}\sigma} \epsilon_{\mathbf{k}\sigma})^2 e^{\tilde{J}_0 S \epsilon_{\mathbf{k}\sigma} / T}. \quad (6.117)$$

We evaluate the zero-field version of this expression in the thermodynamical limit, similarly to the case of the susceptibility.

6.2.4 Staggered correlation length

The energy gap appearing in Eq. (6.50) can be related to the staggered correlation length ξ , as discussed by Takahashi [21]. Assuming for simplicity that a is the lattice constant of the underlying lattice, we may identify

$$\left(\frac{a}{2\xi} \right)^2 = \Delta^2 = \frac{4h_s}{n_0}. \quad (6.118)$$

In the absence of a uniform field the low temperature behavior of ξ has been thoroughly studied by Chakravarty, Halperin and Nelson [17]. Surprisingly, the effect of a uniform field h on ξ has so far not been investigated. We now analyze the asymptotic behavior of ξ at low temperatures. In two spatial dimensions, the limit $T \rightarrow 0$ also implies $h_s \rightarrow 0$. Our self-consistency equations (6.79) and (6.80) can then be solved analytically by isolating divergent contributions to the integrals $I(h, h_s)$ and $R(h, h_s)$ originating from gapless modes in the spin-wave spectrum. In the regular part of the integral, the limit $T \rightarrow 0$ and $h_s \rightarrow 0$ can be taken. For the leading behavior at small uniform fields $h \ll 1$ only the singular part of $I(h, h_s)$ contributes, and we obtain the self-consistency condition

$$0 = n(0) - \frac{I^{\text{sing}}(h, h_s)}{S}. \quad (6.119)$$

Here, $I^{\text{sing}}(h, h_s)$ is the part of the integral $I(h, h_s)$ that diverges for vanishing gaps in the spin-wave dispersions, and $n(0) = n(h = 0, h_s = 0, T = 0)$. For $h \ll 1$, we obtain

$$\begin{aligned} I^{\text{sing}}(h, h_s) &= \frac{T}{\tilde{J}_0 S} \frac{V_u}{2} \sum_{\sigma} \int \frac{d^2 k}{(2\pi)^2} \frac{1}{\epsilon_{\mathbf{k}\sigma}^2} \\ &\approx -\frac{T}{\tilde{J}_0 S} \frac{V_u}{8\pi \ell_x \ell_y} \left[\ln \left(\frac{4h_s}{n_0} \right) + \ln \left(4h^2 + \frac{4h_s}{n_0} \right) \right], \end{aligned} \quad (6.120)$$

to leading logarithmic order. From Eqs. (6.118) and (6.119) we then obtain the following result for the self-consistent energy gap in a small uniform magnetic field

$$\Delta^2(h) = \left(\frac{a}{2\xi(h)} \right)^2 = \sqrt{\Delta_0^4 + \frac{(2h)^4}{4}} - \frac{(2h)^2}{2}, \quad (6.121)$$

where $\Delta_0 = a/2\xi(0)$ is the gap for vanishing uniform field and the temperature dependence of the zero-field staggered correlation length is given by

$$\frac{\xi(0)}{a} \propto \exp \left(\frac{2\pi \tilde{J}_0 S^2 n(0)}{T} \frac{\ell_x \ell_y}{V_u} \right). \quad (6.122)$$

For a square lattice this yields with $\tilde{J}_0 = 4J$ and $\ell_x \ell_y / V_u = 1/4$

$$\frac{\xi(0)}{a} \propto \exp \left(\frac{2\pi J S^2 n(0)}{T} \right), \quad (6.123)$$

which is identical to Takahashi's result (see Eq. (27a) in Ref. [21]), except that we do not include a spin-wave velocity renormalization in our approach. To obtain this renormalization, the spin-wave interaction would have to be treated on the mean-field level in a fully self-consistent way.

The field dependence of the correlation length for fixed temperature is given by Eq. (6.121). For $h \ll \Delta_0(T)$, we have

$$\xi(h) = \xi(0) \left[1 + \frac{1}{2} \left(\frac{h}{\Delta_0} \right)^2 \right], \quad (6.124)$$

whereas for $h \gg \Delta_0(T)$, we obtain

$$\frac{\xi(h)}{a} = 4h \left(\frac{\xi(0)}{a} \right)^2. \quad (6.125)$$

From Eq. (6.121) it is clear that $\xi(h) > \xi(0)$. Thus, the correlation length is increased by a small uniform field due to reduced quantum fluctuations.

The temperature dependence of the correlation length for fixed uniform field h can also be extracted from Eq. (6.121). As long as $\Delta_0(T) \gg 2h$, this temperature dependence is still given by Eq. (6.122). When the temperature is further reduced, Eq. (6.121) predicts a crossover at $\Delta_0(T) \approx 2h$ to the following temperature-dependent correlation length

$$\frac{\xi(h)}{a} \propto \exp \left(\frac{4\pi \tilde{J}_0 S^2 n(0)}{T} \frac{\ell_x \ell_y}{V_u} \right). \quad (6.126)$$

The additional factor of two in the exponent as compared to Eq. (6.122) is due to the fact that at very low temperatures the spin-wave mode $\epsilon_{\mathbf{k}-}$ yields a singular contribution, whereas the mode $\epsilon_{\mathbf{k}+}$ has a gap $2h$ which is fixed by the external field. In contrast, for $h = 0$ both modes contribute equally, leading to Eq. (6.122).

The analysis in this section has been carried out for $h \ll 1$. For larger fields, there are field dependent prefactors of the first logarithm in Eq. (6.120) leading to a field dependent renormalization factor Z_h in the exponent of Eq. (6.126). The field dependence of the correlation length at fixed temperature is then no longer determined by the singular contributions to the integrals and cannot be extracted from the simple analysis presented here. Close to the critical field at $h = 1$ the nature of the divergences changes, since the dispersion of the $\sigma = -$ mode becomes quadratic. As our mean-field calculation is not suitable to describe the true critical behavior in two dimensions, we do not discuss this limit in more detail.

6.3 Applications to an antiferromagnet on a distorted honeycomb lattice

In this final part of the present chapter, we apply the theoretical results obtained above to the special case of a Heisenberg antiferromagnet on a distorted honeycomb lattice. This is motivated by a recent synthesis of a novel low-dimensional metal-organic magnet and the respective experiments, see Sec. 6.3.1. After we introduce the distorted honeycomb lattice in Sec. 6.3.2 we present results for the energy spectrum (Sec. 6.3.3), uniform and staggered magnetization (Secs. 6.3.4, 6.3.5), uniform susceptibility (Sec. 6.3.6) and specific heat (Sec. 6.3.7). In addition, we have performed quantum Monte Carlo calculations using the stochastic series expansion and compare our numerical findings with the spin-wave results. Finally, we fit the experimental curves to consistently extract the strength of the coupling constants.

6.3.1 Experimental motivation

Let us first present the structure of a newly synthesized metal-organic magnet in order to substantiate the study of a two-dimensional Heisenberg antiferromagnet on a distorted honeycomb lattice in the following sections. The synthesis is due to Schmidt et al. [32] and the experiments were performed by Pashchenko et al. [32, 96].

Motivated by the challenge to find low-dimensional metal-organic magnets where the magnetic moments are coupled sufficiently strongly to exhibit interesting collective effects, Schmidt and co-workers synthesized transition metal complexes of o-hydroxynaphthoic acids. These complexes exhibit layered structures with strong magnetic couplings within the layers and weak interactions between the layers. The layer struc-

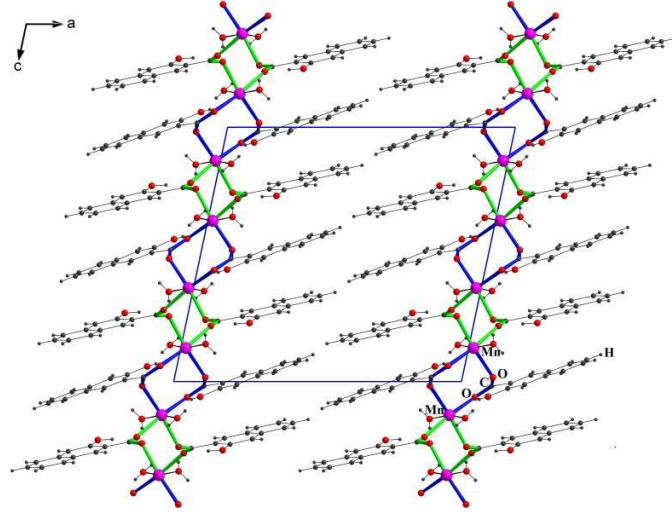


Figure 6.4: View along the b -axis of the metal-organic quantum magnet $\text{Mn}[\text{C}_{10}\text{H}_6(\text{OH})(\text{COO})]_2 \times 2\text{H}_2\text{O}$. Bold lines show exchange paths $\text{Mn}-\text{O}-\text{C}-\text{O}-\text{Mn}$. The unit cell, denoted by the parallelogram, contains four crystallographically equivalent Mn^{2+} ions. This picture is courtesy of V. Pashchenko [96].

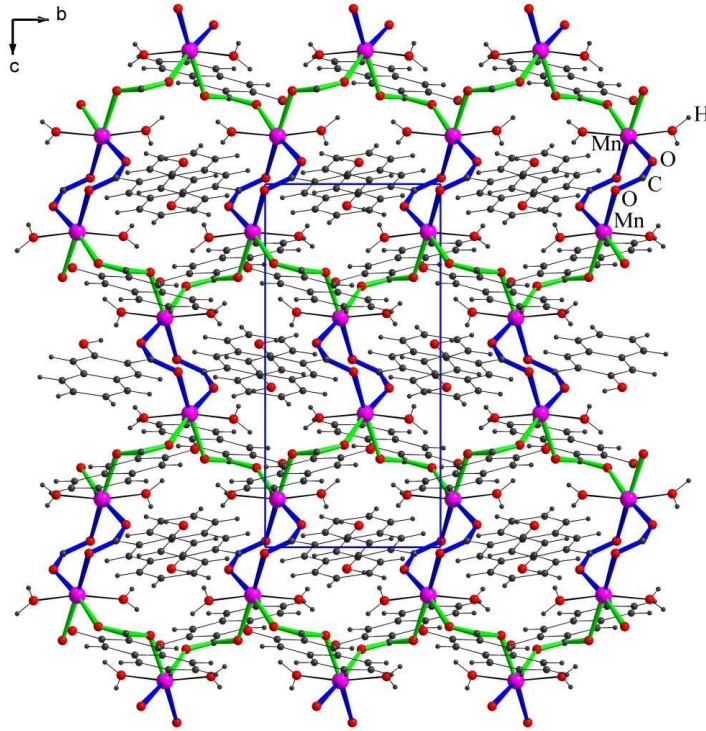


Figure 6.5: View on the (bc) plane of the metal-organic quantum magnet $\text{Mn}[\text{C}_{10}\text{H}_6(\text{OH})(\text{COO})]_2 \times 2\text{H}_2\text{O}$. This picture is courtesy of V. Pashchenko [96].

tures are built up chemically from spin-bearing metal ions (in this case Mn^{2+}), which are connected by short bridges, being separated by organic fragments of considerable size, see Fig. 6.4.

The crystal structure of $\text{Mn}[\text{C}_{10}\text{H}_6(\text{OH})(\text{COO})]_2 \times 2\text{H}_2\text{O}$ (systematic name: manganese(II) 3-hydroxy-2-naphthoate dihydrate) is of particular interest, because the Mn^{2+} ions form a distorted honeycomb lattice (Fig. 6.5). The compound crystallizes in the monoclinic space group $P2_1/c$ with the lattice parameters $a = 17.191(4) \text{ \AA}$, $b = 7.3448(10) \text{ \AA}$, $c = 15.5279(17) \text{ \AA}$, $\beta = 101.964(8)^\circ$, $V = 1918.1(5) \text{ \AA}^3$. The unit cell contains four crystallographically equivalent Mn^{2+} ions.

The coupling layer, parallel to the (bc) plane, contains the Mn^{2+} ions, the COO^- and OH groups as well as water molecules. The isolating layer, having a thickness of about 12 \AA consists of the organic naphthalene moieties. These naphthalene moieties are only bound together by van der Waals contacts between C and H atoms. The relative weakness of these interactions is reflected by the morphology of the crystals: the crystals grow in (b) and (c) direction much faster than in (a) direction, thus forming thin plates parallel to the (bc) plane.

The magnetism is due to the $S = 5/2$ manganese ions which form a distorted honeycomb pattern parallel to the (bc) planes. Neighboring ions are connected by carboxylic groups, which provide an $\text{Mn} - \text{O} - \text{C} - \text{O} - \text{Mn}$ magnetic exchange path. There are two different exchange paths: the first path contains a single $\text{O} - \text{C} - \text{O}$ unit, displayed in green in Fig. 6.5. In the second path (marked with blue color) the Mn^{2+} ions are connected by two $\text{O} - \text{C} - \text{O}$ moieties simultaneously. The honeycomb layers are well separated from each other; the closest distances between Mn^{2+} ions of different layers are as large as 16.282 \AA .

Magnetic measurements were carried out by Pashchenko et al. on a single crystalline sample of the compound $\text{Mn}[\text{C}_{10}\text{H}_6(\text{OH})(\text{COO})]_2 \times 2\text{H}_2\text{O}$ using a Quantum Design SQUID magnetometer MPMS-XL [32, 96]. Isothermal magnetization runs at temperatures between 2 K and 200 K and fields up to 5 T were performed as well as measurements of the susceptibility in the temperature range 2 – 300 K for a magnetic field of 0.05 – 2 T.

6.3.2 Distorted honeycomb lattice

The structure in Fig. 6.5 suggests that the magnetic properties of the material can be modeled by a spin $S = 5/2$ Heisenberg magnet on the distorted honeycomb lattice shown in Fig. 6.6.

The spin at a given site \mathbf{r}_i interacts with its nearest neighbors at $\mathbf{r}_i + \delta_\nu$ via exchange couplings

$$J_\nu = J(\mathbf{r}_i, \mathbf{r}_i + \delta_\nu) \quad , \quad \nu = \mathbf{1}, \mathbf{2}, \mathbf{3} . \quad (6.127)$$

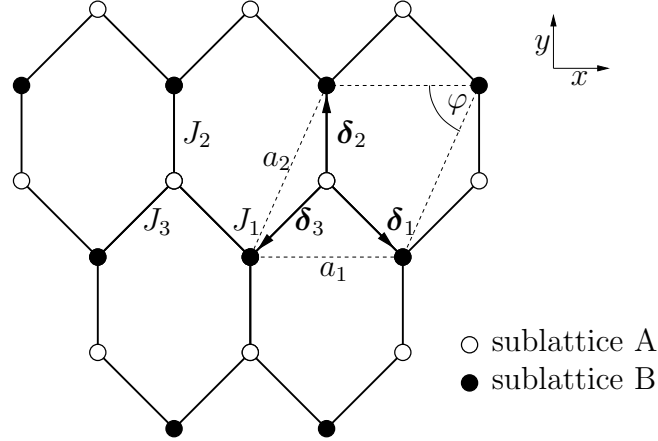


Figure 6.6: Distorted honeycomb lattice. The interactions between spins are displayed as solid lines. The underlying magnetic sublattice is a centered monoclinic Bravais lattice and its primitive cell can be chosen to be the dashed parallelogram. The corresponding primitive vectors are \mathbf{a}_1 and \mathbf{a}_2 .

All exchange integrals J_ν turn out to be positive, and due to the crystal symmetry

$$|\delta_1| = |\delta_3| \equiv \delta_1, \quad (6.128)$$

$$J_1 = J_3. \quad (6.129)$$

A closer look at the crystal structure in Fig. 6.5 and a comparison with the distorted honeycomb lattice in Fig. 6.6 reveals that J_2 acts along two exchange paths while J_1 results from a single exchange path. Therefore we expect J_2 to be roughly twice as large as J_1 . Because the honeycomb lattice is bipartite, for positive J_ν the system is not frustrated, and when quantum fluctuations are neglected the ground state shows classical antiferromagnetic Néel order. More generally, we expect long-range antiferromagnetic order to persist in the quantum mechanical ground state.

Note that the actual structure shown in Fig. 6.5 has an additional distortion in the x direction, resulting in a primitive cell with doubled volume. Due to the low symmetry of the lattice the Dzyaloshinskii-Moriya interaction might play an important role. However, we expect the corresponding energy scale to be small in comparison with J_1 and J_2 , so that in the first approximation we can neglect this effect.

In the following we therefore always work with the magnetically equivalent Bravais sublattices shown in Fig. 6.6. The unit cell is denoted by a dashed parallelogram and the corresponding primitive vectors are

$$\mathbf{a}_1 = a_1 \hat{\mathbf{e}}_x \quad (6.130a)$$

$$\mathbf{a}_2 = a_2 \cos \varphi \hat{\mathbf{e}}_x + a_2 \sin \varphi \hat{\mathbf{e}}_y. \quad (6.130b)$$

Now, after settling these general issues, we can apply the spin-wave results obtained in previous sections of this chapter to the Heisenberg antiferromagnet on the distorted honeycomb lattice.

6.3.3 Energy dispersion

The reciprocal of the Bravais lattice defined in Fig. 6.6 is a monoclinic Bravais lattice with the magnetic Brillouin zone shown in Fig. 6.7. The primitive vectors of the reciprocal lattice are

$$\mathbf{b}_1 = \frac{2\pi}{a_1 \sin \varphi} (\sin \varphi \hat{\mathbf{e}}_x - \cos \varphi \hat{\mathbf{e}}_y) \quad (6.131a)$$

$$\mathbf{b}_2 = \frac{2\pi}{a_2 \sin \varphi} \hat{\mathbf{e}}_y, \quad (6.131b)$$

where a_1 , a_2 and the angle φ are defined in Fig. 6.6.

Now we can apply the general expression (6.44) for the spin-wave spectrum of the Heisenberg antiferromagnet in uniform external magnetic field to our honeycomb lattice with $|\delta_1| = |\delta_3|$ and $J_1 = J_3$. In Fig. 6.8 the dispersion is plotted for vanishing staggered field and different values of the uniform field. For $h = 0$ we obtain a gapless doubly degenerate mode, as expected from Eq. (6.53). For a finite value of $h > 0$ a gap opens in the branch $\epsilon_{\mathbf{k}+}$, while $\epsilon_{\mathbf{k}-}$ remains gapless.

Next, let us consider the long-wavelength limit $\mathbf{k} \rightarrow 0$. If we diagonalize the structure factor $|\gamma_{\mathbf{k}}|$ according to Eq. (6.47), then the eigenvectors of \mathbf{A} are parallel to the x -axis and the y -axis, with respective eigenvalues

$$\ell_x^2 = \frac{J_1}{2\tilde{J}_0} a_1^2, \quad (6.132a)$$

$$\ell_y^2 = \frac{2J_1J_2}{\tilde{J}_0^2} a_2^2 \sin^2 \varphi. \quad (6.132b)$$

The spin-wave velocities $c_\alpha = \tilde{J}_0 S \ell_\alpha$ along the two principal directions are thus

$$c_x = S \sqrt{\frac{J_1 \tilde{J}_0}{2}} a_1, \quad (6.133a)$$

$$c_y = S \sqrt{2J_1J_2} a_2 \sin \varphi. \quad (6.133b)$$

Note that for $J_2 \rightarrow 0$ the velocity c_y vanishes, so that the system becomes one-dimensional, as is obvious from Fig. 6.6. On the other hand, for $J_1 \rightarrow 0$ both velocities vanish, because in this limit the system consists of decoupled dimers.

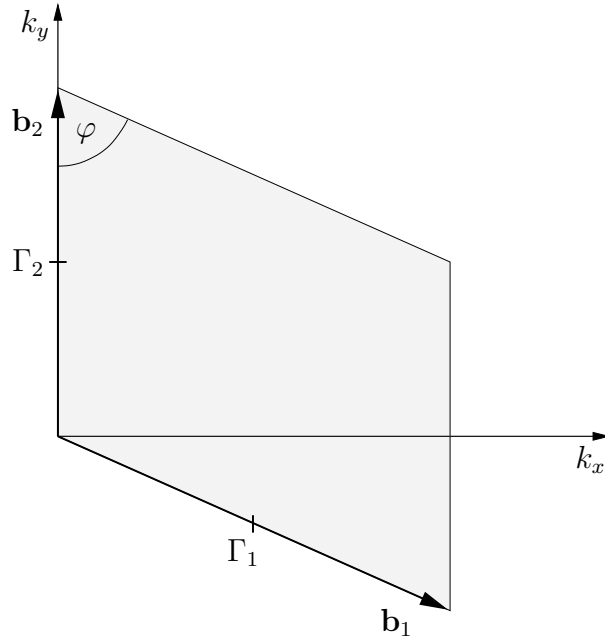


Figure 6.7: Reduced Brillouin zone of the distorted honeycomb lattice shown in Fig. 6.6. The primitive vectors are \mathbf{b}_1 and \mathbf{b}_2 .

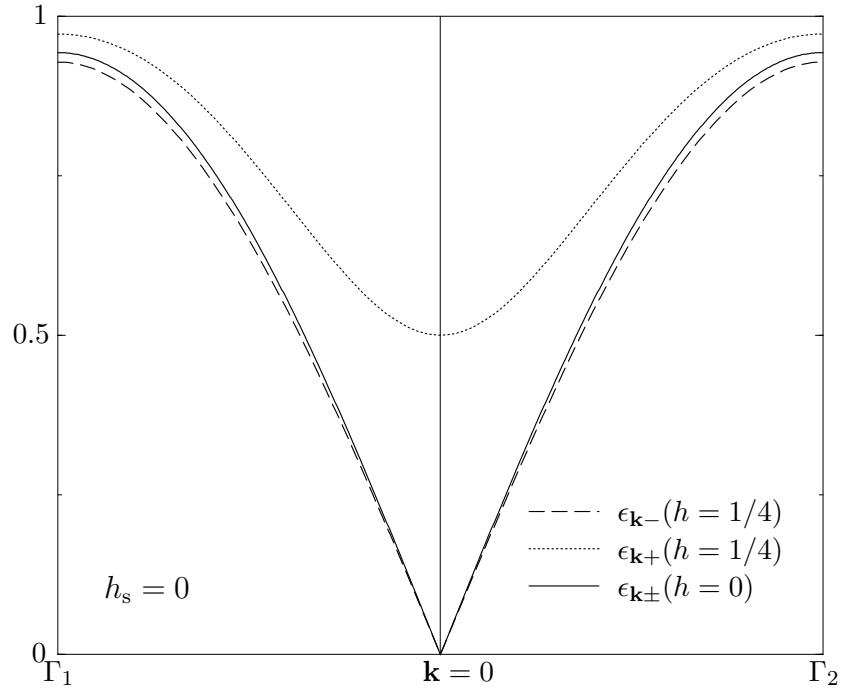


Figure 6.8: Dimensionless spin-wave spectrum of the Heisenberg antiferromagnet on the distorted honeycomb lattice for $h_s = 0$ and different values of h . For symmetry reasons, the dispersion is drawn along the boundaries $\Gamma_1 \rightarrow 0$ and $0 \rightarrow \Gamma_2$ of the reduced Brillouin zone (see Fig. 6.7).

6.3.4 Zero-temperature uniform and staggered magnetization

In this section we focus on the uniform and staggered magnetization at $T = 0$. At the end of Sec. 6.2.1 we have derived the relevant expressions within linear spin-wave theory, see Eqs. (6.82-6.88). We set $h_s = 0$ throughout this section due to the existence of true long-range order at zero temperature. As the deviations from the classical curves are rather small for $S = 5/2$, we alternatively present the curves for the extreme quantum case $S = 1/2$ where appropriate.

The uniform magnetization in Fig. 6.9 shows a positive curvature for all $0 \leq h < 1$ and lies generally below the classical straight line. This has been already observed in Ref. [31] for the square lattice. This tendency is stronger for the honeycomb lattice and is even more pronounced for anisotropic exchange couplings with $J_1 \gg J_2$. The number of nearest neighbors $z = 3$ for the honeycomb lattice is lower than for the square lattice ($z = 4$), and in the limit $J_2 \ll J_1$ the system is almost one-dimensional. The observed tendency thus simply corresponds to increased quantum fluctuations in

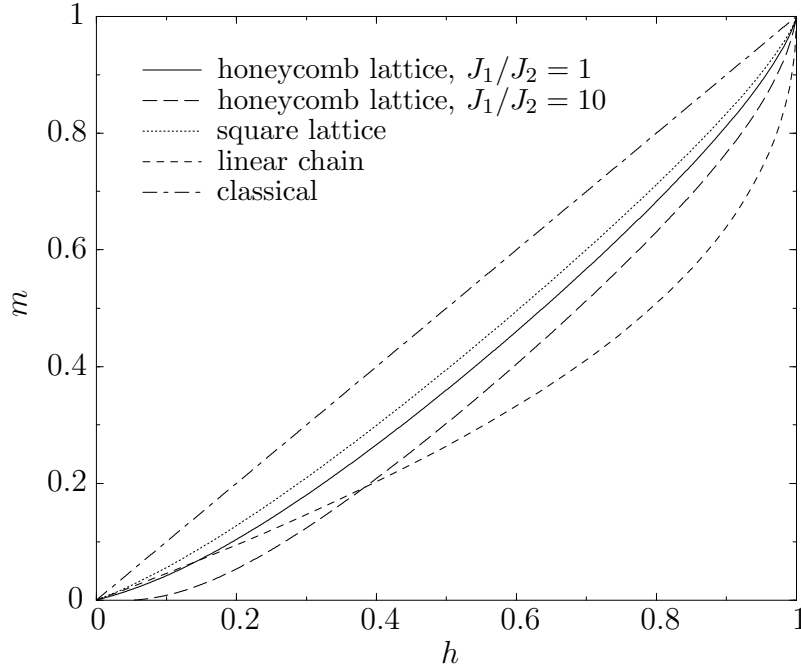


Figure 6.9: Normalized uniform magnetization $m(h)$ for $T = 0$ and $h_s = 0$. The solid line is the zero-temperature magnetization curve for the honeycomb lattice with $S = 1/2$ and $J_1 = J_2$. For comparison we also show the corresponding curve for a square lattice and exact results for a linear antiferromagnetic chain [97]. However, the $S = 1/2$ chain is critical, so it is not surprising that it is poorly described by means of the spin-wave theory. Note that for $h_s = 0$ the classical magnetization is simply $m_0 = h$.

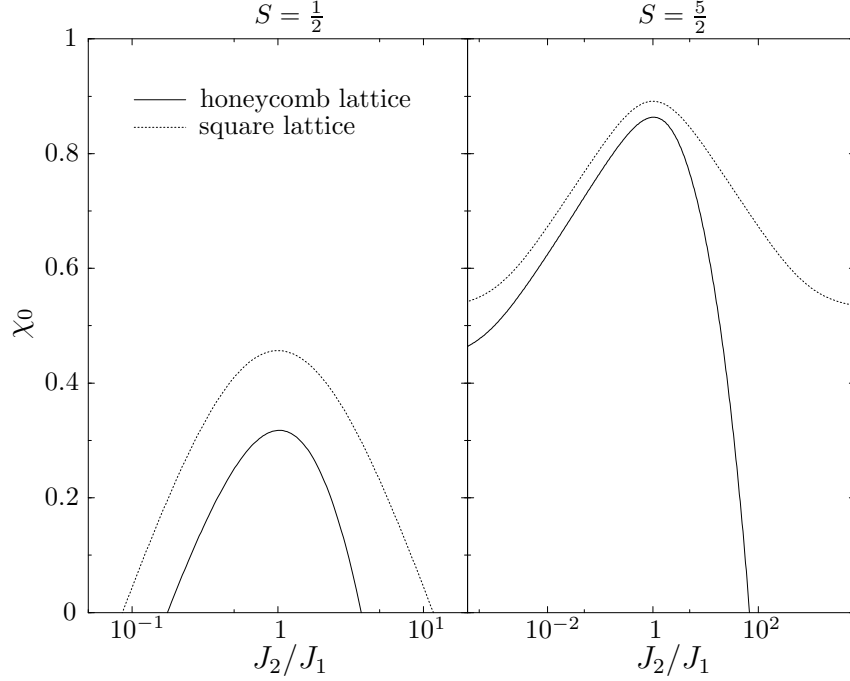


Figure 6.10: Zero-field susceptibility χ_0 as a function of the coupling ratio J_2/J_1 for $S = \frac{1}{2}, \frac{5}{2}$. Results for the distorted honeycomb lattice (solid line) and for the square lattice (dotted line) are compared.

low dimensions.

For small external magnetic fields $h \ll 1$ we can expand the uniform magnetization in powers of h :

$$m(h) = \chi_0 m + \mathcal{O}(h^3), \quad (6.134)$$

with the zero-field susceptibility

$$\chi_0 = 1 - \frac{R(h=0)}{S} = 1 - \frac{1}{2NS} \sum_{\mathbf{k}\sigma} \sigma |\gamma_{\mathbf{k}}| \sqrt{\frac{1 + \sigma |\gamma_{\mathbf{k}}|}{1 - \sigma |\gamma_{\mathbf{k}}|}}. \quad (6.135)$$

Fig. 6.10 shows χ_0 for a varying coupling ratio J_2/J_1 . Note that χ_0 is always below the classical value 1 and is suppressed exponentially with increasing anisotropy. For the honeycomb lattice, this effect is more pronounced for $J_2 \gg J_1$.

Beyond the saturation field $h = 1$ the ground state has full collinear ferromagnetic order. This state as well as single magnon excitations above it are easily shown to be exact eigenstates. As the single magnon states become gapless at exactly the classical value $h = 1$, the saturation field is not changed by quantum fluctuations or magnon interactions.

The limit $h \rightarrow 1$ is reached with infinite slope in $m(h)$. The leading behavior is

given by

$$m = 1 + \frac{V_u}{4\ell_x\ell_y} \frac{\delta h}{\pi S} \ln(4\delta h) , \quad (6.136)$$

where

$$\delta h = 1 - h . \quad (6.137)$$

This logarithmic asymptotics was first discussed in the language of Bose condensation of magnons below the saturation field [98] and was later found for the square lattice ($V_u/4\ell_x\ell_y = 1$) within linear spin-wave theory [31]. For our distorted honeycomb lattice, we have

$$\frac{V_u}{\ell_x\ell_y} = \sqrt{\frac{(2J_1 + J_2)^3}{J_1^2 J_2}} , \quad (6.138)$$

which diverges for $J_1 \rightarrow 0$ or $J_2 \rightarrow 0$ and thus exemplifies the increasing deviations from the classical curve for strongly anisotropic exchange couplings.

The staggered magnetization in Fig. 6.11 shows a non-monotonic dependence on the applied uniform field. For vanishing h the staggered magnetization decreases as we lower the effective dimensionality. For $h = 0$ the expression for the staggered magnetization Eq. (6.88) simplifies to:

$$n(h=0) = 1 - \frac{I(h=0)}{S} = 1 + \frac{1}{2S} - \frac{1}{NS} \sum_{\mathbf{k}} \frac{1}{\epsilon_{\mathbf{k}}} . \quad (6.139)$$

The exponential suppression of the zero-field order parameter $n(h=0)$ with increasing anisotropy and in turn decreasing effective dimensionality is shown in Fig. 6.12. Again, for the honeycomb lattice the effect is stronger for $J_2 \gg J_1$, i.e. the order parameter vanishes faster in the “dimer”-limit.

An external field apparently suppresses quantum fluctuations and $n(h)$ first increases with h before it reaches a maximum and then vanishes for $h \rightarrow 1$ with infinite slope. The asymptotic behavior is given by

$$n = -\frac{V_u}{2\ell_x\ell_y} \frac{\sqrt{\delta h}}{\pi S} \ln(4\delta h) . \quad (6.140)$$

Interestingly, the quantum corrections to the staggered magnetization are positive close to the saturation field and the spin-wave result therefore intersects the classical curve. In a quasi one-dimensional situation ($J_2 \ll J_1$), quantum fluctuations are strong and the leading order spin-wave theory, when pushed to the limit of validity, predicts a quantum disordered phase for small uniform fields.

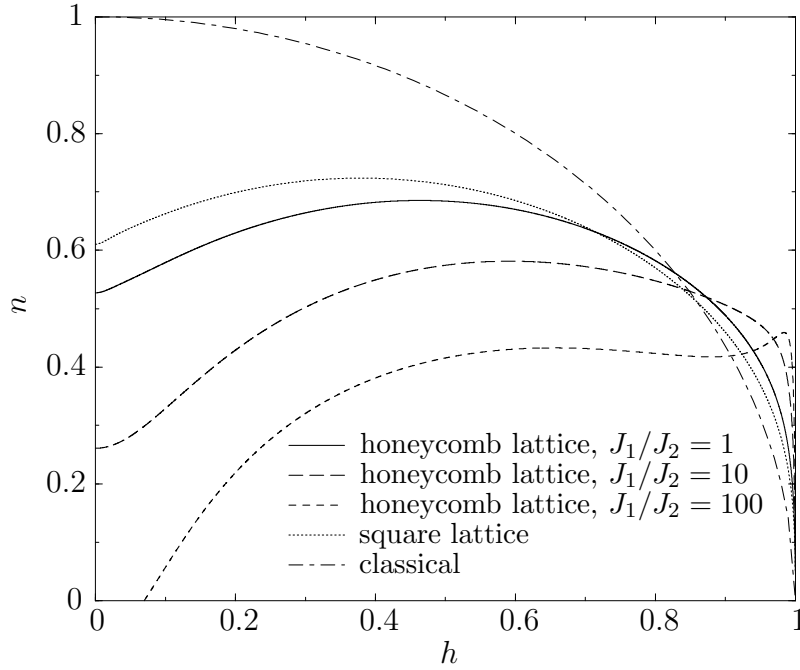


Figure 6.11: Normalized staggered magnetization $n(h)$ at $T = 0$ for honeycomb (solid line) and square lattice with $S = 1/2$ (dotted line). The classical equation $n_0 = \sqrt{1 - h^2}$ is plotted for comparison. We also show the curves for the anisotropic cases $J_1/J_2 = 10, 100$.

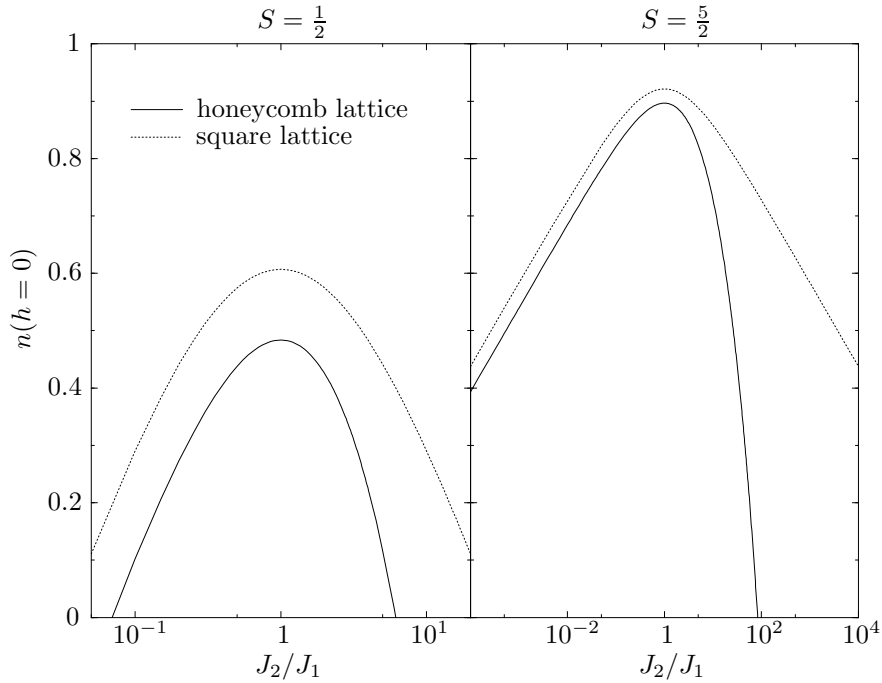


Figure 6.12: Normalized sublattice magnetization $n(h = 0)$ as a function of the coupling ratio J_2/J_1 for $S = \frac{1}{2}, \frac{5}{2}$. Results for the distorted honeycomb lattice (solid line) and for the square lattice (dotted line) are compared.

6.3.5 Finite-temperature magnetization curve

In the first part of this section we present theoretical magnetization curves and compare the results of our spin-wave expansion with numerical findings. In the second part we perform a fit to the experimental magnetization curves and give quantitative estimates for the exchange couplings.

In Fig. 6.13 we show the magnetization curves $m(h)$ for the honeycomb lattice with $S = 5/2$ and $J_1 = J_2$ at different temperatures T as obtained from the spin-wave theory in Sec. 6.2.1. For $T \ll \tilde{J}_0 S$ the magnetization is almost linear throughout the entire field range. At intermediate temperatures $m(h)$ has an S-like shape with a positive curvature at small fields h that changes to a negative curvature with increasing h .

In addition, we have also performed a quantum Monte Carlo simulation for the two-dimensional Heisenberg antiferromagnet on a square lattice. We compare the results of quantum Monte Carlo and spin-wave theory in Fig. 6.14. For low temperatures both magnetization curves show qualitatively the same behavior. In the vicinity of the classical saturation field $h = 1$ the spin-wave magnetization approaches a plateau with $m \approx 1$, while the quantum Monte Carlo curve saturates at larger fields $h > 1$.

It turns out that the magnetization as well as the susceptibility are not very

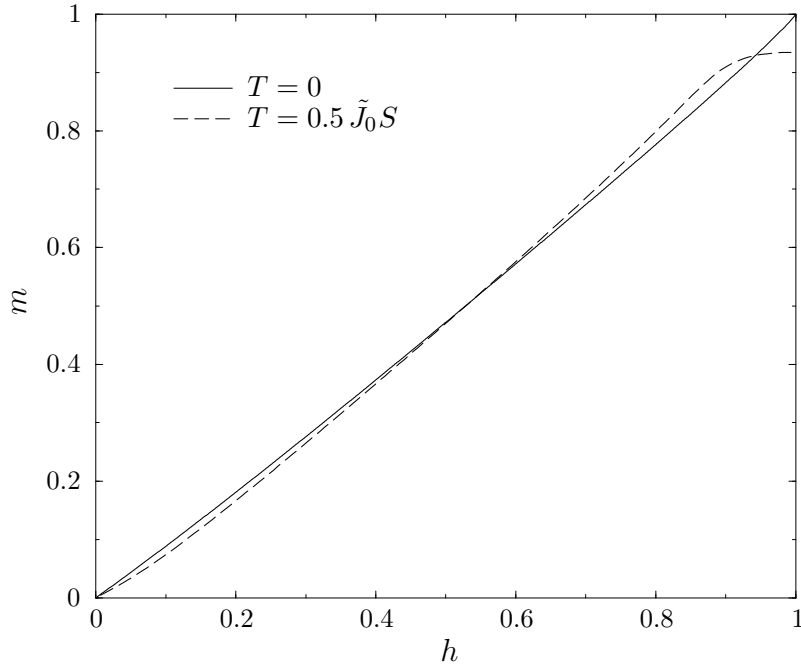


Figure 6.13: Uniform magnetization $m(h)$ for the honeycomb lattice with $S = 5/2$ and $J_1 = J_2$ for two values of T .

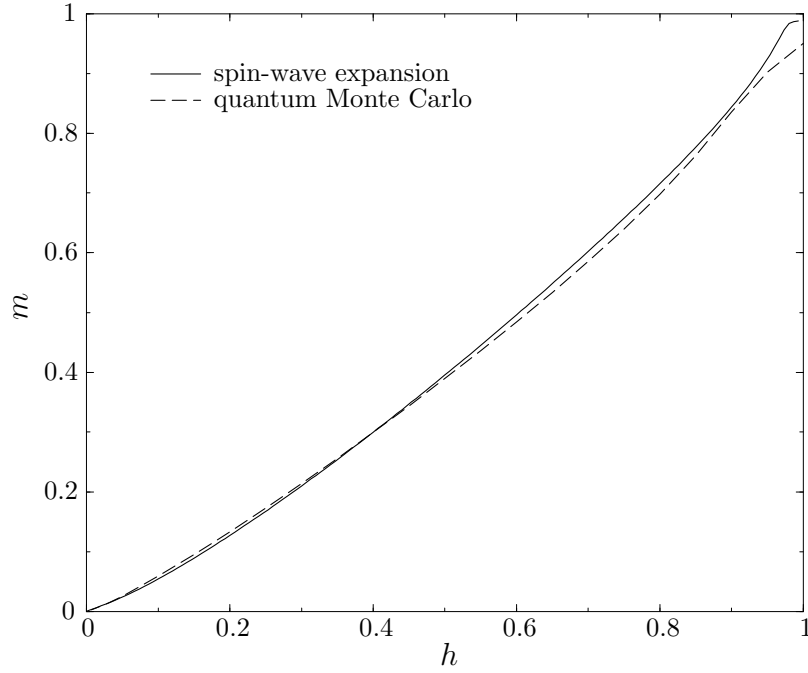


Figure 6.14: Theoretical uniform magnetization $m(h)$ for the square lattice with $S = 1/2$ and $J_1 = J_2$. The results of the spin-wave expansion (solid line) and quantum Monte Carlo (dashed line) show a satisfactory quantitative agreement.

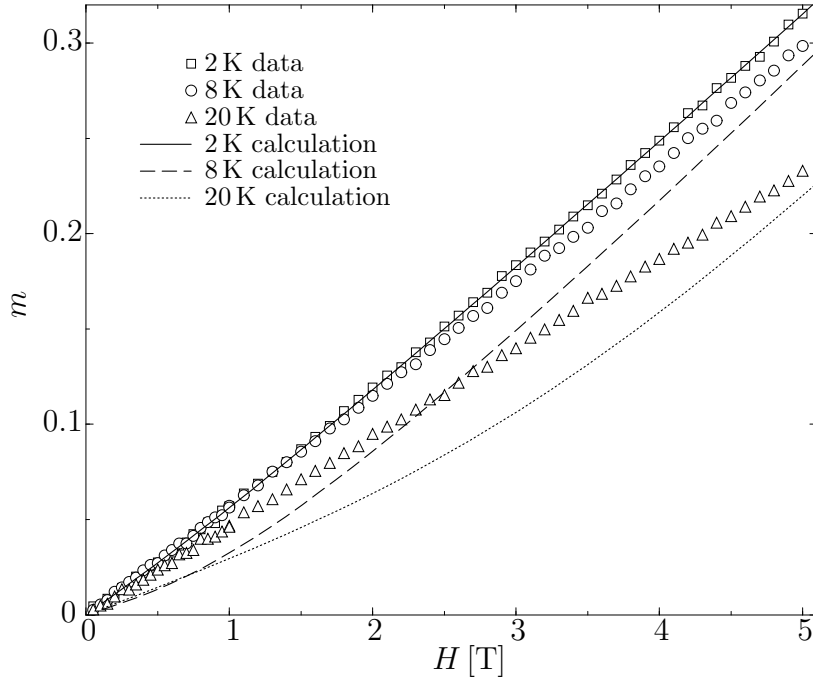


Figure 6.15: Magnetization $m(H)$ of $\text{Mn}[\text{C}_{10}\text{H}_6(\text{OH})(\text{COO})]_2 \times 2\text{H}_2\text{O}$ up to field $H = 5$ T. Experimental data are indicated by squares (2 K), circles (8 K) and triangles (20 K). Theoretical magnetization curves for honeycomb lattice with $S = 5/2$ and $J_2 = 2J_1 = 1.95$ K are denoted by lines.

sensitive to the ratio J_2/J_1 as long as J_1 and J_2 have the same order of magnitude. Thus, from the experimental data we cannot determine the precise value of J_2/J_1 , but our fits are compatible with the assumption $J_2 \approx 2J_1$ motivated in Sec. 6.3.1.

In Fig. 6.15 we show experimental data and theoretical fits for the normalized uniform magnetization $m = M/(NS)$ at different temperatures. The magnetic field $H = 2\tilde{J}_0Sh$ is given in Tesla. At first sight it might seem surprising that all experimental curves are almost straight lines, whereas from Fig. 6.13 one would expect an upward bend of $m(h)$ at higher temperatures. However, we have to take into account that magnetization experiments were performed at field strengths far below the saturation field.

Fits for $T = 2$ K and different ratios $J_1/J_2 \sim \mathcal{O}(1)$ invariably give $\tilde{J}_0 \approx 4$ K. Hence we assume $J_2 = 2J_1$ and fit the theoretical curve to the experimental data at $T = 2$ K. Good agreement is achieved for $J_2 = 1.95$ K. For this value of the exchange couplings, we also plot theoretical magnetization curves at $T = 8$ K and $T = 20$ K in Fig. 6.15. These curves deviate significantly from the data, but one should be aware that $T = 8$ K is already beyond the estimated limit of validity $T \lesssim 0.5\tilde{J}_0S$ of our theoretical approach.

6.3.6 Finite-temperature susceptibility

Another experimentally relevant observable is the uniform zero-field susceptibility, more precisely its temperature dependence. Similarly to the last chapter, we first compare results obtained from different theoretical methods. We close this section with a fit of experimental data.

In Fig. 6.16 we compare the spin-wave result for the susceptibility (6.111) with the quantum Monte Carlo calculations on a honeycomb lattice with $S = 5/2$ and $J_2 = 2J_1$. The two curves show a fairly good agreement over the full temperature range. Although maximum values of the susceptibilities differ in two approaches, the positions of the peaks coincide. The susceptibility peaks are at approximately $10J_1$ and $8J_1$ for the spin-wave and the quantum Monte Carlo curve, respectively. At high temperatures both curves asymptotically approach the correct paramagnetic limit for the susceptibility $S(S+1)/(3T)$.

In Fig. 6.17 the uniform susceptibility is plotted in the experimental units cm^3/mol . When all exchange integrals have the same order of magnitude we expect a peak in the susceptibility for $T \approx \tilde{J}_0S$. Experimentally, the peak is at approximately 7 K so that we have $\tilde{J}_0 \approx 3$ K, in accordance with the fits of the magnetization curves.

For a more quantitative comparison we use the following procedure. First we subtract the temperature-independent contribution from the experimental susceptibility in order to get the correct paramagnetic behavior at high temperatures. Then we fit the theoretical expression (6.111) with $J_2 = 2J_1$ to the full set of data points.

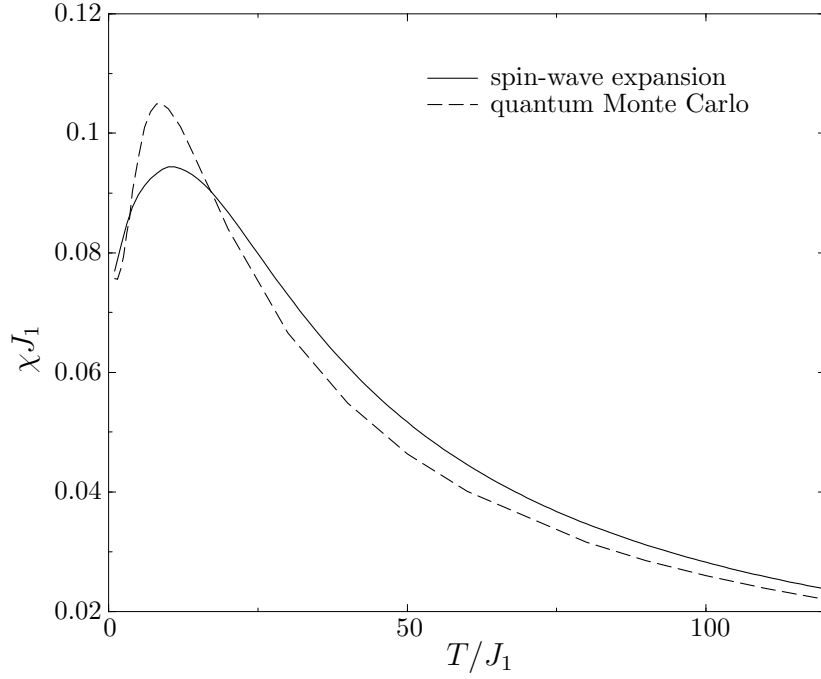


Figure 6.16: Susceptibility χJ_1 as a function of relative temperature T/J_1 for a honeycomb lattice with $S = 5/2$ and $J_2 = 2J_1$. The spin-wave result (solid line) is compared to quantum Monte Carlo calculations (dashed line).

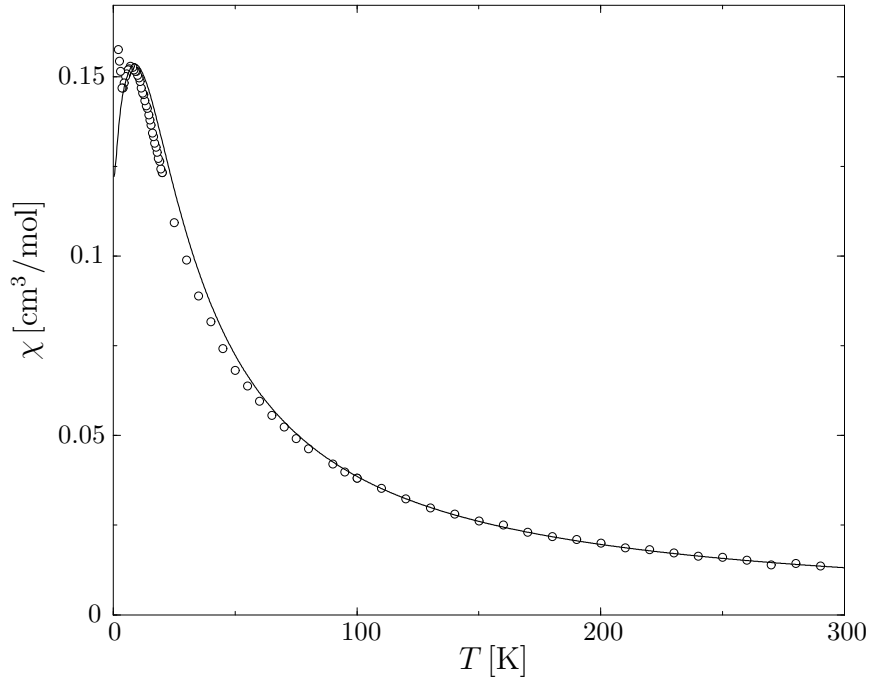


Figure 6.17: Susceptibility $\chi(T)$ of $\text{Mn}[\text{C}_{10}\text{H}_6(\text{OH})(\text{COO})]_2 \times 2\text{H}_2\text{O}$. Circles are experimental data in a field of 2 T. Theoretical fit for honeycomb lattice with $J_2 = 2J_1$ (solid line) gives $J_2 = 1.66\text{K}$.

Circles in Fig. 6.17 are experimental data and the solid line is a fit with $J_2 = 1.66$ K. The theoretical curve reproduces the behavior of the susceptibility very well and it especially gives a good estimate of the position and the form of the peak.

Note that we experimentally observe an increase in the susceptibility below $T_* = 3.0 \pm 0.2$ K. The careful reader will notice at this point that the estimated value of T_* is larger than the temperature $T = 2$ K where we obtained the best fit of our calculated magnetization curve $m(H)$ to the experimental data shown in Fig. 6.15. Hence, at $T = 2$ K the system seems to have some kind of long range magnetic order, which we have ignored in our calculation. However, the precise nature of the order and the mechanism responsible for the ordering are not known at this point. The fact that a strictly 2D model can reasonably well explain the magnetization curve at $T = 2$ K imposes some constraint on possible ordering mechanisms. We suspect that dipole-dipole interactions play an important role in this temperature range, because the long-range nature of the dipole-dipole interaction can give rise to spontaneous antiferromagnetic order even in 2D [99]. This point deserves further attention, both theoretically and experimentally.

6.3.7 Specific heat

In this section we discuss the temperature dependence of the specific heat in the absence of a uniform magnetic field. After the comparison of the theoretical curves we present a thorough discussion of experimental data.

In Fig. 6.18 we plot the zero-field version of the spin-wave expression for the specific heat (6.117) and the corresponding results of the quantum Monte Carlo simulation on a honeycomb lattice with $S = 5/2$ and $J_2 = 2J_1$. At low temperatures the spin-wave curve shows qualitatively correct behavior, as one would expect. However, the spin-wave theory breaks down at higher temperatures and does not correctly describe the peak in the specific heat. Moreover, because the magnon occupation number tends to S for large temperatures the spin-wave specific heat saturates at

$$C_h^{\text{SWT}}(T \rightarrow \infty) \rightarrow 2S(S+1) \ln^2 \left(1 + \frac{1}{S} \right) \approx 1.98. \quad (6.141)$$

This is an artifact of the spin-wave expansion. On the other side, the quantum Monte Carlo data correctly capture the peak in specific heat at approximately $\tilde{J}_0 S$. For high temperatures the quantum Monte Carlo curve decays as T^{-2} , which is the behavior predicted by an ideal paramagnet.

In Fig. 6.19 the molar specific heat is plotted in experimental units mJ/(mol K). Experimental data (circles) were obtained by subtracting the T^3 phonon contribution from the raw data [100]. For a comparison with the experiment, we plot quantum Monte Carlo results (crosses) for a value of $J_1 = 0.83$ K as obtained from the fit of the

susceptibility in the last section. The agreement between the two curves is fairly good at low temperatures. Both the peak position and height are slightly overestimated by quantum Monte Carlo. At high temperatures the error of the corrected experimental data is large due to the subtraction of phononic modes and therefore a reasonable comparison with theoretical findings is not possible.

From the above discussion we conclude that more precise experimental specific heat curves are needed. On the other hand, it would be interesting to compare experimental results with a quantum Monte Carlo calculation of a quasi-two dimensional Heisenberg antiferromagnet on a honeycomb lattice with a small interplane interaction (see Ref. [101] for a similar treatment).

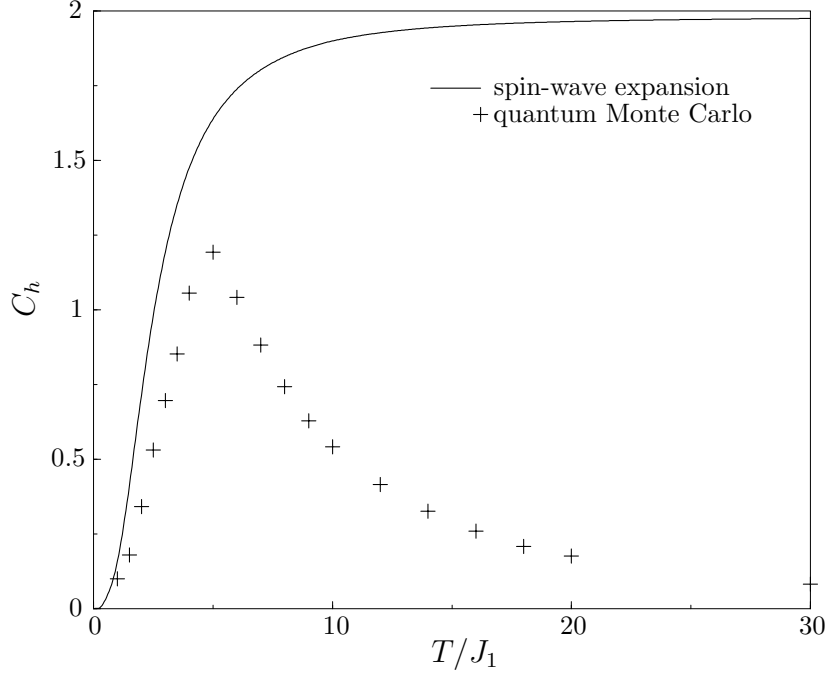


Figure 6.18: Specific heat C_h as a function of relative temperature T/J_1 for a honeycomb lattice with $S = 5/2$ and $J_2 = 2J_1$. The spin-wave result (solid line) is compared to quantum Monte Carlo calculations (crosses).

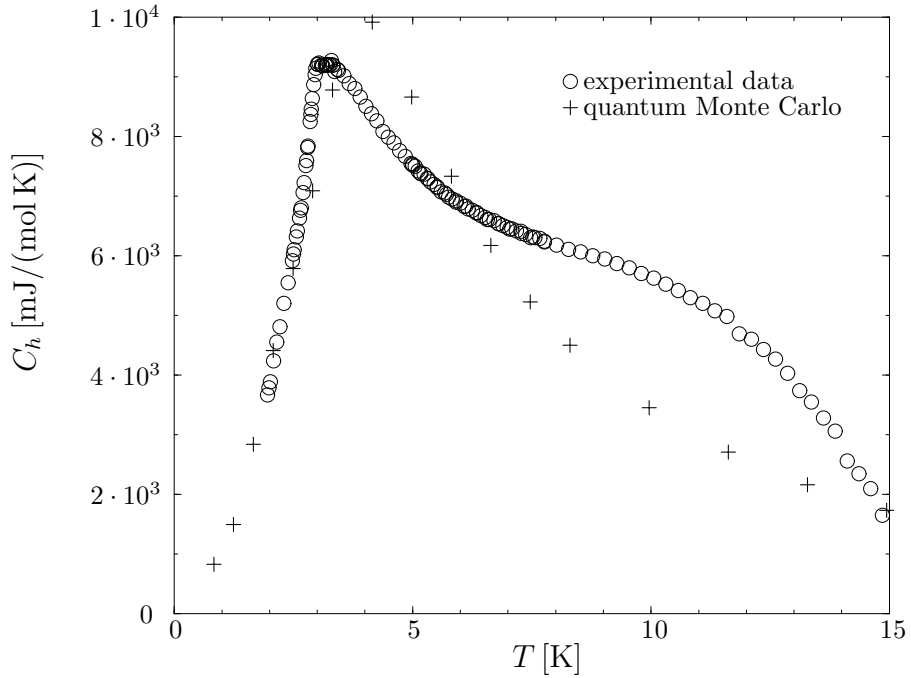


Figure 6.19: Molar specific heat $C_h(T)$ of $\text{Mn}[\text{C}_{10}\text{H}_6(\text{OH})(\text{COO})]_2 \times 2\text{H}_2\text{O}$. Circles are experimental data in a field of 0 T. For comparison, quantum Monte Carlo results for a value of $J_1 = 0.83$ K obtained from the fit of the susceptibility are also plotted (crosses).

Chapter 7

Conclusion

In this thesis, we have discussed the physics of low-dimensional quantum Heisenberg magnets within the framework of spin-wave theory. Although tremendously successful for three-dimensional spin systems, the spin-wave expansion cannot be straightforwardly expanded to magnets in reduced dimensions. The major cause for this is of a fundamental nature: spin waves are fluctuations around the ordered state, but according to the Mermin-Wagner theorem low-dimensional Heisenberg models do not exhibit any long-range order at finite temperatures.

A significant attempt to adapt the spin-wave method to low dimensions was made by Takahashi [19]. He has chosen a variational approach where the Lagrange parameter plays the role of a chemical potential and is determined by the condition of zero order parameter. Takahashi's variant of spin-wave theory works well for ferromagnets [20] and antiferromagnets [21], however for systems with more complex magnetic order like ferrimagnets the method is plagued by ambiguities regarding the choice of the constraint [76]. Furthermore, going beyond the mean-field level within Takahashi's approach turned out to be quite complicated.

In the first part of the thesis we therefore propose an another type of spin-wave theory suitable for low-dimensional systems where the thermodynamic observables are calculated at constant order parameter. In principle, the idea behind our approach is very elementary: a Legendre transformation of the Helmholtz free energy to the Gibbs free energy and a subsequent calculation of the conjugate field and the inverse susceptibility via elementary thermodynamic relations [45]. Within our method we were able to determine the lowest order fluctuation correction to the Helmholtz free energy in a systematical way. In addition, we have calculated the Gibbs free energy and the low-temperature behavior of the susceptibility for the one- and two-dimensional Heisenberg ferromagnet. In three dimensions, we could re-derive the classical Bloch $T^{3/2}$ -law for the spontaneous magnetization of the Heisenberg ferromagnet.

One of the benefits of the approach developed here over Takahashi's modified spin wave theory is that the absence of long range order is obtained as a result and is not set to zero by hand. As we have only demonstrated the method on the simplest case

of a ferromagnet in this work, it would surely be challenging to test it on a model with a more complex ordered state, e.g. a Heisenberg ferrimagnet.

In the second part of the thesis, we treat a two-dimensional Heisenberg antiferromagnet in the presence of a uniform external magnetic field. This work was motivated by experiments performed on a newly synthesized quasi two-dimensional metal-organic $S = 5/2$ antiferromagnet on a distorted honeycomb lattice [32]: an appropriate theoretical interpretation of the measured magnetization curves and the uniform susceptibility was necessary.

Zhitomirsky and Nikuni proposed a spin-wave based method for the calculation of the uniform magnetization of a spin-1/2 Heisenberg square lattice antiferromagnet at zero temperature [31]. By minimizing the classical energy of the system they were able to derive a relation between the tilting angle and the magnitude of the external field. Then, a derivative of the ground-state energy with respect to the uniform field can be made and an expression for the magnetization is obtained.

We generalize the approach of Zhitomirsky and Nikuni to the case of finite temperatures by introducing a formal staggered field such that the staggered magnetization vanishes. For this setup we calculate the linear spin-wave dispersion of a Heisenberg antiferromagnet on an arbitrary two-dimensional bipartite lattice. Subsequently, we obtain the uniform and staggered magnetization by differentiating the Helmholtz free energy with respect to the uniform and staggered field, respectively. We show that within our framework only the longitudinal spin-spin correlation function contributes to the zero-field uniform susceptibility. A comparison of the spin-wave calculations with the results of quantum Monte Carlo yields a satisfactory agreement. By relating the staggered correlation length to the gap in the antiferromagnetic branch of the energy dispersion we determine the field dependence of the correlation length at fixed finite temperature. The temperature behavior of the correlation length for a small fixed field is given and the result for zero field obtained previously in Takahashi's approach is also re-derived.

Finally, we apply our method to an experimentally motivated case of the distorted honeycomb lattice in order to determine the strength of the exchange interactions. Under the assumption of an approximate magnitude of 1 K for the interaction along a single bond, theoretical spin-wave curves show a fairly good agreement with the measured magnetizations for low temperatures. For this value of magnetic interaction strength the calculated susceptibility and specific heat also fit well to the experimentally obtained curves.

An increase of the experimental susceptibility below 2 K might be evidence for antiferromagnetic long-range order. We suspect that at such low temperatures dipole-dipole interactions could be the driving force behind a spontaneous ordering even in two spatial dimensions. Therefore it would be convenient to take the dipole-dipole interaction into account in a further treatment of the problem.

Bibliography

- [1] N. Taniguchi, On the Basic Concept of Nano-Technology, in *Proceedings of the International Conference on Production Engineering*, Tokyo, 1974.
- [2] R. P. Feynman, There's Plenty of Room at the Bottom, Meeting of the American Physical Society, Pasadena, 1959.
- [3] G. Binasch, P. Grünberg, F. Saurenbach, and W. Zinn, *Phys. Rev. B* **39**, 4828 (1988).
- [4] R. P. Feynman, *Int. J. Theor. Phys.* **21**, 467 (1982).
- [5] D. Deutsch, *Proc. Roy. Soc. London* **A400**, 97 (1985).
- [6] D. DiVincenzo, *Fortschr. Physik* **48**, 771 (2000).
- [7] C. Walter, *Sci. Am. Dig.* (2005).
- [8] G. E. Moore, *Electronics* **38**, 114 (1965).
- [9] National Nanotechnology Initiative (NNI), <http://www.nano.gov/>.
- [10] Nanotechnologies and nanosciences, knowledge-based multifunctional materials and new production processes and devices (NMP), <http://www.cordis.lu/nmp/>.
- [11] E. Ising, *Z. Physik* **31**, 253 (1925).
- [12] H. Bethe, *Z. Physik* **71**, 205 (1931).
- [13] N. D. Mermin and H. Wagner, *Phys. Rev. Lett.* **17**, 1133 (1966).
- [14] P. C. Hohenberg, *Phys. Rev.* **158**, 383 (1967).
- [15] A. W. Sandvik and J. Kurkijärvi, *Phys. Rev. B* **43**, 5950 (1991).
- [16] J. G. Bednorz and K. A. Müller, *Z. Physik B* **64**, 189 (1986).
- [17] S. Chakravarty, B. I. Halperin, and D. R. Nelson, *Phys. Rev. B* **39**, 2344 (1988).

- [18] D. P. Arovas and A. Auerbach, Phys. Rev. B **38**, 316 (1988).
- [19] M. Takahashi, Prog. Theor. Phys. Suppl. **87**, 233 (1986).
- [20] M. Takahashi, Phys. Rev. Lett. **58**, 168 (1987).
- [21] M. Takahashi, Phys. Rev. B **40**, 2494 (1989).
- [22] F. J. Dyson, Phys. Rev. **102**, 1217 (1956).
- [23] F. J. Dyson, Phys. Rev. **102**, 1230 (1956).
- [24] S. V. Maleev, Sov. Phys. JETP **6**, 776 (1957).
- [25] E. Dagotto, Rev. Mod. Phys **66**, 763 (1994).
- [26] P. Lemmens and P. Millet, in *Quantum Magnetism*, edited by U. Schollwöck, J. Richter, D. i. J. Farnell, and R. F. Bishop, page 435, Springer Verlag, Berlin, 2004.
- [27] P. W. Anderson, Science **235**, 1196 (1987).
- [28] S. Sachdev, *Quantum Phase Transitions*, Cambridge University Press, Cambridge, 1999.
- [29] M. Oshikawa, M. Yamanaka, and I. Affleck, Phys. Rev. Lett. **78**, 1984 (1996).
- [30] J. Richter, J. Schulenburg, and A. Honecker, in *Quantum Magnetism*, edited by U. Schollwöck, J. Richter, D. J. Farnell, and R. F. Bishop, page 85, Springer Verlag, Berlin, 2004.
- [31] M. E. Zhitomirsky and T. Nikuni, Phys. Rev. B **57**, 5013 (1998).
- [32] M. U. Schmidt, E. Alig, L. Fink, M. Bolte, R. Panisch, V. Pashchenko, B. Wolf, and M. Lang, Acta. Cryst. C **61**, m361 (2005).
- [33] N. W. Ashcroft and N. D. Mermin, *Solid State Physics*, Saunders College Publishing, Philadelphia, 1976.
- [34] A. Auerbach, *Interacting Electrons and Quantum Magnetism*, Springer Verlag, New York, 1994.
- [35] N. Spaldin, *Magnetic Materials*, Cambridge University Press, Cambridge, 2003.
- [36] P. W. Atkins and R. Friedman, *Molecular Quantum Mechanics*, Oxford University Press, Oxford, 2005.
- [37] W. Heitler and F. London, Z. Physik **44**, 455 (1927).

- [38] C. Herring, in *Magnetism*, edited by G. T. Rado and H. Suhl, Academic Press, New York, 1965.
- [39] M. Shimizu, Rep. Prog. Phys. **44**, 329 (1981).
- [40] P. W. Anderson, Phys. Rev. **79**, 350 (1950).
- [41] L. D. Landau and E. M. Lifschitz, *Statistische Physik*, Akademie Verlag Berlin, Berlin, 1987.
- [42] N. N. Bogoliubov, Physik. Abhandl. Sowjetunion **6**, 1, 113, 229 (1962).
- [43] D. Ioffe, S. B. Shlosman, and Y. Velenik, Commun. Math. Phys. **226**, 433 (2002).
- [44] F. D. M. Haldane, Phys. Lett. **93A**, 464 (1983).
- [45] J. W. Negele and H. Orland, *Quantum Many-Particle Systems*, Addison-Wesley, Redwood City, 1988.
- [46] J. Goldstone, Nuovo Cimento **19**, 154 (1961).
- [47] R. V. Lange, Phys. Rev. **146**, 301 (1966).
- [48] F. Bloch, Z. Physik **61**, 206 (1930).
- [49] T. Holstein and H. Primakoff, Phys. Rev. **58**, 1098 (1940).
- [50] P. W. Anderson, Phys. Rev. **86**, 694 (1952).
- [51] R. Kubo, Phys. Rev. **87**, 568 (1952).
- [52] A. B. Harris, D. Kumar, H. B. I., and P. C. Hohenberg, Phys. Rev. B **3**, 961 (1971).
- [53] N. Metropolis and S. Ulam, J. Am. Stat. Assoc. **44**, 335 (1949).
- [54] D. C. Handscomb, Proc. Cambridge Phil. Soc. **58**, 594 (1962).
- [55] D. C. Handscomb, Proc. Cambridge Phil. Soc. **60**, 115 (1964).
- [56] J. W. Lyklema, Phys. Rev. Lett. **49**, 88 (1982).
- [57] A. W. Sandvik, Phys. Rev. B **59**, R14157 (1999).
- [58] ALPS Project: Algorithms and Libraries for Physics Simulations, <http://alps.comp-phys.org/>.

- [59] F. Alet, S. Wessel, and M. Troyer, Phys. Rev. E **71**, 036706 (2005).
- [60] D. C. Mattis, *The Theory of Magnetism I: Statics and Dynamics*, Springer-Verlag, Berlin Heidelberg & New York, 1981.
- [61] P. Kopietz, P. Scharf, M. S. Skaf, and S. Chakravarty, Europhys. Lett. **9**, 465 (1989).
- [62] F. Schütz, M. Kollar, and P. Kopietz, Phys. Rev. Lett. **91**, 017205 (2003).
- [63] I. Spremo, F. Schütz, P. Kopietz, V. Pashchenko, B. Wolf, M. Lang, J. W. Bats, C. Hu, and M. U. Schmidt, Phys. Rev. B **72**, 174429 (2005).
- [64] P. Kopietz, *Low Dimensional Quantum Magnetism and Applications to High-Temperature Superconductors*, PhD thesis, University of California Los Angeles, 1990.
- [65] N. Hasselmann and P. Kopietz, unpublished.
- [66] J. Schwinger, in *Quantum Theory of Angular Momentum*, edited by L. Biedenharn and H. Van Dam, Academic Press, New York, 1965.
- [67] P. Kopietz, Phys. Rev. B **41**, 9228 (1990).
- [68] P. Kopietz and S. Chakravarty, Phys. Rev. B **40**, 4858 (1989).
- [69] A. E. Trumper, L. O. Manuel, C. J. Gazza, and L. O. Ceccatto, Phys. Rev. Lett. **78**, 2216 (1997).
- [70] S.-K. Ma, *Statistical Mechanics*, chapter 27, World Scientific, Singapore, 1985.
- [71] A. Georges and J. S. Yedidia, Phys. Rev. B **43**, 3475 (1991).
- [72] P. Zedler and P. Kopietz, Phys. Rev. B **72**, 184404 (2005).
- [73] E. S. Pisanova, N. B. Ivanov, and N. S. Tonchev, Phys. Rev. B **65**, 212404 (2001).
- [74] X. Wan, K. Yang, and R. N. Bhatt, Phys. Rev. B **66**, 014429 (2002).
- [75] S. Yamamoto and T. Nakanishi, Phys. Rev. Lett. **89**, 157603 (2002).
- [76] S. Yamamoto, T. Fukui, K. Maisinger, and U. Schollwöck, J. Phys.: Condens. Matter **10**, 11033 (1998).
- [77] K. Huang, *Introduction to Statistical Physics*, Taylor & Francis, New York, 2001.

- [78] F. London, *Superfluids II*, John Wiley and Sons, New York, 1954, Appendix.
- [79] M. Abramowitz and I. Stegun, editors, *Handbook of Mathematical Functions*, Dover Publications Inc., New York, 1964.
- [80] J. E. Robinson, Phys. Rev. **83**, 678 (1951).
- [81] M. Takahashi and M. Yamada, J. Phys. Soc. Jpn **54**, 2808 (1985).
- [82] M. Yamada and M. Takahashi, J. Phys. Soc. Jpn **55**, 2024 (1986).
- [83] P. Kopietz, Phys. Rev. B **40**, 5194 (1989).
- [84] P. Schlottmann, Phys. Rev. Lett. **54**, 2131 (1985).
- [85] P. Schlottmann, Phys. Rev. B **33**, 4880 (1986).
- [86] E. Brézin and D. J. Wallace, Phys. Rev. B **7**, 1967 (1973).
- [87] G. F. Mazenko, Phys. Rev. B **14**, 3933 (1976).
- [88] V. G. Vaks, A. Larkin, and S. Pikin, Sov. Phys. JETP **26**, 647 (1968).
- [89] M. E. Zhitomirsky and A. L. Chernyshev, Phys. Rev. Lett. **82**, 4536 (1999).
- [90] S. V. Maleyev, Phys. Rev. Lett. **85**, 3281 (2000).
- [91] A. V. Syromyatnikov and S. V. Maleyev, Phys. Rev. B **65**, 12401 (2001).
- [92] T. Oguchi, Phys. Rev. **117**, 117 (1960).
- [93] P. Kopietz and S. Chakravarty, Phys. Rev. B **56**, 3338 (1997).
- [94] M. Y. Veillette, J. T. Chalker, and R. Coldea, Phys. Rev. B **71**, 214426 (2005).
- [95] A. L. Fetter and J. D. Walecka, *Quantum Theory of Many-Body Systems*, McGraw-Hill, New York, 1971.
- [96] V. Pashchenko, private communication.
- [97] R. B. Griffiths, Phys. Rev. **133**, A768 (1964).
- [98] S. Gluzman, Z. Phys. B **90**, 313 (1993).
- [99] C. Pich and F. Schwabl, Phys. Rev. B **47**, 7957 (1993).
- [100] A. Brühl, private communication.

- [101] P. Sengupta, A. W. Sandvik, and R. R. P. Singh, Phys. Rev. B **68**, 094423 (2003).
- [102] K. E. Drexler, *Engines of Creation: the Coming Era of Nanotechnology*, Doubleday Anchor, New York, 1986.

Deutsche Zusammenfassung

Nanotechnologie wird heute als eine der Schlüsseltechnologien der Zukunft angesehen [102]. Unter diesem Sammelbegriff werden Aktivitäten zur Erforschung der Physik auf der Sub-Mikrometer-Skala und Verfahren zur Herstellung von Strukturen mit entsprechenden Dimensionen zusammengefasst.

Als einer von vielen Zweigen der Nanotechnologie hat sich die *Spintronik* (kurz für spin-basierte Elektronik) etabliert. Als Geburtsstunde der Spintronik gilt die Entdeckung des Riesen-Magnetowiderstandes (Engl. giant magnetoresistance, kurz GMR) in den späten 1980-er Jahren [3]. Heute wird dieser Begriff für alle elektronischen Geräte benutzt, die zusätzlich zu den Ladungs- auch die Spinfreiheitsgrade des Elektrons ausnutzen. Das prominenteste Beispiel eines spintronischen Geräts - zumindest gedanklich - ist der Quantencomputer. In einem Quantencomputer werden die Quantenbits (kurz Qubits) durch die Spinfreiheitsgrade des Elektrons dargestellt [4, 5]. Praktische Realisierung eines Quantencomputers stellt aufgrund vieler prinzipieller Probleme, wie z.B. Dekohärenz, nach wie vor eine technische Herausforderung dar.

Von den am Markt erhältlichen spintronischen Produkten sind Drehventile (auch spin-valves genannt) am weitesten verbreitet. Ein Drehventil besteht aus magnetischen Dünnschichten mit jeweils unterschiedlichem Hystereseverhalten, deren elektrische Leitfähigkeit von der Richtung des angelegten Magnetfeldes abhängt. Sie werden in der Automobilindustrie als Sensoren und in Festplatten als Leseköpfe eingesetzt. Das so genannte Krydersche Gesetz besagt, dass sich die Speicherdichte von Festplatten alle 18 Monate verdoppelt [7]. Die gleiche Rate gilt nach dem bekannten Mooreschen Gesetz für Anzahl der Transistoren auf integrierten Schaltungen [8]. Daraus folgt, dass die technische Entwicklung der Spintronik ungefähr so schnell wie die konventionelle Mikroelektronik voranschreitet.

Obwohl die Spintronik und das gesamte Feld der Nanotechnologie erst ein geringes Marktvolumen aufweisen, sind deren Potenziale unübersehbar. Dies spiegelt sich auch in dem stetig wachsenden Forschungsaufwand wider. Eine Vielzahl von öffentlich geförderten Programmen wurden ausgeschrieben, um mit 'National Nanotechnology Initiative' (NNI) in den Vereinigten Staaten [9] und 'Nanotechnologies and nanosciences, knowledge-based multifunctional materials and new production processes and devices' (NMP) der Europäischen Union [10] nur zwei der Größten zu nennen.

Aus wissenschaftlicher Sicht wird die Spintronik maßgeblich durch die Physik niedrigdimensionaler Quantenspinsysteme vorangetrieben. Die Disziplin des niedrigdimensionalen Magnetismus wurde durch zwei bahnbrechende theoretische Arbeiten begründet: das Aufstellen des gleichnamigen Modells durch Ising im Jahre 1925 [11] und die Berechnung des exakten Grundzustandes des eindimensionalen Heisenbergmodells durch Bethe im Jahre 1931 [12]. In Ermangelung geeigneter experimenteller Realisierungen wurde in den darauffolgenden 40 Jahren vorwiegend theoretische Forschung betrieben. Aus einer Vielzahl von exakten Ergebnissen ist das so genannte Mermin-Wagner Theorem [13] besonders hervorzuheben. Dieses besagt, dass in isotropen ein- und zweidimensionalen Heisenbergmagneten bei endlichen Temperaturen keine spontane Symmetriebrechung möglich ist. Diese Aussage werden wir bei den in der vorliegenden Arbeit durchgeführten Berechnungen mehrfach benutzen.

Ein weiteres exaktes Resultat, dass für die Physik der Quantenspinsysteme und insbesondere für die vorliegende Arbeit von zentraler Bedeutung ist, ist das *Goldstone'sche Theorem* [46]. Das Goldstonesche Theorem besagt, dass die spontan gebrochene kontinuierliche Symmetrie im Grundzustand des Hamiltonoperators mit kurzreichweitiger Wechselwirkung die Existenz niederenergetischer Anregungen ohne Bandlücke bedingt. Die Energie dieser so genannten Goldstoneschen Moden verschwindet bei den Werten für den Impuls, für die die Spin-Spin-Korrelationsfunktion divergiert. Goldstonesche Moden treten auch in Heisenbergmagneten auf; hier haben diese kollektiven Anregungen bosonischen Charakter und heißen *Spinwellen* bzw. *Magnonen*.

Spinwellentheorie wurde von Bloch [48] und Holstein und Primakoff [49] unabhängig voneinander zur Behandlung von Ferromagneten entwickelt. Da die Spinwellenamplitude bei niedrigen Temperaturen gering ist, können Wechselwirkungen zwischen den Magnonen vernachlässigt werden. Dies ist Inhalt der *linearen* Spinwellentheorie. Mit diesem Zugang leitete Bloch das bekannte $T^{3/2}$ -Gesetz für die spontane Magnetisierung eines dreidimensionalen Magneten ab.

Die Spinwellentheorie wurde in den 1950-er Jahren von Anderson [50] und Kubo [51] zur Beschreibung des antiferromagnetischen Néel-Zustandes herangezogen. Dyson bestimmte asymptotisch die thermodynamischen Variablen eines dreidimensionalen Ferromagneten bei niedrigen Temperaturen [22, 23]. Der Dysonsche Zugang wurde von Harris und Mitarbeitern verallgemeinert, um die dynamischen Eigenschaften wie Spin-Spin Korrelationen und Spinwellendämpfung von Heisenberg-Antiferromagneten systematisch zu berechnen [52].

Formal werden in der Spinwellentheorie die Komponenten des Spinoperators auf kanonische Boseoperatoren - Magnonen - abgebildet. Der so erhaltene bosonische Hamiltonoperator ist nach Potenzen des inversen Spins geordnet; dies erlaubt eine systematische Behandlung von Wechselwirkungen. Der Term quadratisch in Magnonen ist wechselwirkungsfrei und kann durch geeignete kanonische Transformation auf den harmonischen Oszillator abgebildet werden. In der vorliegenden Arbeit benutzen

wir die Dyson-Maleev-Transformation [22, 24]. Wir formulieren die Abbildung für den allgemeinen Fall des Heisenbergmagneten im homogenen externen Magnetfeld. Der so erhaltene Dyson-Maleev-Hamiltonoperator enthält Terme mit bis zu sechster Ordnung in bosonischen Freiheitsgraden. In der Literatur wird anstelle von Dyson-Maleev- oft die Holstein-Primakoff-Transformation [49] verwendet. Hier hat der bosonische Hamiltonoperator unendlich viele Wechselwirkungsterme und muss in geeigneter Weise trunziert werden. Die Holstein-Primakoff-Darstellung ist äquivalent zur Dyson-Maleev-Darstellung, d.h. beide liefern äquivalente Ergebnisse für physikalische Observable.

Obwohl sich die Spinwellentheorie als sehr erfolgreiche analytische Methode für dreidimensionale Spinsysteme etablieren konnte, kann sie nicht ohne Weiteres auf niedrigdimensionale Magnete angewendet werden. Spinwellen sind Fluktuationen um den geordneten Zustand; dieser wird aber laut Mermin-Wagner-Theorem in reduzierten Dimensionen bei endlichen Temperaturen zerstört. Nichtsdestotrotz können die niederenergetischen Anregungen vieler Magnete, die keine langreichweitige magnetische Ordnung aufweisen, mit Hilfe von *renormierten* Spinwellen beschrieben werden. Als Beispiel seien zweidimensionale Heisenberg-Ferromagnete [68] und -Antiferromagnete [17] bei niedrigen, aber dennoch endlichen Temperaturen genannt. In diesen Fällen ist die Korrelationslänge ξ des Ordnungsparameters exponentiell groß und Spinwellen mit dem Wellenvektor $|\mathbf{k}| \gg \xi^{-1}$ sind wohldefinierte elementare Anregungen [64]. Weitere Systeme, die bei niedrigen Temperaturen dieses Verhalten zeigen, sind Antiferromagnete mit der Haldane-Lücke und eindimensionale Ferromagnete mit beliebigem Spin.

Die Entdeckung der Hochtemperatur-Supraleitung in den 1980-er Jahren belebte das Interesse an niedrigdimensionalen Quantenmagneten [16]. Die Kupferoxid-Schichten in den Hochtemperatursupraleitern - das bekannteste Beispiel ist La_2CuO_4 - sind eine sehr gute experimentelle Realisierung des zweidimensionalen $S = 1/2$ Heisenberg-Antiferromagneten auf dem Quadratgitter [17]. Das Problem wurde mit Hilfe unterschiedlicher theoretischer Methoden behandelt, unter anderem im Rahmen des Nichtlinearen Sigmamodells [17] und der Schwinger-Boson-Theorie [18].

In einer Reihe von wichtigen Arbeiten versuchte Takahashi, die Spinwellentheorie auf niedrigdimensionale Modelle zu verallgemeinern [19, 20, 21]. Er wählte einen Variationsansatz, in dem der Lagrangeparameter physikalisch die Bedeutung des chemischen Potentials hat. In Übereinstimmung mit dem Mermin-Wagner-Theorem wird der Lagrangeparameter so festgelegt, dass der Ordnungsparameter verschwindet. Takahashis Methode liefert zufriedenstellende Ergebnisse für ferromagnetische [20] und antiferromagnetische [21] Heisenbergmodelle, läßt sich aber aufgrund von Mehrdeutigkeiten nicht ohne Weiteres auf Systeme mit komplexerer magnetischer Ordnung wie Ferrimagnete anwenden [76]. Außerdem erwies es sich als schwierig, in diesem Zugang über die Molekularfeldnäherung hinauszugehen.

In der vorliegenden Arbeit schlagen wir eine neue Spinwellen-Methode für niedrig-dimensionale Spinsysteme vor. Sie basiert auf der konventionellen Spinwellentheorie, mit dem Unterschied, dass bei den thermodynamischen Berechnungen der Ordnungsparameter M konstant gehalten wird. Der Grundgedanke unseres Zuganges beruht auf einer elementaren Umformung: der Legendre-Transformation der Helmholtzschen Freien Energie zur Gibbschen Freien Enthalpie und anschließender Berechnung des zum Ordnungsparameter konjugierten Feldes H und der inversen Suszeptibilität mittels thermodynamischer Gleichungen [45].

Wir wenden die Spinwellentheorie bei konstantem Ordnungsparameter auf Heisenberg-Ferromagneten auf hyperkubischen Gittern in 1,2 und 3 Dimensionen an. In der Hartree-Fock-Näherung konnten wir Takahashis Ergebnisse reproduzieren, z.B. für die Suszeptibilitäten in einer Dimension

$$\frac{\chi_{D=1}}{N} = \frac{2JS^4}{T^2} \left[1 - \frac{3}{S} \frac{\zeta(\frac{1}{2})}{2\sqrt{\pi}} \sqrt{\frac{T}{JS}} + \mathcal{O}\left(\frac{T}{JS}\right) \right], \quad (7.1)$$

und in zwei Dimensionen

$$\chi_{D=2} = \frac{e^{4\pi JS^2/T}}{4\pi JS} \left[1 + \mathcal{O}\left(\frac{T}{JS}\right) \right], \quad (7.2)$$

wobei J die Austauschwechselwirkung, T die Temperatur, S der Spin und N die Anzahl der Gitterplätze sind. Darüber hinaus haben wir die Zwei-Schleifen-Korrektur zur Freien Energie bestimmt und damit die Suszeptibilitäten in dieser Näherung berechnet

$$\frac{\chi_{D=1}^{(2)}}{N} \sim C_\chi \frac{JS^4}{T^2}, \quad (7.3)$$

mit $C_\chi \approx 1.96$, und

$$\chi_{D=2}^{(2)} \sim T^2 e^{4\pi JS^2/T}. \quad (7.4)$$

Das Quanten-Monte-Carlo Ergebnis $C_\chi = 1.58 \pm 0.03$ für die $S = 1/2$ Heisenberg-Kette [83] legt die Vermutung nahe, dass die höheren Korrekturen den Wert von C_χ renormieren werden. Für den Heisenberg-Ferromagneten auf dem Quadratgitter wurde gezeigt, dass sich das Resultat für die Suszeptibilität $\chi_{D=2}^{(2)}$ auch unter Berücksichtigung höherer Ordnungen in der Störungstheorie nicht ändert [17, 68].

Wir konnten unsere Methode am Beispiel des dreidimensionalen Heisenberg-Ferromagneten auf dem kubischen Gitter verifizieren, indem wir die Magnetisierung pro Gitterplatz im thermodynamischen Limes bestimmt haben

$$\frac{M_{D=3}(H)}{N} = S - \frac{\zeta(\frac{3}{2})}{(2\sqrt{\pi})^3} \left(\frac{T}{JS}\right)^{3/2} + \mathcal{O}(H^{1/2}). \quad (7.5)$$

Bei verschwindendem Magnetfeld $H = 0$ erhalten wir das bekannte Blochsche Gesetz für die führende Korrektur der spontanen Magnetisierung im geordneten Zustand.

Anders als in Takahashis modifizierter Spinwellentheorie erhalten wir in unserem Zugang die Abwesenheit der Fernordnung als Ergebnis und müssen den Ordnungsparameter nicht a priori gleich Null setzen. Ein anderer Vorteil unserer Methode ist die Möglichkeit, systematisch höhere Ordnungen in der Störungstheorie berechnen zu können.

Wir haben die Spinwellentheorie bei konstantem Ordnungsparameter nur auf den einfachsten Fall des Heisenberg-Ferromagneten angewendet. Es wäre daher von besonderem Interesse, die Methode auf Systeme mit komplexerer magnetischer Ordnung wie z.B. Ferrimagnete anzuwenden.

Im zweiten Teil der vorliegenden Arbeit widmen wir uns zweidimensionalen Heisenberg-Antiferromagneten mit Nächste-Nachbar-Wechselwirkung in Anwesenheit eines homogenen externen Magnetfeldes. Die Auswirkungen eines homogenen äußeren Feldes auf Quanten-Antiferromagnete wurden in Vergangenheit intensiv untersucht [31, 89]. Insbesondere der Bereich des hohen Magnetfeldes nahe der Sättigung ist von theoretischem Interesse [89].

Die Berechnung der homogenen Magnetisierung des $S = 1/2$ Heisenberg-Antiferromagneten bei $T = 0$ im Rahmen der Spinwellentheorie geht auf Zhitomirsky und Nikuni zurück [31]. In ihrem Zugang wird zunächst die klassische Grundzustandsenergie des Systems minimiert und dadurch die Beziehung zwischen der Feldstärke und dem Kippwinkel zwischen homogener Magnetisierung und dem Feld bestimmt. Dadurch kann man die Energie des Spinwellengrundzustandes durch das äußere Feld parametrisieren; durch die Ableitung der Energie nach dem äußeren Feld erhält man einen Ausdruck für die homogene Magnetisierung.

Wir verallgemeinern die Methode von Zhitomirsky und Nikuni auf Heisenberg-Antiferromagnete mit *beliebigem* Spin auf einem *zweidimensionalen bipartiten* Gitter bei *endlichen* Temperaturen. Wir führen in dem Modell-Hamiltonoperator ein formales alternierendes Magnetfeld senkrecht zum externen homogenen Magnetfeld ein. Bei $T > 0$ wird dieses alternierende Feld so gewählt, dass die konjugierte Untergitter-Magnetisierung gemäß dem Mermin-Wagner Theorem verschwindet.

Wir formulieren die Spinwellenentwicklung um den klassischen nicht-kollinearen Zustand, indem wir die lokalen z -Quantisierungsachsen auf die klassischen Spinvektoren legen. Anschließend bestimmen wir das feldabhängige Spinwellenspektrum für den wechselwirkungsfreien Dyson-Maleev-Hamiltonoperator. Im Limes des verschwindenden äußeren Magnetfeldes können wir die bekannte zweifach entartete Spinwellendispersion rekonstruieren [92].

Die führende Spinwellen-Korrektur zur homogenen bzw. Untergitter-Magnetisierung berechnen wir durch Ableiten der Helmholtzschen freien Energie nach homogenem bzw. alternierendem Magnetfeld. Für $T = 0$ und den speziellen Fall des Qua-

dratgitters bekommen wir einen identischen Ausdruck für die Magnetisierung wie Zhitomirsky und Nikuni [31]. Bei endlichen Temperaturen setzen wir die Untergitter-Magnetisierung gleich Null und erhalten somit die homogene Magnetisierung in Abhängigkeit vom äußeren Feld und der Temperatur.

Außerdem zeigen wir, dass in unserer Methode nur die longitudinale Spin-Spin-Korrelationsfunktion zur homogenen Suszeptibilität beiträgt. Wir bestimmen die Feldabhängigkeit der antiferromagnetischen Korrelationslänge bei fester Temperatur mit Hilfe der Energielücke im antiferromagnetischen Zweig der Dispersion. Wir geben auch die Temperaturabhängigkeit der Korrelationslänge bei schwachem externen Magnetfeld an und leiten das bekannte Ergebnis für das verschwindende Feld ab [21].

Wir vergleichen die im Rahmen der Spinwellennäherung gewonnenen Observable mit den entsprechenden Quanten-Monte-Carlo-Ergebnissen. Sowohl homogene Magnetisierung als auch Suszeptibilität stimmen qualitativ zufriedenstellend mit den exakten Resultaten überein.

Abschließend wenden wir unsere Ergebnisse auf den experimentell motivierten Fall eines neuartigen zweidimensionalen metall-organischen $S = 5/2$ Heisenberg-Antiferromagneten auf einem verzerrten Wabengitter [32] an, um die Kopplungsstärke der Austauschwechselwirkung zu bestimmen. Aus den Fits der Magnetisierung bei tiefen Temperaturen und der Suszeptibilität an die experimentellen Kurven erhalten wir einen konsistenten Wert von ungefähr 1 K für die Wechselwirkungsstärke entlang eines einfachen Bindungspfades. Dies wird durch die Quanten Monte Carlo-Berechnung der spezifischen Wärme bestätigt.

Wir können den Anstieg der experimentellen Suszeptibilität unterhalb von 2 K mit unserem einfachen Modell allerdings nicht erklären. Da wir langreichweitige Dipol-Dipol-Wechselwirkungen als Ursache für dieses Verhalten vermuten, wäre es sinnvoll, diese bei weiterer Behandlung des Problems zu berücksichtigen.

Veröffentlichungen

1. Peter Kopietz und Ivan Spremo
Comment on Spin Dynamics of the 2D Spin 1/2 Quantum Antiferromagnet Copper Deuteroformate Tetradeuterate (CFTD),
Phys. Rev. Lett. **89**, 079701 (2002).
2. Marcus Kollar, Ivan Spremo, und Peter Kopietz,
Spin wave theory at constant order parameter,
Phys. Rev. B **67**, 104427 (2003).
3. Ivan Spremo, Florian Schütz, Peter Kopietz, Volodymyr Pashchenko, Bernd Wolf, Michael Lang, Jan W. Bats, Chunhua Hu, und Martin U. Schmidt,
Magnetic properties of a metal-organic antiferromagnet on a distorted honeycomb lattice,
Phys. Rev. B **72**, 174429 (2005).
4. Nils Hasselmann, Florian Schütz, Ivan Spremo, und Peter Kopietz,
Effective spin-wave action for ordered Heisenberg antiferromagnets in a magnetic field,
Proceedings of the Symposium on Spin and charge correlations in molecular based materials, Königstein (Taunus), October 2005

Lebenslauf

Zur Person

Name	Ivan Spremo
Geburtsdatum	26. Oktober 1976
Geburtsort	Ljubljana, Slowenien
Staatsangehörigkeit	Slowenisch

Berufserfahrung

seit 10/2005	<i>Wissenschaftlicher Mitarbeiter</i> in Zentraler Forschung und Vorauentwicklung Abteilung Werkstoffe Robert Bosch GmbH, Stuttgart
07/2002 - 09/2005	<i>Systemadministrator</i> im Institut für Theoretische Physik Universität Frankfurt

Bildungsgang

seit 03/2001

Doktorarbeit in theoretischer Festkörperphysik

Thema: Spin-Wave Calculations for Low-Dimensional
Magnets

Betreuer: Prof. Dr. Peter Kopietz

Universität Frankfurt

11/2000

Diplom in Physik, Note: Sehr Gut

Universität Göttingen

06/1999 - 11/2000

Diplomarbeit in theoretischer Festkörperphysik

Thema: Die Wegnersche Flußgleichungsmethode im Vergleich
mit direkten Verfahren für inhomogene Elektronensysteme

Betreuer: Prof. Dr. Kurt Schönhammer

Universität Göttingen

10/1997

Vordiplom in Physik, Note: Gut

Universität Göttingen

10/1995 - 11/2000

Studium der Physik

Universität Göttingen

06/1995

International Baccalaureate, Note: Sehr Gut

09/1991 - 06/1995

Gimnazija Bežigrad, Ljubljana

09/1983 - 06/1991

Osnovna šola Ledina, Ljubljana

Danksagung

Dank oder auch Dankbarkeit ist eine Eigenschaft von Menschen, die von anderen Menschen etwas erhalten haben (egal ob Geld, Gefühle, Wissen oder Gegenstände) und sich darüber freuen. Es ist die Anerkennung empfangenen Wohlvollens und die Bereitschaft, es zu erwidern.

Wikipedia

An dieser Stelle möchte ich mich bei den Menschen bedanken, die mich auf vielfältige Weise unterstützt und so die Fertigstellung vorliegender Arbeit erst ermöglicht haben. Ganz besonders danke ich meinem Betreuer, Prof. Dr. Peter Kopietz, der die Bearbeitung des Themas ermöglichte und mir sowohl durch physikalischen Weitblick, als auch durch seine Geduld und Präsenz während der gesamten Zeit eine große fachliche und menschliche Bereicherung war.

Prof. Dr. Maria-Roser Valenti danke ich für interessante Diskussionen und die Begutachtung der Arbeit.

Nils Hasselmann und Florian Schütz danke ich für gute Zusammenarbeit, konstruktive Kritik, schnelle und gründliche Korrektur der Arbeit und für entlastende Gespräche in gemeinsamen Pausen. Nicht zu vergessen sind auch Lorenz Bartosch, Tom Busche und Miodrag Kulić, mit denen ich viele fachliche sowie fachfremde Diskussionen geführt habe.

Volodymyr Pashchenko war stets bereit, mich in experimentellen Fragen zu beraten. In Stefan Wessel hatte ich einen kompetenten Ansprechpartner bezüglich Quanten Monte Carlo. Ich danke beiden für ihre Unterstützung.

Des weiteren gilt mein Dank Alexander Schinner, Felicien Capraro, Andrea Salguero, Gregor Kaczor, Alexander Achenbach und Gebhard Zeeb für die kollegiale und gute Zusammenarbeit in der Systemadministration. Durch ihre Unterstützung war die Doppelbelastung bewältigbar. Nils Lerch und Andreas Kreisel danke ich für die verantwortungsvolle Weiterführung meines Amtes als Systemadministrator.

Ein herzliches Dankeschön geht an unsere Sekretärinnen Frau Vogel, Frau Dinges und Frau Kolokotsa sowie Joe Laperal-Gomez und Andreas Mimler für die häufige Ermöglichung des ‘kleinen Dienstweges’.